

## Abstract

Title of Dissertation: Semiclassical surface of section  
perturbation theory

Oleg A. Zaitsev, Doctor of Philosophy, 2001

Dissertation directed by: Professor Richard E. Prange  
Department of Physics, University of Maryland

We derive analytic expressions for the wavefunctions and energy levels in the semiclassical approximation for perturbed integrable systems. We find that some eigenstates of such systems are substantially different from any of the unperturbed states, which requires some sort of a resonant perturbation theory. We utilize the semiclassical surface of section method by Bogomolny that reduces the spatial dimensions of the problem by one. Among the systems considered are the circular billiard with a perturbed boundary, including the short stadium; the perturbed rectangular billiard, including the tilted square and the square in magnetic field; the bouncing ball states in the stadium and slanted stadium; and the whispering gallery modes. The surface of section perturbation theory is compared with the Born-Oppenheimer approximation, which is an alternative way to describe some classes of states in these systems. We discuss the derivation of the trace formulas from Bogomolny's transfer operator for the chaotic, integrable, and almost integrable systems.

# Semiclassical surface of section perturbation theory

by

Oleg A. Zaitsev

Dissertation submitted to the Faculty of the Graduate School of the  
University of Maryland, College Park in partial fulfillment  
of the requirements for the degree of  
Doctor of Philosophy  
2001

Advisory Committee:

Professor Richard E. Prange, Chairman/Advisor  
Assoc. Professor Steven Anlage  
Assoc. Professor Brian R. Hunt  
Asst. Professor Wolfgang Losert  
Professor Edward Ott

# Preface

The main purpose of this work is to study the perturbed integrable systems in the semiclassical regime [63]. The examples of such systems include a circular or rectangular billiard with a distorted boundary, a rectangular billiard with a weak magnetic field, coupled quartic oscillators — any system that is a “small” perturbation of an integrable system. In a classical integrable system even an infinitesimal perturbation produces a qualitatively big effect — it changes the topology of the phase space near the periodic orbits. Whether this change will affect the quantum states depends on the energy of the particle.

As will be explained in due course, these systems possess the special spatially localized states related to the classical periodic orbits. Localization may take place even for relatively small perturbations. For example, in the case of a distorted boundary even a perturbation smaller than the wavelength may lead to a strong effect.

We use the Bogomolny  $T$ -operator method throughout this work. It provides the semiclassical description for the Poincaré surface of section. With this approach we reduce the dimensionality of the problem by one. In particular, for the two-dimensional systems one can derive a one-dimensional Schrödinger equation on the surface of section. It is often easy to find the qualitative behavior of its solutions and thus predict the localized states even without doing extensive calculations. In some cases the  $T$ -operator method produces the results similar to the Born-Oppenheimer approximation that we also consider.

Here is a brief description of the work. Chapter 1 is of an introductory character. We review the  $T$ -operator method in general for the reader’s convenience. We also demonstrate its connection with the boundary integral method for billiards. The Maslov phases are discussed as well.

In Chapter 2 the perturbation theory is derived and discussed from various aspects. Possible

experiments are suggested. Although the theory is formulated for the circular billiard with a perturbed boundary, the general character of the derivation and results is emphasized. In the following chapters we apply the method to other systems without detailed explanations.

In the first part of Chapter 3 we adapt the theory to the rectangular billiard with a perturbed boundary. We consider a tilted square as an example. In the rest of the chapter we study several non-perturbative systems where the perturbation theory still can be used for special classes of states, perhaps after some modification. Among such states are the bouncing ball and the whispering gallery modes. We also show how the whispering gallery mode near the boundary with a point of zero curvature can be described in terms of scattering.

In Chapter 4 we consider an example where the perturbation is not a distorted boundary, but a magnetic field. We analyze the square billiard in uniform magnetic field and with an off-center Aharonov-Bohm flux line. Experimental possibilities are also discussed.

The Born-Oppenheimer approximation is a subject of Chapter 5. We revisit some of the examples of earlier chapters and analyze them with this method. We compare this approach with the  $T$ -operator perturbation theory.

In Chapter 6 we derive the trace formulas for chaotic, integrable, and almost integrable systems starting with the  $T$ -operator. We consider an example of coupled quartic oscillators. Finally, in Chapter 7 we summarize the results of this work.

# Dedication

*To my parents*

## Acknowledgements

It is my pleasure to thank my advisor Prof. Richard Prange for the inspiration he provided and patience while working with me and answering my numerous questions. Needless to say, his ideas formed the skeleton of this work. At the same time, he left me enough room to work on my own initiatives, giving a good advice, when needed.

I am indebted to my colleague Dr. Romanas Narevich for the countless discussions and help. He co-authored many of the results presented in this work and created many of the figures.

# Table of Contents

<b>Preface</b>	<b>ii</b>
<b>List of Tables</b>	<b>ix</b>
<b>List of Figures</b>	<b>x</b>
<b>1 Introductory chapter: Elements of the semiclassical theory</b>	<b>1</b>
1.1 Stationary phase approximation . . . . .	1
1.2 Boundary integral method . . . . .	2
1.3 Surface of section map . . . . .	5
1.4 $T$ -operator: the general case . . . . .	6
1.5 Properties of the $T$ -operator . . . . .	8
1.6 Maslov phase and the change of variables . . . . .	9
1.7 Two-dimensional separable system . . . . .	13
1.8 Conclusions . . . . .	18
<b>2 Perturbation theory</b>	<b>19</b>
2.1 Perturbed integrable systems . . . . .	20
2.2 Formulation of the theory . . . . .	22
2.2.1 Perturbed circular billiard . . . . .	22
2.2.2 Simplest case: $(1, 2)$ resonance, $k\epsilon \ll 1$ . . . . .	27
2.2.3 General case: $(p, q)$ resonance, $k\epsilon^{3/2} \ll 1$ . . . . .	29
2.2.4 Quantization conditions . . . . .	35
2.2.5 Third order theory: $k\epsilon^2 \ll 1 \sim k\epsilon^{3/2}$ . . . . .	38

2.2.6	Non-resonant case . . . . .	38
2.3	Comments and discussion . . . . .	39
2.3.1	Classical interpretation . . . . .	39
2.3.2	Resonant or non-resonant? . . . . .	44
2.3.3	Close to a large resonance . . . . .	45
2.3.4	Localization in angular momentum . . . . .	46
2.3.5	Numerical computations . . . . .	47
2.3.6	Possible experiments . . . . .	49
2.4	Two-dimensional wavefunctions . . . . .	51
2.5	Additional remarks . . . . .	54
2.5.1	The prefactor . . . . .	55
2.5.2	Fourier expanded perturbation . . . . .	56
2.5.3	Direct quantization of classical perturbation theory . . . . .	57
2.5.4	Perturbed spherical billiard . . . . .	62
2.6	Conclusions . . . . .	62
<b>3</b>	<b>Rectangular billiard and other systems</b>	<b>64</b>
3.1	Rectangular billiard — general case . . . . .	64
3.1.1	Classification of trajectories . . . . .	64
3.1.2	Perturbation theory . . . . .	67
3.1.3	Two-dimensional wavefunction . . . . .	70
3.1.4	Example: tilted square . . . . .	71
3.2	Billiards without small parameter . . . . .	76
3.3	Whispering gallery modes . . . . .	82
3.4	Scattering problem . . . . .	85
3.4.1	Classical theory . . . . .	87
3.4.2	Semiclassical theory . . . . .	90
3.5	Conclusions . . . . .	93
<b>4</b>	<b>Square billiard in magnetic field</b>	<b>95</b>
4.1	Uniform field . . . . .	96



4.1.1	Limits of applicability . . . . .	96
4.1.2	Effective potential and eigenstates . . . . .	97
4.1.3	Magnetic response . . . . .	101
4.1.4	Visual representation of eigenstates . . . . .	103
4.2	Aharonov-Bohm flux line . . . . .	119
4.3	Experimental suggestions . . . . .	123
4.4	Conclusions . . . . .	126
<b>5</b>	<b>Quasiclassical Born-Oppenheimer approximations</b>	<b>128</b>
5.1	Textbook example . . . . .	129
5.2	Bouncing ball states . . . . .	130
5.3	Channeling approximation . . . . .	134
5.4	BOA in the asymptotic region . . . . .	136
5.5	Whispering gallery modes . . . . .	139
5.6	Conclusions . . . . .	142
<b>6</b>	<b>Trace formulas</b>	<b>143</b>
6.1	General derivation of the trace formula . . . . .	143
6.2	Gutzwiller trace formula . . . . .	145
6.3	Berry-Tabor formula . . . . .	146
6.4	Perturbed Berry-Tabor formula . . . . .	146
6.5	Example: coupled quartic oscillators . . . . .	148
6.6	Conclusions . . . . .	149
<b>7</b>	<b>Summary</b>	<b>153</b>
	<b>Bibliography</b>	<b>157</b>

# List of Tables

2.1	Numerical ( $\omega_{\text{num}}$ ) and theoretical ( $\omega_{\text{theor}}$ ) eigenphases modulo $2\pi$ , compared for states with different $m$ , but all belonging to the same low angular momentum resonance. . . . .	50
2.2	Energies $k$ with different quantum numbers $n$ , but same $m = 11$ , computed numerically and found solving Eq. (2.34). . . . .	51

# List of Figures

1.1	The classical orbit from point $q'$ to point $q$ on the boundary. . . . .	4
1.2	Two orbits that touch the caustic and lie almost in the same plane. . . . .	11
1.3	Poincaré map from $\theta_x = \theta'$ to $\theta_x = \theta$ on the surface of section $\theta_y = \text{const.}$ . . .	14
1.4	Step-wise phase $f(\theta)$ from Eq. (1.56). . . . .	17
2.1	The surface of section (boundary phase space) of a perturbed circular billiard. .	23
2.2	The surface of section for (a) “short stadium” and (b) “smoothed stadium.” (c) Husimi plots for the numerical states of Fig. 2.4. . . . .	24
2.3	Short Bunimovich stadium $R(\theta) = R_0 + \epsilon\Delta R(\theta)$ with $\epsilon = 0.3$ . . . . .	26
2.4	Examples of the low angular momentum states $\psi_m(\theta)$ in the short stadium. . .	30
2.5	The low angular momentum state $n = 10, m = 2$ for the short stadium with $\epsilon = 0.1$ . . . . .	31
2.6	Contour plot of the numerical low angular momentum state $n = 25, m = 3$ for the short stadium with $\epsilon = 0.01$ . . . . .	32
2.7	Numerical and theoretical surface of section wavefunctions for the (1,3) reso- nance in the short stadium. . . . .	36
2.8	Contour plot of a numerically obtained state for the (1,4) resonance in the short stadium. . . . .	37
2.9	Numerical and theoretical surface of section wavefunctions for the non-resonant state on the golden mean torus. . . . .	40
2.10	Exact and approximate invariant loops near the (1,4) and (1,28) resonances in the smoothed stadium. . . . .	42
2.11	Exact and approximate golden mean torus for the smoothed stadium. . . . .	43

2.12 Two orbits with angular momentum $l_{pq}$ arriving at point $(r, \theta)$ in the circular billiard. . . . .	53
3.1 Perturbed rectangular billiard. . . . .	65
3.2 Method of images for the rectangular billiard. . . . .	66
3.3 Four classical orbits that contribute to the wavefunction in a rectangle. . . . .	71
3.4 Function $\hat{\psi}_0(x)$ for the tilted square. . . . .	73
3.5 Two-dimensional wavefunction in the tilted square. . . . .	74
3.6 Density plot for the wavefunction of Fig. 3.5. . . . .	74
3.7 The cross-section of the numerical wavefunction for the state of Figs. 3.4-3.6 along the diagonals. . . . .	75
3.8 Ice-cream cone billiard. . . . .	77
3.9 Bunimovich stadium billiard. . . . .	78
3.10 Bouncing ball mode in the Bunimovich stadium. . . . .	78
3.11 Bouncing ball mode in the slanted stadium. . . . .	79
3.12 Localized state in the “baseball” stadium. . . . .	79
3.13 Short periodic orbit and a nearby orbit in a generic billiard. . . . .	81
3.14 Whispering gallery mode in the short stadium. . . . .	83
3.15 Classical orbit of length $L(\rho, s; s')$ from point $s'$ on the boundary to point $(\rho, s)$ inside the billiard. . . . .	86
3.16 $\epsilon s^{-2/3}$ at the bounce points $s_i$ for a classical orbit. . . . .	88
3.17 Values of adiabatic invariant for 100 orbits after they pass the singular region. . . . .	89
3.18 Two orbits that preserve the adiabatic invariant. . . . .	90
4.1 Method of images for the square in magnetic field. . . . .	98
4.2 $\partial E_m / \partial \hat{B}$ as a function of $\hat{E}$ . . . . .	104
4.3 Decomposition of the state $m = 14, n = 62, B = 25$ into $B = 0$ basis states. . . . .	105
4.4 Absolute square of the numerical wavefunction for the localized paramagnetic state $m = 0, n = 62, B = 31.4$ . . . . .	107
4.5 Numerical wavefunction and current for the state in Fig. 4.4. . . . .	108

4.6	Absolute square of the numerical wavefunction for the state $m = 1, n = 60,$ $B = 31.4.$ . . . . .	109
4.7	Numerical wavefunction and current for the state in Fig. 4.6. . . . .	110
4.8	Theoretical wavefunction and current for the state in Fig. 4.6. . . . .	111
4.9	Almost non-magnetic state $m = 10, n = 62, B = 25.$ . . . . .	113
4.10	Normal derivative $ \partial\Psi_{nm}/\partial y _{y=-1/2}$ , obtained numerically, and the theoretical surface of section function $\hat{\psi}_m(x)$ for the state of Fig. 4.9. . . . .	114
4.11	Numerical wavefunction and current for the state of maximum diamagnetism $m = 14, n = 62, B = 25.$ . . . . .	115
4.12	Theoretical wavefunction and current for the state in Fig. 4.11. . . . .	116
4.13	Numerical wavefunction and current for the diamagnetic state $m = 14, n = 62,$ $B = 31.4.$ . . . . .	117
4.14	Streamlines for the sequence of states $m = 6, 8, 10, 12, n = 62, B = 25.$ . . . . .	118
4.15	State $m = 0, n = 86$ in the square with the flux line, $a = \frac{1}{4}, \phi = 0.1\phi_0, \rho = 0.01.$	121
4.16	Absolute value of the wavefunction, $n = 58, m = 0$ , for an ideal single flux line, $a = \frac{1}{4}, \phi = 0.1\phi_0.$ . . . . .	122
4.17	Ideal flux line at the center of the square, $\phi = 0.1\phi_0.$ Current in the state $n = 82, m = 0$ , symmetric under the $90^\circ$ rotation. . . . .	124
4.18	Possible microwave experiment with ferrite. . . . .	127
5.1	Cross-sections of the numerical wavefunctions for the $(0, 1)$ resonance in the tilted square. . . . .	132
5.2	Density plot of $ \Psi_{55,2}(x, y) ^2$ , the state of Fig. 5.1 (c). . . . .	133
6.1	$\hat{W}(\theta)$ for the $(1, 1)$ family of orbits of the quartic oscillators with $x^2y^2$ coupling.	150
6.2	Real part of $I_W$ as a function of $\epsilon/\hbar.$ . . . . .	151
6.3	Imaginary part of $I_W$ as a function of $\epsilon/\hbar.$ . . . . .	151

## Chapter 1

# Introductory chapter: Elements of the semiclassical theory

We begin with a review of the semiclassical methods that provide the framework for the perturbation theory developed in the subsequent chapters. The starting point for most of our calculations will be the Bogomolny  $T$ -operator equation, which is essentially a semiclassical Green's function method adapted to the Poincaré surface of section. In billiards the procedure is related to the boundary integral method.

### 1.1 Stationary phase approximation

Almost any semiclassical theory takes advantage of the *stationary phase approximation* ( $S\Phi$ ), which provides the most direct connection with the underlying classical behavior. Since it is used consistently throughout this work it seems necessary to remind the reader of the application of this method. The problem that often arises is to evaluate an integral of the form

$$I = \int dx e^{iS(x)/\hbar} \tag{1.1}$$

asymptotically for  $\hbar \rightarrow 0$ . It is argued that under certain conditions the main contribution comes from the neighborhoods of the points where the derivative of  $S(x)$  vanishes, the so called *stationary points*. Near such point  $x_{\text{st}}$  we can expand

$$S(x) = S(x_{\text{st}}) + \frac{1}{2}S''(x_{\text{st}})(x - x_{\text{st}})^2 + O[(x - x_{\text{st}})^3] \tag{1.2}$$

and the integral is approximately equal to

$$I \approx \sum_{x_{\text{st}}} \sqrt{\frac{2\pi\hbar}{-iS''(x_{\text{st}})}} e^{iS(x_{\text{st}})/\hbar}. \quad (1.3)$$

The square root is analytically continued from the real positive numbers. Equation (1.3) is a good approximation to the integral if the third order terms that we left out are small within the region  $|x - x_{\text{st}}| < \sqrt{\hbar/|S''(x_{\text{st}})|}$  that contributes the most to the integral. This translates into the condition

$$|S''(x_{\text{st}})|^{3/2} \gg \hbar^{1/2} |S'''(x_{\text{st}})| \quad (1.4)$$

which is normally satisfied for small  $\hbar$  unless  $|S''(x_{\text{st}})|$  is unusually small.

## 1.2 Boundary integral method

The perturbation theory that is the subject of this work is based on the *semiclassical surface of section transfer operator* (or *T-operator*) method developed in generality by Bogomolny [19] and discussed below. This method is especially convenient in billiards where the surface of section can be associated with the boundary. It is instructive to see how the *T-operator* formulation follows explicitly from a version of the *boundary integral method* [18, 33] designed to solve the Helmholtz equation in billiards.

The wavefunction  $\Psi(r)$  for a particle of mass  $m$  and energy  $E$  moving freely inside a two-dimensional domain  $B$  with the impenetrable boundary  $\partial B$  is determined by the Schrödinger equation

$$(\nabla'^2 + k^2) \Psi(r') = 0 \quad (1.5)$$

with the Dirichlet boundary conditions

$$\Psi(r')|_{\partial B} = 0. \quad (1.6)$$

Here the wavenumber  $k = \sqrt{2mE}/\hbar$  and  $\nabla'^2$  is the two-dimensional Laplacian acting on  $r'$ . The *free-space* Green function  $G_0(r', r)$  (that does not satisfy the boundary conditions on  $\partial B$ ) is defined by the equation

$$(\nabla'^2 + k^2) G_0(r', r) = \delta(r' - r) \quad (1.7)$$

which is solved by the Hankel function [41]

$$G_0(r', r) = -\frac{i}{4} H_0^{(1)}(k|r' - r|). \quad (1.8)$$

Multiplying Eq. (1.5) by  $-G_0(r', r)$  and Eq. (1.7) by  $\Psi(r')$ , adding them together and integrating over the billiard's area we arrive to the integral equation

$$\Psi(r) = \int_B d^2r' [\Psi(r') \nabla'^2 G_0(r', r) - G_0(r', r) \nabla'^2 \Psi(r')]. \quad (1.9)$$

With the help of Green's theorem we transform it to the boundary integral

$$\Psi(r) = \oint_{\partial B} dq' \left[ G_0(q', r) \frac{\partial \Psi(q')}{\partial n'} - \Psi(q') \frac{\partial G_0(q', r)}{\partial n'} \right] \quad (1.10)$$

where  $q'$  is the coordinate along the boundary and  $n'$  is the normal at point  $q'$  directed inside the boundary. The second term vanishes due to the boundary conditions. Taking point  $r = q$  on the boundary and introducing the new function

$$\mu(q) = \frac{\partial \Psi(q)}{\partial n} \quad (1.11)$$

we can write the integral equation which is *equivalent* to the original Helmholtz equation (1.5),

$$\mu(q) = \int dq' \frac{\partial G_0(q', q)}{\partial n} \mu(q'). \quad (1.12)$$

Its kernel has a  $\delta$ -function type singularity at  $q' = q$ . Indeed,

$$\frac{\partial G_0(q', q)}{\partial n} = \frac{ik}{4} H_0^{(1)'}[kL(q, q')] \frac{\partial L(q, q')}{\partial n} \quad (1.13)$$

with

$$\frac{\partial L(q, q')}{\partial n} = \begin{cases} |\hat{p} \cdot n|, & q' \neq q \\ 1, & q' = q \end{cases} \quad (1.14)$$

where  $L(q, q')$  is the length of the classical orbit (chord) going from point  $q'$  to  $q$  and  $\hat{p}$  is a unit vector along this orbit (or a unit momentum) (Fig. 1.1). Using the asymptotic expansion for the derivative of Hankel's function for small argument [41] we find

$$\frac{\partial G_0(q', q)}{\partial n} \sim \begin{cases} -\frac{|\hat{p} \cdot n|}{2\pi L(q, q')} \sim -\frac{1}{4\pi}, & q' \rightarrow q \\ \infty, & q' = q \end{cases}. \quad (1.15)$$

The  $-1/4\pi$  is written under the assumption of a convex boundary with non-vanishing curvature, but this assumption is not essential for extracting the  $\delta$ -singularity. So, we may assume



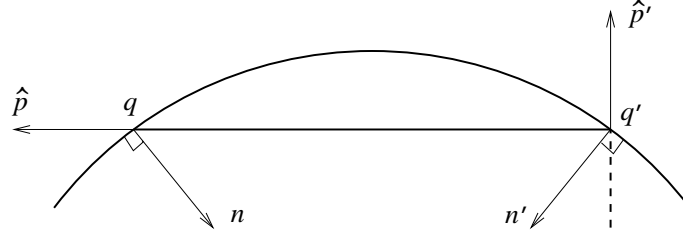


Figure 1.1: The classical orbit from point  $q'$  to point  $q$  on the boundary. The dashed line shows the orbit incident at  $q'$ .

that the boundary is locally a straight line. Then, for any  $q$  and  $q'$ ,  $\partial L(q, q')/\partial n = \lim_{n \rightarrow 0} n/\sqrt{(q - q')^2 + n^2}$  and the singular part of the kernel

$$\left( \frac{\partial G_0(q', q)}{\partial n} \right)_{\text{sing}} = \lim_{n \rightarrow 0} \frac{n}{2\pi [(q - q')^2 + n^2]} = \frac{1}{2} \delta(q - q'). \quad (1.16)$$

The integral equation (1.12) may now be rewritten as

$$\mu(q) = \int dq' K(q, q') \mu(q') \quad (1.17)$$

with the regular kernel

$$K(q, q') = 2 \left( \frac{\partial G_0(q', q)}{\partial n} \right)_{\text{reg}}. \quad (1.18)$$

Thus the problem is reduced to the one-dimensional integral equation (1.17) for  $\mu(q)$ . This function contains most of the information about the state and  $\det(1 - K) = 0$  is the quantization condition. [The second quantization condition comes from the periodicity requirements on  $\mu(q)$ .] If needed, the wavefunction  $\Psi(r)$  can be subsequently determined from Eq. (1.10).

Our goal is to develop a semiclassical approximation to this scheme. When  $kL \gg 1$  we may use the large argument asymptotics for the Hankel function [41] and the kernel now becomes

$$\begin{aligned} K(q, q') &\approx -\sqrt{\frac{k}{2\pi L(q, q')}} |\hat{p} \cdot n| e^{ikL(q, q') - i\pi/4} \\ &= -\sqrt{\frac{1}{2\pi} \frac{\partial^2 S(q, q')}{\partial q \partial q'}} \frac{|\hat{p} \cdot n|}{|\hat{p}' \cdot n'|} e^{iS(q, q') - i\pi/4}. \end{aligned} \quad (1.19)$$

We introduced the reduced action (measured in units of  $\hbar$ )

$$S(q, q') = kL(q, q') \quad (1.20)$$

for the classical orbit  $q' \mapsto q$ . Clearly,  $K(q, q')$  is not symmetric. The semiclassical approximation allows to symmetrize it. First, notice that, in spite of the notation, both  $|\hat{p} \cdot n|$  and  $|\hat{p}' \cdot n'|$  are the functions of two coordinates,  $q$  and  $q'$ . The essential part of the semiclassical approach, however, is to evaluate all the integrals containing the fast changing action at the exponent in the stationary phase approximation. It will be clear from the following chapters (and is well known) that this approximation amounts to extracting those  $q$  and  $q'$  that are connected by a classical orbit. Thus we may consider, say,  $|\hat{p} \cdot n|$  to be a function of  $q$  only (as well as the two fixed parameters related to the initial conditions, one of which is the total energy). Similarly,  $|\hat{p}' \cdot n'|$  will be a function of  $q'$ .

Define a function

$$\psi(q) = \frac{\mu(q)}{\sqrt{|\hat{p} \cdot n|}}. \quad (1.21)$$

Then the semiclassical analog to Eq. (1.17) is

$$\psi(q) = \int_{\partial B} dq' T(q, q') \psi(q') \quad (1.22)$$

where the  $T$ -operator

$$T(q, q'; E) = K(q, q'; E) \sqrt{\frac{|\hat{p}' \cdot n'|}{|\hat{p} \cdot n|}} = -\sqrt{\frac{1}{2\pi i} \frac{\partial^2 S(q, q'; E)}{\partial q \partial q'}} e^{iS(q, q'; E)}. \quad (1.23)$$

Unlike  $K(q, q')$ , the  $T$ -operator is symmetric and unitary (semiclassically). See Sec. 1.5 for more details. Clearly, Eq. (1.22) has a solution if  $\det(1 - T) = 0$ . The original wavefunction  $\Psi(r)$  can be found from  $\psi(q)$  (see Sec. 1.4). We emphasize once again that the stationary phase approximation is expected when dealing with the  $T$ -operator. In the next section we discuss the relationship between the  $T$ -operator and the classical surface of section map.

### 1.3 Surface of section map

In the previous section we reduced the two-dimensional problem in a billiard to a one-dimensional problem on its boundary. The state of the system can be equivalently described by either 2D-wavefunction  $\Psi(r)$  or 1D-wavefunction  $\psi(q)$ . In the classical language, we reduced the continuous motion in the four-dimensional phase space of the billiard to a map in the two-dimensional phase space of the boundary. It is an example of a *surface of section map*. Again, this map contains all the information about the continuous motion.

Formally, the map  $(p', q') \mapsto (p, q)$  is implicitly given by the equations

$$p = \frac{\partial S(q, q')}{\partial q}, \quad p' = -\frac{\partial S(q, q')}{\partial q'}. \quad (1.24)$$

The generalized momentum (in the units of  $\hbar$ )  $p$  is the projection of the total momentum onto the boundary. To connect the classical and quantum descriptions consider a version of Eq. (1.22)

$$\psi(q) = \int dq' T(q, q') \psi'(q') \quad (1.25)$$

describing the propagation of a wavepacket. We write the wavefunction  $\psi'(q')$  on a locally defined Lagrangian manifold  $p'(q')$  in the semiclassical form (Sec. 6.3.c in Ref. [74])

$$\psi'(q') = \sqrt{\frac{\partial^2 S(P, q')}{\partial P \partial q'}} e^{i \int p'(q') dq'} = \sqrt{-\left(\frac{\partial Q}{\partial q'}\right)_P} e^{i \int p'(q') dq'} \quad (1.26)$$

where  $S(P, q')$  is the Legendre transform of  $S(q, q')$  to the canonical coordinates  $(P, Q)$  such that  $P$  is a local integral of motion. We substitute it in Eq. (1.25) and integrate by the  $S\Phi$ . The stationary point  $q'_{\text{st}}$  is determined by the second of the Eqs. (1.24). In the neighborhood of point  $q$  we define the function  $p(q)$  by

$$\int^q p(q'') dq'' = S[q, q'_{\text{st}}(q)] + \int^{q'_{\text{st}}(q)} p'(q'') dq''. \quad (1.27)$$

This definition satisfies the first of the Eqs. (1.24). Thus the integral

$$\begin{aligned} \int dq' T(q, q') \psi'(q') &= -\sqrt{\frac{-\frac{\partial^2 S}{\partial q \partial q'} \left(\frac{\partial Q}{\partial q'}\right)_P}{\frac{\partial^2 S}{\partial q'^2} + \frac{dp'}{dq'}}} e^{i \int p(q) dq} \\ &= -\sqrt{\left(\frac{\partial q'}{\partial q}\right)_P \left(\frac{\partial Q}{\partial q'}\right)_P} e^{i \int p(q) dq} = \sqrt{\frac{\partial^2 S(q, P)}{\partial q \partial P}} e^{i \int p(q) dq - i\pi} = \psi(q). \end{aligned} \quad (1.28)$$

(To prove the second equality differentiate the equation  $\partial S(q, q')/\partial q' + p'(q') = 0$ . The Maslov phase  $-\pi$  results from the reflection at the billiard's boundary.) This shows that if a manifold  $p'(q')$  evolves into the manifold  $p(q)$  the  $T$ -operator provides the evolution of the wavefunction defined on this manifold.

## 1.4 $T$ -operator: the general case

The phase space of billiard boundary is an example of a *Poincaré surface of section* (PSS). The above discussion makes it clear now why the  $T$ -operator is called the surface of section

transfer operator. In general, PSS is a  $(2N - 2)$ -dimensional manifold in the phase space of an  $N$ -dimensional system crossed by all classical trajectories. Bogomolny [19] derived the expression for the  $T$ -operator in the case when PSS is an  $(N - 1)$ -dimensional manifold in the coordinate space of the system together with its conjugate momenta. He assumed the Hamiltonian has the form

$$H(\hat{p}, r) = \frac{1}{2}\hat{p}^2 + V(r) \quad (1.29)$$

but presumably his result is more general. The  $T$ -operator is now

$$T(q, q'; E) = \frac{1}{(2\pi i)^{(N-1)/2}} \sum_{\text{cl. tr.}} \left| \det \left[ \frac{\partial^2 S(q, q'; E)}{\partial q \partial q'} \right] \right|^{1/2} e^{iS(q, q'; E) - i\frac{\pi}{2}\nu}. \quad (1.30)$$

The sum is over all classical trajectories that go from  $q'$  to  $q$  on PSS and correspond to *one* Poincaré mapping. All trajectories should leave the PSS with the positive, say, normal component of the momentum. The reduced action  $S(q, q'; E)$  is still measured in the units of  $\hbar$ . The *Maslov index*  $\nu$  is determined by the number and type of caustics encountered by the trajectory [11]. For example, a regular caustic of dimension  $(N - 1)$  increases  $\nu$  by 1; a hard wall increases  $\nu$  by 2. We discuss the origin of Maslov phase in Sec. 1.6. In a billiard with its boundary as a PSS<sup>1</sup>  $\nu = 2$  and there is only one trajectory  $q' \mapsto q$ . Then Eq. (1.23) follows.

A surface of section wavefunction is determined from the integral equation

$$\psi(q) = \int_{\text{PSS}} dq' T(q, q') \psi(q') \quad (1.31)$$

that we will call *Bogomolny's equation* and the quantization condition is

$$\det(1 - T) = 0. \quad (1.32)$$

The original wavefunction can be found by propagating  $\psi(q)$ ,

$$\Psi(r) = \int_{\text{PSS}} dq \tilde{G}(r, q; E) \psi(q) \quad (1.33)$$

where

$$\tilde{G}(r, q; E) = \frac{i^{1/2}}{(2\pi i)^{(N-1)/2}} \sum_{\text{cl. tr.}} \left| \frac{1}{v(r)} \det \left[ \frac{\partial^2 S(r, q; E)}{\partial r_{\perp} \partial q} \right] \right|^{1/2} e^{iS(r, q; E) - i\frac{\pi}{2}\nu}. \quad (1.34)$$

---

<sup>1</sup>In the billiard problems it is sometimes convenient to choose PSS infinitesimally close to the hard wall, not on the hard wall.

The trajectories start at point  $q$  on PSS with the positive normal component of the momentum and end at point  $r$  of the interior;  $v(r)$  is the modulus of the velocity at point  $r$ ;  $r_\perp$  is the direction perpendicular to the trajectory at point  $r$ . In the case of a billiard one can show that Eqs. (1.33) and (1.34) agree with Eqs. (1.10) and (1.21) up to normalization if the asymptotic form of Hankel's function is used.

## 1.5 Properties of the $T$ -operator

In this section we review some of the properties of the  $T$ -operator [19]. As was noticed by Bogomolny,  $T$ -operator is similar to the time-dependent semiclassical Green's function [cf. Eq. (1.25)]. It is therefore not surprising that they share some of the properties. To simplify notation we assume the system to be two-dimensional and omit the Maslov indices.

First, note that the  $T$ -operator vanishes for short trajectories, i.e.  $T(q, q') \rightarrow 0$  as  $q \rightarrow q'$ . Indeed, in this case  $S(q, q') \sim p|q - q'|$ , so the prefactor in Eq. (1.30) vanishes.

As was mentioned before, the  $T$ -operator, unlike the exact kernel  $K(q, q')$ , is unitary in semiclassical approximation. To see this we evaluate the integral

$$(T^\dagger T)(q_1, q_2) = \frac{1}{2\pi} \int dq \sum \sum \left[ \frac{\partial^2 S(q, q_1)}{\partial q \partial q_1} \frac{\partial^2 S(q, q_2)}{\partial q \partial q_2} \right]^{1/2} e^{i[S(q, q_2) - S(q, q_1)]} \quad (1.35)$$

by the  $S\Phi$ . The stationary phase condition  $\partial S(q, q_1)/\partial q = \partial S(q, q_2)/\partial q$  requires that the orbits  $q_1 \mapsto q$  and  $q_2 \mapsto q$  have the same final momentum in the PSS. For a deterministic map it means they are the same orbit, i.e.  $q_1 = q_2$ . Expand  $S(q, q_2) \cong S(q, q_1) + (q_2 - q_1)\partial S(q, q_1)/\partial q_1$ . Then the integral becomes

$$(T^\dagger T)(q_1, q_2) = \frac{1}{2\pi} \int dq \left( \frac{\partial p_1}{\partial q} \right)_{q_1} e^{ip_1(q_2 - q_1)} \cong \delta(q_2 - q_1). \quad (1.36)$$

The sum over classical orbits disappeared because the integration over  $dp_1$  takes care of all the orbits leaving  $q_1$ . The  $\delta$ -function is not ideal since  $|p_1|$  is limited by the fixed total energy but it is a good approximation semiclassically. The unitarity of the  $T$ -operator leads to the resurgence of the spectral determinant [33].

Another useful property, the  $n$ th power of the  $T$ -operator has the form of the  $T$ -operator for  $n$  Poincaré mappings, that is  $T^n(q, q'; E)$  is given by Eq. (1.30) but the orbits now cross

the PSS  $n$  times. Consider, for example,

$$T^2(q, q') = \frac{1}{2\pi} \int dq'' \sum \sum \left[ -\frac{\partial^2 S(q, q'')}{\partial q \partial q''} \frac{\partial^2 S(q'', q')}{\partial q'' \partial q'} \right]^{1/2} e^{i[S(q, q'') + S(q'', q')]} \quad (1.37)$$

The  $S\Phi$  condition  $\partial S(q, q'')/\partial q'' + \partial S(q'', q')/\partial q'' = 0$  ensures that the orbits  $q' \mapsto q''$  and  $q'' \mapsto q$  have the same momentum at  $q''$ . In other words, it selects the classical orbits  $q' \mapsto q'' \mapsto q$  that cross the PSS twice. To complete the proof we need to show that

$$\frac{\frac{\partial^2 S(q, q'')}{\partial q \partial q''} \frac{\partial^2 S(q'', q')}{\partial q'' \partial q'}}{\frac{\partial^2 S_2(q, q')}{\partial q''^2}} = \frac{\partial^2 S_2(q, q')}{\partial q'' \partial q'} \quad (1.38)$$

where  $S_2(q, q') = S(q, q'') + S(q'', q')$ . For this we differentiate the  $S\Phi$  condition by  $q$  and by  $q'$ . The composition property is important for the derivation of the trace formula using the  $T$ -operator (see Sec. 6.1) and for the semiclassical Fredholm theory [33, 34, 30].

The  $T$ -operator in momentum representation is semiclassically a finite matrix if the PSS has a finite length  $\mathcal{L}$ . Suppose the PSS is a closed line. We define a complete set of the momentum eigenfunctions

$$\phi_p(q) = \frac{1}{\sqrt{\mathcal{L}}} e^{ipq} \quad (1.39)$$

where  $p = (2\pi/\mathcal{L}) \times \text{integer}$ . The  $T$ -operator matrix is

$$T_{pp'} = \frac{1}{\mathcal{L}} \int dq dq' T(q, q') e^{i(p'q' - pq)}. \quad (1.40)$$

The  $S\Phi$  condition requires that  $p$  and  $p'$  be equal to the projection of the classical momentum at points  $q$  and  $q'$ , respectively. But this projection is limited by  $\sqrt{2mE}$  by the absolute value. Hence the size of the matrix is no greater than  $\mathcal{L}\sqrt{2mE}/\pi$  or  $2\mathcal{L}/\lambda$  where  $\lambda$  is the de Broglie wavelength.

## 1.6 Maslov phase and the change of variables

A neighborhood of a caustic in a multidimensional system, like a turning point in one dimension, is the region where the semiclassical approximation breaks down. It turns out that the  $T$ -operator and the wavefunctions acquire additional phases, called *Maslov's phases*, in the regions of validity [54]. The Maslov phases will change, in general, the overall probability density and the quantization conditions and thus it is important to understand their origin and be able to properly account for them.

The central point in Bogomolny's derivation of the  $T$ -operator is the use of the semiclassical approximation to the Green function in the energy representation [40]

$$G(r, r'; E) = \frac{1}{i(2\pi i)^{(N-1)/2}} \sum_{\text{cl. tr.}} \left| \frac{1}{v(r)v(r')} \det \left[ \frac{\partial^2 S(r, r'; E)}{\partial r_{\perp} \partial r'_{\perp}} \right] \right|^{1/2} \times e^{iS(r, r'; E) - i\frac{\pi}{2}\nu}. \quad (1.41)$$

It satisfies  $(E - H)G(r, r'; E) = \delta(r - r')$  and is not valid for short trajectories, at least in two dimensions.  $r_{\perp}, r'_{\perp}$  are the local coordinates perpendicular to the velocity at  $r, r'$ , respectively.  $v = |\partial H / \partial p|$  is the modulus of the velocity (actions and momenta are defined in the units of  $\hbar$ ). The Maslov index  $\nu$  in the  $T$ -operator (1.30) is inherited from this Green's function.

Let us follow a particular orbit starting from  $r'$ . At some points along the orbit one or more eigenvalues of the matrix  $\partial^2 S / \partial r_{\perp} \partial r'_{\perp}$  may become infinite and change sign [11]. That is what happens when the orbit touches a caustic (see below). If  $m$  eigenvalues change sign (caustic of order  $m$ ) the determinant in Eq. (1.41) changes by  $(-1)^m$ . If we drop the modulus and analytically continue the determinant in the complex space "around" the singularity [45] as in the one-dimensional case [49] we will find that the Green function acquired the phase  $-m\pi/2$ . One has to assume the function is exponentially small in the classically forbidden region beyond the caustic. (This method does not work near a hard wall.) The Maslov index of an orbit is the sum of the contributions from all caustics the orbit encounters. Each caustic increases  $\nu$  by  $m$ , each hard wall increases  $\nu$  by 2. In particular, if  $r' = q'$  and  $r = q$  lie on the surface of section and the orbit makes one Poincaré mapping, this index enters the  $T$ -operator.

So far we defined the Maslov index in terms of singularities of the matrix  $\partial^2 S / \partial r_{\perp} \partial r'_{\perp}$ . Now we give it the geometrical interpretation [26, 11]. Let us surround the orbit of the previous paragraph (we call it the central orbit) with a sufficiently narrow tube of trajectories with the same energy  $E$  all of which originate from point  $r'$ . They form an  $(N - 1)$ -parameter family that can be parametrized by the vector  $\partial S / \partial r'_{\perp}$ , which depends on  $r$ . For a given orbit in the family we will choose  $r$  to be on the caustic. It is possible that *all* the trajectories within the tube (remember, the tube is narrow) touch an  $(N - m)$ -dimensional surface which is independent of the shape of the tube. This surface is called a *caustic of order  $m$* . Suppose the central orbit touches the caustic surface at point  $r$ . The caustic has  $m - 1$  dimensions less than the number of parameters in the tube. This accounts for  $m - 1$  infinite eigenvalues of

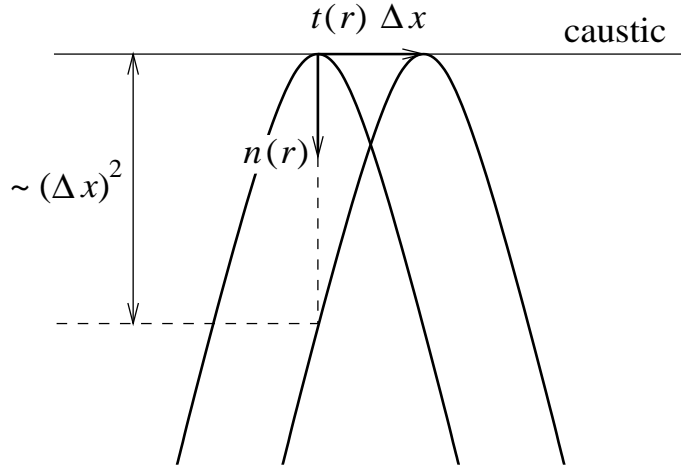


Figure 1.2: Two orbits that touch the caustic and lie almost in the same plane.

$\partial^2 S / \partial r_{\perp} \partial r'_{\perp}$ . (When different trajectories touch the caustic at the same point, the derivative of the parametrization vector becomes infinite.) Without the loss of generality we can always assume that the caustic is locally flat by making an appropriate coordinate transformation. The orbits are parabolic near the caustic. Consider an orbit that touches the caustic a small distance  $\Delta x$  from the central orbit and lies locally in almost the same plane (Fig. 1.2). (To find this orbit note that the plane of the parabola of the central orbit is fixed by two unit vectors: one is the tangent vector  $t(r)$  at the point of touch, another,  $n(r)$ , is orthogonal to the caustic at the point of touch. If the neighboring orbit touches the caustic at  $r + t(r)\Delta x$ , its tangent at this point is almost parallel to  $t(r)$  by continuity. Its second vector  $n[r + t(r)\Delta x]$  belongs to the  $m$ -dimensional complement to the caustic, so its direction can be fixed by  $m - 1$  free parameters mentioned above.) Now, the difference in parameters for these two orbits is of order  $\Delta x$ , but the distance between them at point  $r$  in the direction of  $n(r)$  is of order  $(\Delta x)^2$ . This brings another singular eigenvalue of  $\partial^2 S / \partial r_{\perp} \partial r'_{\perp}$ . Thus, this matrix has  $m$  singular eigenvalues in total.

A special case is the caustic associated with the original point  $r'$ . Creagh *et al.* [26] argue that each negative eigenvalue of  $-\partial^2 S / \partial r_{\perp} \partial r'_{\perp}$  for positive time  $t = 0+$  decreases the Maslov index by  $-1$ . (Here one has to be careful to preserve the orientation of the local basis  $(\mathbf{e}_{\parallel}, \mathbf{e}_{\perp}^i)$ ,



$i = 1, \dots, N - 1$ , along the orbit, where  $\mathbf{e}_{\parallel}$  points in the direction of propagation.) This apparently contradicts the statement in Ref. [11] that  $\nu = 0$  for short trajectories since there are no caustics in between. Notice, however, that for the kinetic-plus-potential systems all eigenvalues of  $-\partial^2 S / \partial r_{\perp} \partial r'_{\perp}$  are positive [26]. In general, as the example in the next section shows, this additional Maslov index is important for the quantization conditions.

It is sometimes convenient to evaluate the classical action in the canonical coordinates, other than the original ones. For example, in the next section the action-angle variables are used. It would be desirable to be able to construct the  $T$ -operator and solve for the wavefunction directly in the new coordinates. Let us analyze how the Green function (1.41) transforms under canonical transformation  $(p, q) \mapsto (P, Q)$ . We rewrite Eq. (1.41) in an equivalent form [11]

$$G(q, q'; E) = \sum_{\text{cl. tr.}} G_1(q, q'; E) \equiv \sum_{\text{cl. tr.}} \frac{\sqrt{\Delta(q, q'; E)}}{i (2\pi i)^{(N-1)/2}} e^{iS(q, q'; E)}, \quad (1.42)$$

$$\Delta(q, q'; E) = - \left( \frac{\partial^2 S}{\partial E^2} \right)^{1-N} \det \left( \frac{\partial^2 S}{\partial E^2} \frac{\partial^2 S}{\partial q \partial q'} - \frac{\partial^2 S}{\partial E \partial q} \frac{\partial^2 S}{\partial E \partial q'} \right). \quad (1.43)$$

Note that we removed the modulus from under the square root together with the Maslov index. For a given trajectory we can define the coordinate transformations  $Q = Q(q, q')$  and  $Q' = Q'(q, q')$  which can be multivalued. The probability density for a semiclassical wavefunction is a sum of probabilities for individual orbits, therefore the transformed Green's function

$$G^{(Q)}(Q, Q') = \sum_{\text{cl. tr.}} G_1(q, q') \sqrt{\left| \det \frac{\partial q}{\partial Q} \right| \left| \det \frac{\partial q'}{\partial Q'} \right|} \quad (1.44)$$

where  $q$  and  $q'$  are the functions of  $Q$  and  $Q'$ . But  $\Delta(q, q') = \Delta(Q, Q') \det(\partial Q / \partial q) \det(\partial Q' / \partial q')$ . Finally, the Green function

$$G^{(Q)}(Q, Q'; E) = \sum_{\text{cl. tr.}} \sqrt{\Delta(Q, Q'; E) \operatorname{sgn} \left( \det \frac{\partial Q}{\partial q} \det \frac{\partial Q'}{\partial q'} \right)} \frac{e^{iS^{(Q)}(Q, Q'; E)}}{i (2\pi i)^{(N-1)/2}} \quad (1.45)$$

where  $S^{(Q)}(Q, Q'; E) = S(q, q'; E)$ . Equation (1.45) has the same form as Eq. (1.42) except for the signature of the Jacobians. Let us fix  $q'$  and follow  $q$  along the trajectory. If  $Q = Q(q)$  is a multivalued function, some eigenvalues of  $\partial Q / \partial q$  become singular and change sign as the orbit goes from one sheet of  $Q(q)$  to another. This happens if a caustic in  $q$ -space is completely or partially removed in  $Q$ -space by making  $Q(q)$  multivalued. If, for instance, the caustic is removed completely, the number of singular eigenvalues is equal to the order

of the caustic. Suppose  $k$  eigenvalues become singular. Then the matrix inside  $\Delta(Q, Q'; E)$  has  $k$  singular eigenvalues less than the matrix inside  $\Delta(q, q'; E)$ . Thus the total number of singular eigenvalues, and, consequently, the Maslov index, is invariant under the coordinate transformation.<sup>2</sup> The important conclusion from this discussion is that the semiclassical Green function or the  $T$ -operator can be evaluated with Eqs. (1.41) or (1.30) in any set of canonical coordinates, apart from the Maslov index which is determined by the topology of the orbits in the *physical space*. This result is quite different from the classical assumption that all canonical coordinates are equivalent.

## 1.7 Two-dimensional separable system

As an illustration of the  $T$ -operator technique we apply it to a two-dimensional system which is separable in the Cartesian coordinates. We will solve the problem in the action-angle (AA) variables. They change the topology of the orbits and thus bring certain complications. It will be helpful to understand them before moving on to the perturbation theory of the following chapters. The results are, of course, well known from simpler methods. The quantization of the rotationally invariant integrable systems in two and three dimensions using Bogomolny's  $T$ -operator was done by Goodings and Whelan [36].

For a separable system we can define the action-angle variables  $(I_x, \theta_x)$  and  $(I_y, \theta_y)$  in  $x$  and  $y$  directions, respectively. We choose the  $x$  axis ( $y = 0$ ) as the PSS which corresponds to  $\theta_y = \text{const}$ . One Poincaré mapping  $x' \mapsto x$  is described as  $\theta'_x \mapsto \theta_x, \theta_y \mapsto \theta_y + 2\pi$  in the AA variables (Fig. 1.3). Note that by definition  $\theta_x > \theta'_x$ ; the actions  $I_i = (2\pi)^{-1} \oint p_i dx_i$  ( $i = x, y$ ) are integrals of motion; the functions  $x(\theta_x)$  and  $y(\theta_y)$  have period  $2\pi$ . We made a transformation to the AA variables because in these coordinates the  $T$ -operator has a particularly simple form:

$$T(\theta, \theta'; E) = \left( \frac{1}{2\pi i} \left| \frac{\partial^2 S}{\partial \theta \partial \theta'} \right| \right)^{1/2} e^{iS(\Delta\theta; E) - i\frac{\pi}{2}\nu(\theta, \theta'; E)} \quad (1.46)$$

where we dropped the subscript “ $x$ ” in  $\theta_x$  and, apart from the Maslov index,  $T(\theta, \theta'; E)$  depends only on the difference  $\Delta\theta = \theta - \theta'$ . We assumed there is only one trajectory connecting  $\theta'$

<sup>2</sup>If there is a new caustic of order  $m$  in  $Q$ -space that did not exist in  $q$ -space then  $m$  eigenvalues of  $\partial Q/\partial q$  go through zero and change sign but in the opposite direction than the corresponding  $m$  singular eigenvalues of  $\Delta(Q, Q'; E)$ . Thus, again, the Maslov index does not change.

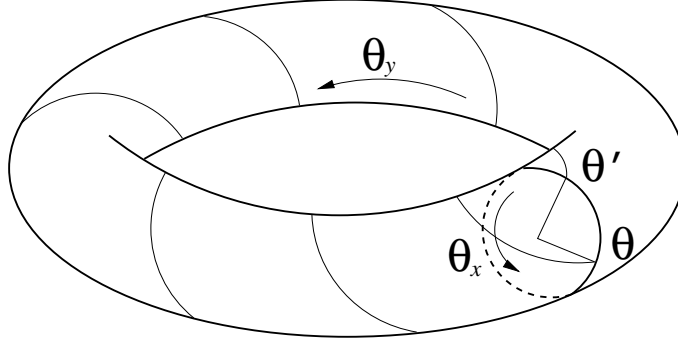


Figure 1.3: Poincaré map from  $\theta_x = \theta'$  to  $\theta_x = \theta$  on the surface of section  $\theta_y = \text{const.}$

and  $\theta$ . If there are more than one trajectory with the same energy, they will have different  $I$ 's, and the PSS wavefunctions  $\psi(\theta) \propto e^{iI_x\theta}$  can be treated independently in the semiclassical approximation.

The action

$$S(\Delta\theta; E) = \Delta\theta I_x + 2\pi I_y \quad (1.47)$$

where the  $I$ 's should be expressed in terms of  $\Delta\theta$  and  $E$ . One relation is the Hamiltonian

$$H(I_x, I_y) = E. \quad (1.48)$$

Suppose it can be solved for  $I_y$ ,

$$I_y = g_E(I_x). \quad (1.49)$$

Define the frequency ratio

$$\alpha \equiv \alpha_E(I_x) \equiv \frac{\omega_x}{\omega_y} = \frac{(\partial H / \partial I_x)_{I_y}}{(\partial H / \partial I_y)_{I_x}} \quad (1.50)$$

where  $I_y$  was substituted from Eq. (1.49). Then the second relation is

$$\alpha_E(I_x) = \frac{\Delta\theta}{2\pi}. \quad (1.51)$$

Eqs. (1.49) and (1.51) allow one to write the action  $S(\Delta\theta; E)$ .<sup>3</sup> Note a useful formula [76]

$$\alpha = -g'_E(I_x) \quad (1.52)$$

<sup>3</sup>The  $T$ -operator is not well defined for a two-dimensional harmonic oscillator where  $\Delta\theta = \text{const.}$

which can be derived by differentiating Eqs. (1.48) and (1.49).

The Maslov index  $\nu(\theta, \theta'; E)$  counts the number of caustics encountered by the orbit in the Cartesian coordinates. Suppose there are two turning points in both  $x$ - and  $y$ -directions that produce the first order caustics. The Maslov index

$$\nu(\theta, \theta') = \nu_0 + \nu_x(\theta, \theta') + \nu_y, \quad \nu_y = 2. \quad (1.53)$$

Here  $\nu_x, \nu_y$  are the number of times the orbit goes through the turning points in  $x$ - and  $y$ -directions, respectively, and  $\nu_0 = -\Theta(\partial^2 S / \partial r_\perp \partial r'_\perp |_{t \rightarrow 0})$  is related to the starting point caustic (see the previous section),  $\Theta$  is the Heaviside function. Assume for the definitiveness that the turning points in  $x$  are located at  $\theta \bmod 2\pi = 0, \pi$  (they must be separated by  $\pi$  because of the time-reversal symmetry). Suppose  $\pi n < \Delta\theta < \pi(n+1)$ , for some  $n = 0, 1, \dots$ . Then, depending on the end point  $\theta$ , the orbit encounters  $n$  or  $n+1$  turning points in  $x$ . It is easy to find

$$\nu_x(\theta, \Delta\theta) = \begin{cases} n+1, & 0 < \theta < \Delta\theta - \pi n \\ n, & \Delta\theta - \pi n < \theta < \pi \end{cases} \quad (1.54)$$

continued in  $\theta$  with period  $\pi$ . The additional Maslov index  $\nu_0$  can be conveniently expressed as [76]

$$\nu_0 = -\Theta[g''_E(I_x)]. \quad (1.55)$$

To solve Bogomolny's equation (1.31) we make an ansatz

$$\psi(\theta) = e^{iI\theta + if(\theta)} \quad (1.56)$$

where  $I = \text{const}$  to be determined and  $f(\theta)$  is a step-function. With  $T$  given by Eq. (1.46) Bogomolny's equation becomes

$$e^{if(\theta)} = \int d(\Delta\theta) \left[ \frac{|S''(\Delta\theta)|}{2\pi i} \right]^{1/2} e^{i[S(\Delta\theta) - I\Delta\theta + f(\theta - \Delta\theta) - \frac{\pi}{2}\nu(\theta, \Delta\theta)]} \quad (1.57)$$

where the integration variable has been changed from  $\theta'$  to  $\Delta\theta$  and  $e^{iI\theta}$  was canceled on both sides. The stationary phase condition is

$$I = S'(\Delta\theta_{\text{st}}) = I_x(\Delta\theta_{\text{st}}, E). \quad (1.58)$$

The second equality follows from Eq. (1.47) taking into account that  $\left(\frac{\partial I_y}{\partial \Delta\theta}\right)_E = g'_E(I_x) \left(\frac{\partial I_x}{\partial \Delta\theta}\right)_E = -\frac{\Delta\theta}{2\pi} \left(\frac{\partial I_x}{\partial \Delta\theta}\right)_E$  [see Eqs. (1.51) and (1.52)]. Note that  $f$  and  $\nu$  do not change the stationary

point. We expand  $S(\Delta\theta)$  near the stationary point and integrate. Equation (1.57) becomes

$$e^{if(\theta)} = \left[ \frac{|S''(\Delta\theta_{\text{st}})|}{S''(\Delta\theta_{\text{st}})} \right]^{1/2} e^{i[2\pi I_y(\Delta\theta_{\text{st}}, E) + f(\theta - \Delta\theta_{\text{st}}) - \frac{\pi}{2}\nu(\theta, \Delta\theta_{\text{st}})]}. \quad (1.59)$$

Applying another chain of equalities  $S''(\Delta\theta) = \left(\frac{\partial I_x}{\partial \Delta\theta}\right)_E = \frac{1}{2\pi} \left(\frac{\partial I_x}{\partial \alpha}\right)_E = -\frac{1}{2\pi g''_E}$  we find that the pre-exponential factor cancels the Maslov index  $\nu_0$ . Let us require that

$$f(\theta) - f(\theta - \Delta\theta_{\text{st}}) + \frac{\pi}{2}\nu_x(\theta, \Delta\theta_{\text{st}}) = 0 \quad (1.60)$$

for all  $\theta$ . Then Eq. (1.59) is solved if

$$I_y(\Delta\theta_{\text{st}}, E) = n_y + \frac{1}{2} \quad (1.61)$$

for some  $n_y = 0, 1, \dots$ . This is, of course, a well known Einstein-Brillouin-Keller (EBK) quantization of an action variable. One can check that the step-wise function (Fig. 1.4)

$$f(\theta) = 0 \text{ if } 0 < \theta < \pi; \quad f(\theta + \pi) - f(\theta) = -\frac{\pi}{2} \quad (1.62)$$

satisfies Eq. (1.60). The second quantization condition

$$I_x(\Delta\theta_{\text{st}}, E) = n_x + \frac{1}{2}, \quad n_x = 0, 1, \dots \quad (1.63)$$

comes from the  $2\pi$ -periodicity of  $\psi(\theta)$  Eq. (1.56). (This requirement ensures that  $\psi(\theta)$  is uniquely defined on the cross-section of an invariant torus  $0 \leq \theta \leq 2\pi$ ,  $\theta_y = \text{const.}$ )

Thus, after all this trouble, we arrive to the familiar EBK expression for the energy

$$E_{n_x, n_y} = H\left(I_x = n_x + \frac{1}{2}, I_y = n_y + \frac{1}{2}\right) \quad (1.64)$$

with the PSS wavefunction

$$\psi(\theta) = e^{i(n_x + \frac{1}{2})\theta + if(\theta)}. \quad (1.65)$$

This function is discontinuous at  $\theta = \pi n$ . This may seem to be unphysical, but remember that the semiclassical approximation breaks down near the turning points. Therefore Eq. (1.65) should not be used near  $\theta = \pi n$ . The exact wavefunction would smoothly join the discontinuity. If there were hard walls instead of caustics the actions would be integral and  $f(\theta)$  would have the steps of size  $\pi$ .

The wavefunction in  $x$ -representation can be recovered by the standard procedure  $\psi(x) = \psi(\theta) \sqrt{|\partial\theta/\partial x|}$ . Note that  $\partial\theta/\partial x = \omega_x/v_x$ , where  $v_x$  is the velocity, and  $I_x\theta = \int p_x dx$ . Suppose

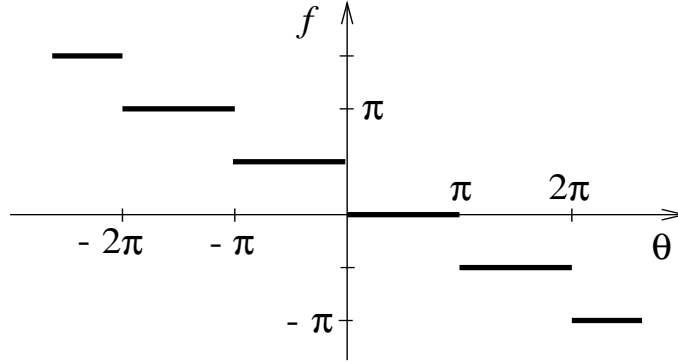


Figure 1.4: Step-wise phase  $f(\theta)$  from Eq. (1.56).

$x(\theta = 0)$  is the turning point on the left. Then  $\psi(x)$  has two branches:

$$\begin{aligned}\psi_1(x) &\propto \frac{1}{\sqrt{|v_x|}} e^{i \int_{x(0)}^x |p_x| dx'}, & 0 < \theta < \pi, \\ \psi_2(x) &\propto \frac{1}{\sqrt{|v_x|}} e^{-i \int_{x(0)}^x |p_x| dx' + i \frac{\pi}{2}}, & -\pi < \theta < 0,\end{aligned}\tag{1.66}$$

which makes

$$\psi(x) \propto \frac{1}{\sqrt{|v_x|}} \cos \left[ i \int_{x(0)}^x |p_x| dx' - i \frac{\pi}{4} \right],\tag{1.67}$$

the one-dimensional bound state wavefunction [49].

Finally, we note that the algorithm we used to solve the semiclassical problem in the AA coordinates (or other coordinates that change the topology of the trajectories) may be not unique. Both in this and in the previous section, where we considered the change of coordinates in the  $T$ -operator, we assumed that the wavefunctions do not acquire Maslov's index on caustics — we always took the *absolute value* of the Jacobian:  $\psi(q) = \psi(Q) \sqrt{|\partial Q / \partial q|}$ . Alternatively, we could drop the modulus or add the Maslov phase. Then the Maslov phase of the  $T$ -operator would be determined by the caustics in the current coordinates (not physical space) and the wavefunction  $\psi$  would not have the unnatural discontinuities as in the above example. However, the straightforward quantization conditions would be incorrect, for instance, the actions would be integral instead of half-integral. Thus the special formulation of the quantization conditions would be necessary, again giving significance to the physical coordinates. Whichever method

is used, the physically important quantities, the wavefunction  $\psi(x)$  and the quantized energy, will be the same.

## 1.8 Conclusions

Bogomolny's  $T$ -operator is a powerful tool that combines the semiclassical approximation and Poincaré's surface of section. Bogomolny's equation determines the surface of section wavefunction and the energy levels. The full wavefunction can be reconstructed from the surface of section wavefunction with the help of a semiclassical propagator. In billiards the method is related to the boundary integral method. The properties of  $T$ -operator include unitarity, the composition property, and the finite size in the momentum representation, all within the stationary phase approximation. The  $T$ -operator propagates the semiclassical wavepacket consistently with the classical surface of section map. The regions where the semiclassical approximation breaks down, like caustics and walls, are responsible for the additional (Maslov) phases in the  $T$ -operator and wavefunctions. One should be careful, when making coordinate transformations with singular points, not to change the Maslov phase. For the integrable systems the  $T$ -operator method is consistent with the EBK quantization.

## Chapter 2

# Perturbation theory

In this chapter we present a systematic derivation of the perturbation theory that provides a semiclassical description for almost integrable systems [62]. In a theory of this type there are two competing quantities: the large action (compared to the Planck constant) and the small perturbation from integrability. Their interplay determines to what degree the structure of classical phase space is reflected in the quantum results.

It is a well-known fact of the classical theory [52] that the topology of invariant tori near the periodic orbits changes under perturbation. One needs a resonant classical perturbation theory in order to describe it. On the other hand, the standard EBK quantization procedure relies on the classical invariant tori, which means that a resonant semiclassical theory might be necessary for some classes of states. Here is a simple estimate. For a periodic orbit of action  $I$  the perturbation of size  $\epsilon$  changes the topology of the tori within the layer  $\delta I \sim \sqrt{\epsilon}I$ . If  $\delta I \gtrsim \hbar$ , several quantum levels become mixed, i.e. the resonant theory is required.

For a billiard of linear size  $L$  with the perturbed boundary the condition becomes  $kL\sqrt{\epsilon} \gtrsim 1$  where  $k = 2\pi/\lambda$  is the wavenumber. This means that, unless the perturbation  $\delta L \ll \lambda^2/L$ , the billiard will have strongly perturbed states.<sup>1</sup> Note that even the distortion of the boundary shorter than the wavelength may be strong enough to mix several energy levels.

In the following sections we derive the analytic expressions for the wavefunctions and energy levels of the states associated with the classical resonances. Although our theory is effectively

---

<sup>1</sup>In a billiard the level spacing  $\hbar^2/mL^2$  should be compared to the shift of a given level  $\hbar^2k^2\delta L/mL$ , which results in the same criterion. (Noted by M. Sieber.)



a resonant perturbation theory, the diagonalization of unperturbed states is not explicit. The Bogomolny equation allows to express the results in a simple, easy to visualize form.

We use the circle billiard with a perturbed boundary as an example. Several papers published in recent years [21, 32, 20, 25] discuss the localization and diffusion in angular momentum space of this system. We too find the angular momentum localized, with the degree of localization depending on the smoothness of the perturbation.

There are several other methods that deal with almost integrable systems that are sometimes similar, sometimes complementary to the following theory. For instance, the quantization of Birkhoff-Gustavson normal form [15, 38, 68] is useful for the perturbed harmonic oscillators — the case to which our theory does not directly apply. The Born-Oppenheimer approximation (Ch. 5) is similar to the perturbation theory in some cases. The perturbed Berry-Tabor formula (Ch. 6) expresses the contributions of the periodic orbits to the density of states consistently with the perturbation theory.

## 2.1 Perturbed integrable systems

An  $N$ -dimensional Hamiltonian system is called *integrable* if it has  $N$  independent integrals of motion in involution [74]. Its motion in the phase space is confined to an  $N$ -dimensional manifold that has the topology of a torus. It is called an *invariant torus*. The integrals of motion can be chosen to be the action variables  $I_i$ ,  $i = 1, \dots, N$ . Then the angle variables  $\theta_i$  (identified with  $\theta_i + 2\pi$ ) provide the natural coordinates on the torus. The Hamiltonian of the system depends only on the actions,  $H_0(I) = E$ . The equations of motion  $\dot{\theta}_i = \partial H_0 / \partial I_i \equiv \omega_i(I)$  can be easily integrated.

In the case  $N = 2$  we can choose the Poincaré surface of section (PSS) as, say,  $\theta_2 = 0$  (Fig. 1.3). The dynamics of the system induces the PSS map  $(I', \theta') \mapsto (I, \theta)$  (we dropped the subscript “1”) simply as  $I = I'$ ,  $\theta = \theta' + 2\pi\omega_1/\omega_2$ . If all points  $(I, \theta)$  belonging to a certain trajectory are plotted  $I$  vs  $\theta$ ,  $0 < \theta < 2\pi$ , they all will lie on a horizontal line  $I = \text{const}$ . The line will either be covered densely if  $\omega_1/\omega_2$  is irrational or have a finite number of points if it is rational. We may say that the line  $I = \text{const}$  is an intersection of an invariant torus with the PSS. The reduced action  $S(\theta, \theta') = S_0(\theta - \theta') = (\theta - \theta')I_1 + 2\pi I_2$  [cf. Eq. (1.47)] is a generating function for this map:  $I = \partial S / \partial \theta$ ,  $I' = -\partial S / \partial \theta'$  (Sec. 1.3). Note that  $S(\theta, \theta')$  depends only

on the difference  $\theta - \theta'$ . The action variables must be regarded as functions of  $\theta - \theta'$  and  $E$  (see Sec. 1.7 for details).

The Hamiltonian of a *perturbed integrable system*

$$H = H_0(I_1, I_2) + \epsilon H_2(I_1, I_2, \theta_1, \theta_2) + \epsilon^2 H_4 + \dots \quad (2.1)$$

differs from an integrable Hamiltonian by the terms proportional to a small parameter  $\epsilon$ . Likewise, the action of such system

$$S(\theta, \theta') = S_0(\theta - \theta') + \epsilon S_2(\theta, \theta') + \epsilon^2 S_4 + \dots \quad (2.2)$$

is expanded in powers of  $\epsilon$ . (We reserve the odd subscripts for half-integral powers of  $\epsilon$  that will appear in other expansions.) The classical perturbation theory [52], in principle, allows one to find the corrections to the action if the Hamiltonian is known, for example,  $S_2 = - \int H_2 dt$ . Since only short orbits are involved, the problem of small divisors does not arise. In the case of a billiard with a perturbed boundary,  $S(\theta, \theta')$  can be easily deduced directly.

Of course, when the perturbation is on,  $I$ 's are no longer integrals of motion. Consequently, the orbits on the PSS are no longer confined to the lines  $I = \text{const}$ . One can imagine several possibilities. The lines could be slightly deformed, they could change their topology, or disappear completely (i.e. the orbit would densely cover a two-dimensional area in the PSS). As a matter of fact, all three cases may be present within one system, depending on the region in the phase space.

According to the Kolmogorov-Arnold-Moser (KAM) theorem, for small enough  $\epsilon$  and smooth enough perturbation most of the tori continue to exist and remain close to the unperturbed tori. The measure of the destroyed or considerably modified tori tends to zero as  $\epsilon \rightarrow 0$ . The destroyed tori are located near the *rational*, or *resonant*, original tori. These are the tori that have a rational winding number  $\omega_1/\omega_2$ , i.e. they support a *periodic orbit*, or *resonance*. Consider a  $(p, q)$  resonance, i.e. the winding number is  $p/q$ , an irreducible fraction. Then all points on the line  $I = \text{const}$  are the fixed points of  $\mathcal{T}^q$ , where  $\mathcal{T}$  is one Poincaré mapping. The Poincaré-Birkhoff fixed point theorem [74] states that under the perturbation only an even number, a multiple of  $2q$ , of fixed points will remain. They will alternate between stable and unstable.

As Fig. 2.1 illustrates, the tori form resonant islands around the fixed points. The size

of the islands is proportional to  $\sqrt{\epsilon}$ . Thus most of the tori near a rational torus change their topology under the perturbation and form a new system of tori. The new tori, in turn, form secondary resonance chains (as in the example of  $(2, 5)$  resonance in the figure) although they are exponentially smaller than the primary resonances [52]. There is a chaotic region near the separatrix formed by numerous intersections of stable and unstable manifolds. It too is exponentially small [50]. The size of the resonant islands reduces rapidly with  $q$  (see Sec. 2.3.2), so the total measure of the strongly modified phase space is finite and proportional to  $\sqrt{\epsilon}$ . The rest of the tori are slightly perturbed on the scale of  $\epsilon$ . Figure 2.1 shows the torus with the “most irrational” golden mean (GM) winding number. It is supposedly the last torus to be destroyed with the increase of the perturbation, although this is not a subject of this work. The figure also illustrates how the rational numbers with large  $q$  tend to become “closer” to irrational numbers. If one disregards the small island chains in  $(7, 16)$  or  $(15, 32)$  resonances the overall curve is similar to a perturbed irrational torus. Its oscillation is of order of  $\epsilon$ . This effect is relevant to the semiclassical theory since the quantization misses those details of the phase space that have a typical area less than  $2\pi\hbar$  (see Secs. 2.3.1 and 2.3.2).

If the perturbation is not smooth enough (so that the KAM theorem does not apply) the invariant tori may not exist at all [Fig. 2.2 (a)]. In this case the semiclassical perturbation theory needs diffraction corrections, although the simplest version still reflects the main features of the states for small  $\epsilon$ .

## 2.2 Formulation of the theory

### 2.2.1 Perturbed circular billiard

The perturbation theory we are about to present is based on the  $T$ -operator and requires a careful choice of coordinates and surface of section. From the theoretical point of view the natural choice would be the action-angle (AA) variables where the unperturbed action depends only on the difference of the angles. In practice working in the AA variables is not always physically transparent and may require a complicated transformation from the original coordinates and back. On the other hand, billiards with a perturbed boundary have an advantage that the reduced action is just a geometrical quantity proportional to the length

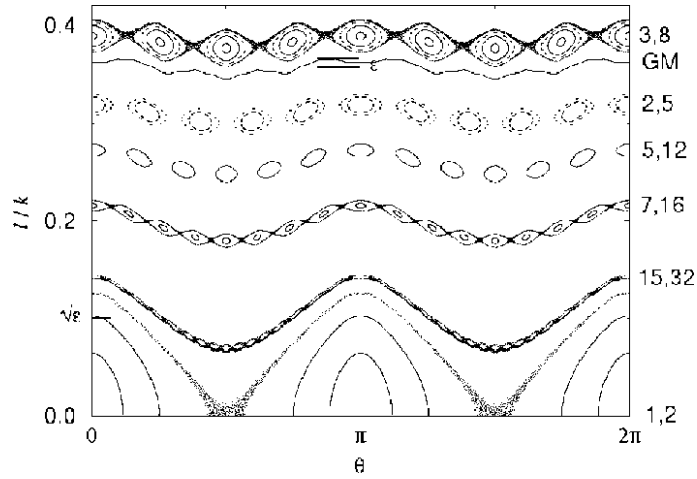


Figure 2.1: The surface of section (boundary phase space) of a perturbed circular billiard.  $l/k$  is an angular momentum normalized to its maximal value and  $\theta$  is an angular coordinate along the boundary. The numbers on the right denote the orbits near the  $(p, q)$  resonances perturbed by order  $\sqrt{\epsilon}$ . GM is an orbit with the golden mean winding number perturbed by order  $\epsilon$ . The secondary resonances and the chaotic regions near the separatrices, that are exponentially small when  $\epsilon \rightarrow 0$ , can also be observed. Here the perturbation is the “smoothed stadium” with the parameters  $\epsilon = 0.1$ ,  $\eta = 0.19$  defined in Sec. 2.2.1.

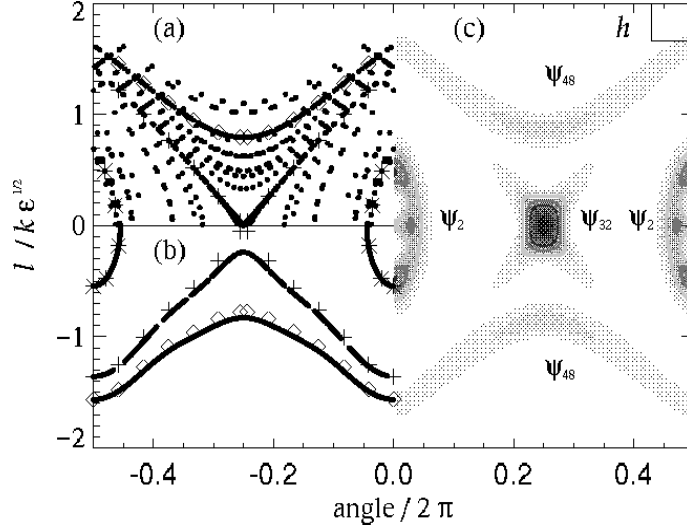


Figure 2.2: The surface of section for (a) “short stadium” and (b) “smoothed stadium” of Sec. 2.2.1 with  $\epsilon = 0.01$ ,  $\eta = 0.15$ .  $l/k$  as in Fig. 2.1. The points  $\diamond$ ,  $+$ , and  $*$  denote the intersection of the invariant tori with the surface of section,  $l_{\text{inv}}(\theta)$ , as given by the perturbation theory (see Sec. 2.3.1), for the non-resonant, separatrix, and resonant orbits, respectively. In (a), where KAM fails, orbits started at symbols were iterated forward and backward 15 times (appear as dots  $\bullet$ ). Only short time structure is regular. In (b), where KAM applies, three orbits, each iterated 1000 times, coalesce into solid lines. (c) Husimi plots for the numerical states of Fig. 2.4, as well as the scar state  $\psi_{32}$ , for the short stadium. The square has area  $h$ .

of the orbit. A perturbed circular billiard whose boundary in the polar coordinates is  $r(\theta) = R_0 + \epsilon \Delta R(\theta)$  is a particularly convenient system since the angle  $\theta$  together with the (modulus of) angular momentum  $l$  are, in fact, the AA variables (when  $\epsilon = 0$ , of course). (We can always make the angular average of  $\Delta R$  vanish and assume  $\Delta R \sim R_0$ .) We will formulate the perturbation theory for this system, which allows the simple mathematical description and direct physical interpretation. There should be no principal difficulty to generalize the theory or tailor it to other systems, as we do in the subsequent chapters. We would like to point out some limitations that will become more apparent as we proceed. First, the theory is the most useful in two-dimensional systems, where the PSS has a one-dimensional space component. Second, the unperturbed action  $S_0$  should depend only on the difference of coordinates in the PSS which may force one to use the AA variables. Finally, the theory is not suitable for the perturbed two-dimensional harmonic oscillator since  $S_0$  is not well defined (see the footnote on p. 14).

From now on we assume  $R_0 = 1$ . A wavenumber  $k$  also becomes dimensionless. (To restore the proper units one should substitute  $k$  by  $kR_0$ .) A perturbation of the form  $\Delta R(\theta) = |\sin \theta| - 2/\pi$  models the short Bunimovich stadium that recently received a lot of attention [21, 20, 25]. The straight segments in this stadium have length  $2\epsilon$ . Our perturbed circle approximates it to the order of  $\epsilon$  and has a discontinuous derivative (Fig. 2.3) [we neglected the straight segments when deriving  $\Delta R(\theta)$ , which thus describes the outer boundary of two circles with their centers being  $2\epsilon$  apart]. Although the invariant tori do not exist, our theory still works if  $k\epsilon^{3/2} \ll 1$ . We also consider a “smoothed stadium”  $\Delta R(\theta) = \sqrt{\sin^2 \theta + \eta^2} - C_\eta$ , where  $C_\eta$  makes the angular average vanish. If  $\epsilon$  is sufficiently small compared to  $\eta$  the invariant tori exist [Fig. 2.2 (b)]. We choose  $\eta \sim \sqrt{\epsilon}$  in our numerical examples.

We associate the PSS with the boundary of the billiard. We parametrize it by the angle  $\theta$  with the conjugate momentum  $l$ . Our goal is to construct the  $T$ -operator (1.23) and solve Bogomolny’s equation (1.22) perturbatively. For convenience we assume  $\hbar = 1$  and the mass  $m = 1/2$ . Then the energy  $E = k^2$ . The action

$$S(\theta, \theta') = kL(\theta, \theta') = k[L_0(\theta - \theta') + \epsilon L_2(\theta, \theta') + \dots] \quad (2.3)$$

where  $L(\theta, \theta')$  is the chord length between points  $\theta$  and  $\theta'$  on the boundary. For a perfect

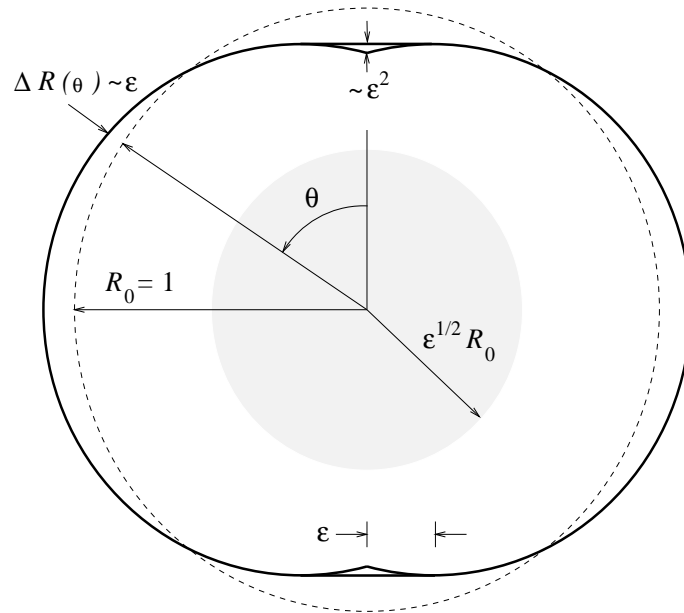


Figure 2.3: Short Bunimovich stadium  $R(\theta) = R_0 + \epsilon\Delta R(\theta)$  with  $\epsilon = 0.3$ . The straight segments have length  $2\epsilon$ . The dashed line denotes the circle of radius  $R_0 = 1$ . The difference between the actual stadium and the approximation for  $\Delta R(\theta)$  that we use is of order  $\epsilon^2$ . The classical orbits that pass through the shaded region are affected by the  $l = 0$  resonance.

circle we find

$$L_0(\theta - \theta') = 2 \left| \sin \frac{\theta - \theta'}{2} \right| \quad (2.4)$$

and the correction

$$L_2(\theta, \theta') = \left| \sin \frac{\theta - \theta'}{2} \right| [\Delta R(\theta) + \Delta R(\theta')]. \quad (2.5)$$

We always assume  $k \gg 1$  and  $\epsilon \ll 1$  as general requirements for the semiclassical and perturbation theories, respectively.

An example of the PSS is shown on Fig. 2.1. Note that in a perfect circle of radius 1 the angular momentum is bounded,  $|l| \leq k$ . The resonances correspond to the periodic trajectories in a circle. For instance, the (1, 2) resonance is related to the  $l = 0$  orbit passing through the center of the circle. The (1, 3) resonance is a triangle shaped periodic orbit, etc. Our theory is designed to find the quantum states located primarily within a given resonance.

### 2.2.2 Simplest case: (1, 2) resonance, $k\epsilon \ll 1$

The theory simplifies significantly for the states near (1, 2) resonance, partly due to the symmetry of the perturbation  $L_2(\theta, \theta')$ . We also assume the perturbation to be sufficiently weak,  $k\epsilon \ll 1$ , a requirement that will be later relaxed. It was explained in the chapter's introduction that as long as  $k\sqrt{\epsilon} \gtrsim 1$  the resonant perturbation theory is needed. The relevant classical orbits have the angular momentum  $l \sim k\sqrt{\epsilon}$  and pass through the shaded region in Fig. 2.3.

In a perfect circle the resonant trajectory maps point  $\theta'$  to  $\theta = \theta' + \pi$ . We therefore expand the  $T$ -operator in  $\delta\theta' = \theta' - \theta + \pi$ , as well as in  $k\epsilon$ . In this case Eq. (1.23) becomes

$$T(\theta, \theta') \simeq -\sqrt{\frac{k}{4\pi i}} (1 + \dots) e^{i(2k - \frac{k}{4}\delta\theta'^2 + \dots)} [1 + ik\epsilon V(\theta) + \dots] \quad (2.6)$$

where  $V(\theta) = L_2(\theta, \theta - \pi) = \Delta R(\theta) + \Delta R(\theta - \pi)$ . We also expand the wavefunction

$$\psi(\theta') = \psi(\theta - \pi) + \delta\theta' \psi'(\theta - \pi) + \frac{\delta\theta'^2}{2} \psi''(\theta - \pi) + \dots \quad (2.7)$$

that solves Bogomolny's equation  $\psi = T\psi$ . We evaluate the integral  $\int T(\theta, \theta') \psi(\theta') d\theta'$  in the stationary phase approximation ( $S\Phi$ ) thus justifying the smallness of  $\delta\theta'$ . The equation is reduced to

$$\psi(\theta) = e^{i(2k + \frac{\pi}{2})} \left[ \psi(\theta - \pi) - \frac{i}{k} \psi''(\theta - \pi) + ik\epsilon V(\theta) \psi(\theta - \pi) \right]. \quad (2.8)$$



Assume we can expand  $\psi(\theta-\pi) \simeq e^{-i(2k+\frac{\pi}{2})\theta} \psi(\theta) - ik\epsilon E_m \psi(\theta-\pi)$ , making  $\psi(\theta-\pi) = e^{-i\omega} \psi(\theta)$  where

$$\omega(k) \simeq 2k + \frac{\pi}{2} + k\epsilon E_m. \quad (2.9)$$

The constant  $E_m$  is to be determined. We find that  $\psi(\theta)$  has to satisfy the ordinary differential equation

$$\psi''(\theta) + k^2\epsilon [E_m - V(\theta)] \psi(\theta) = 0, \quad (2.10)$$

which is a one-dimensional Schrödinger equation. We will refer to  $V(\theta)$  as a “potential” and to  $E_m$  as a “(surface of section) energy” when it does not cause a confusion. Note that the strength of the potential is scaled as  $(k\sqrt{\epsilon})^2$ .

The eigenstates  $\psi_m(\theta)$  of Eq. (2.10) with the eigenenergy  $E_m$  solve Bogomolny’s equation,  $m$  is a quantum number that labels the states. Since  $V(\theta)$  has period  $\pi$  we can always find the  $2\pi$ -periodic solutions such that  $\psi_m(\theta) = \pm \psi_m(\theta - \pi)$ . The second quantization condition is then

$$\omega(k) = 2\pi n + \omega_m \quad (2.11)$$

where  $\omega_m = 0$  or  $\pi$  (depending on  $m$ ) and  $n$  is integer. This provides an equation for  $k$  and the total energy  $E_{nm}$

$$k_{nm} = \sqrt{E_{nm}} = \frac{2\pi(n - \frac{1}{4}) + \omega_m}{2 - \epsilon E_m}. \quad (2.12)$$

Note that  $E_m$  and  $\psi_m$  weakly depend on  $n$  via the parameter  $k^2\epsilon$ .

Eq. (2.10) can be solved by standard methods either numerically or analytically. If  $k\sqrt{\epsilon} \gg 1$  we can approximate its solution in WKB:

$$\psi_m(\theta) \propto \frac{1}{\sqrt{f'(\theta)}} e^{ik\sqrt{\epsilon}f(\theta)} \quad (2.13)$$

where

$$f(\theta) = \pm \int d\theta \sqrt{E_m - V(\theta)}. \quad (2.14)$$

If  $E_m > V(\theta)$  for all  $\theta$ , we may quantize  $E_m$  by the condition

$$k\sqrt{\epsilon} \int_0^\pi d\theta \sqrt{E_m - V(\theta)} = \omega_m + 2\pi m. \quad (2.15)$$

We call this the “rotational” case since all  $\theta$  are in the “classically allowed region.” As will be clarified later, these states quantize the classical orbits in the surface of section that lie

near the resonance chain though *outside* of the separatrix (Fig. 2.1). In the KAM language, the topology of the tori did not change as a result of the perturbation, but they are strongly distorted by the nearby resonance. If we compare a picture of a resonance chain with the phase portrait of a pendulum, these tori would be analogous to the rotational trajectory of a pendulum.

Likewise, if  $E_m < \max V(\theta)$  the motion will be librational. These are the tori that lie inside the separatrix and surround the stable periodic orbit. Their topology is changed by the perturbation. The potential  $V(\theta)$  has at least two wells between 0 and  $2\pi$ . If the tunneling between the wells can be neglected the degenerate levels will be given by the Bohr-Sommerfeld conditions [49]

$$k\sqrt{\epsilon} \int_{\theta_{m-}}^{\theta_{m+}} d\theta \sqrt{E_m - V(\theta)} = \pi \left( m + \frac{1}{2} \right). \quad (2.16)$$

Here the limits of the integration are the classical turning points. The wavefunction inside the well is

$$\psi_m(\theta) = [E_m - V(\theta)]^{-1/4} \sin \left( \int_{\theta_{m-}}^{\theta} d\theta' \sqrt{E_m - V(\theta')} + \frac{\pi}{4} \right). \quad (2.17)$$

Figures 2.2 (c) and 2.4 show the examples of the rotational and librational states. The two-dimensional wavefunctions for the librational states with  $m = 2, 3$  are shown in Figs. 2.5, 2.6, respectively.

### 2.2.3 General case: $(p, q)$ resonance, $k\epsilon^{3/2} \ll 1$

In this section we quantize the orbits near an arbitrary  $(p, q)$  resonance. We also lift the restriction  $k\epsilon \ll 1$ . Instead, we construct the perturbation series  $\psi(\theta) = \exp \{ ik [f_0(\theta) + bf_1(\theta) + b^2f_2(\theta) + \dots + b^M f_M(\theta)] \}$ , where  $b = \sqrt{\epsilon}$  and  $f'_i \sim 1$ . We call  $M$  the order of the perturbation theory. The large and small parameters  $k$  and  $b$  should satisfy the conditions  $kb^{M-1} \gg 1$  and  $kb^{M+1} \ll 1$ . Equation (2.13), for example, is the case  $M = 1$ . The first condition ensures the validity of this WKB-type ansatz by making the phase fast varying. In other words, the quantum system will reflect the classical structure to order  $M$ . The second condition allows to neglect the terms of order  $M + 1$ . In practice, the procedure becomes very tedious for  $M > 2$  and the results are not interesting qualitatively. In this case one can simply solve the problem numerically. Although we derive the expressions for up to  $M = 3$  we do not go beyond  $M = 2$  in the examples studied in this work.

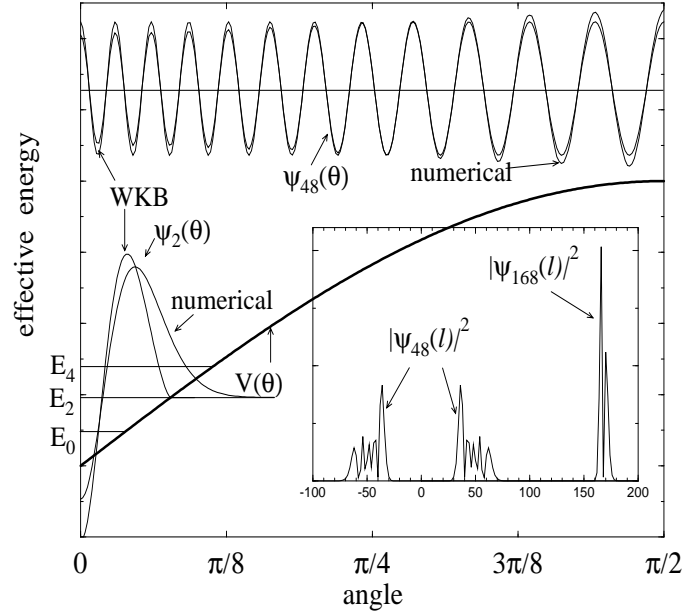


Figure 2.4: Examples of the low angular momentum states  $\psi_m(\theta)$  in the short stadium. The effective potential  $V(\theta)$  is shown as a thick line. The WKB solutions of Eq. (2.10) are compared with the numerical solutions of Bogomolny's equation  $\psi = T\psi$  (see Sec. 2.3.5). The zero axis for each state is its WKB effective energy  $E_m$ . For the librational state the simplistic boundary condition  $\psi_2(\theta) = 0$  at the turning point was taken in the WKB case. The states and the potential are symmetric at  $\theta = 0$ .  $k\sqrt{\epsilon} = 42.3$  is fixed. Inset: the angular momentum representation of the rotational states  $m = 48$  and  $m = 168$  (Sec. 2.3.4).

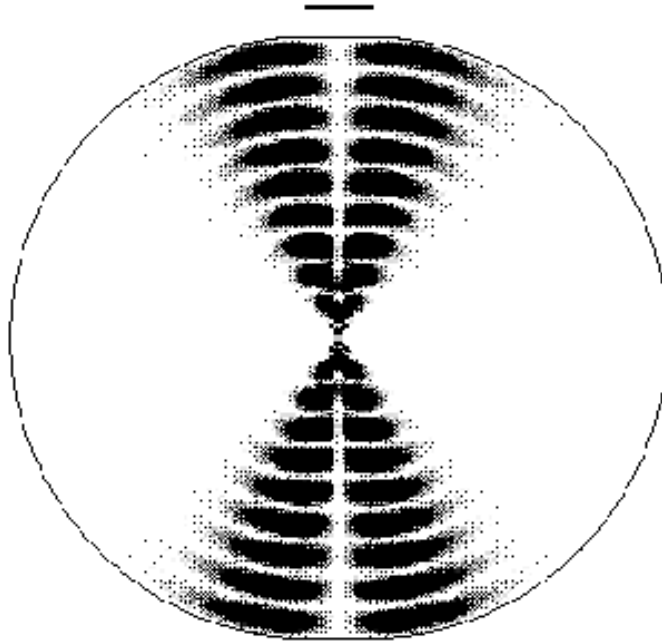


Figure 2.5: The low angular momentum state  $n = 10$ ,  $m = 2$  for the short stadium with  $\epsilon = 0.05$ . The absolute square of the wavefunction is calculated from the perturbation theory. The theoretical wavefunction is inaccurate near the center of the billiard (see Sec. 2.4). The line segment indicates the length and position of the straight parts of the boundary.

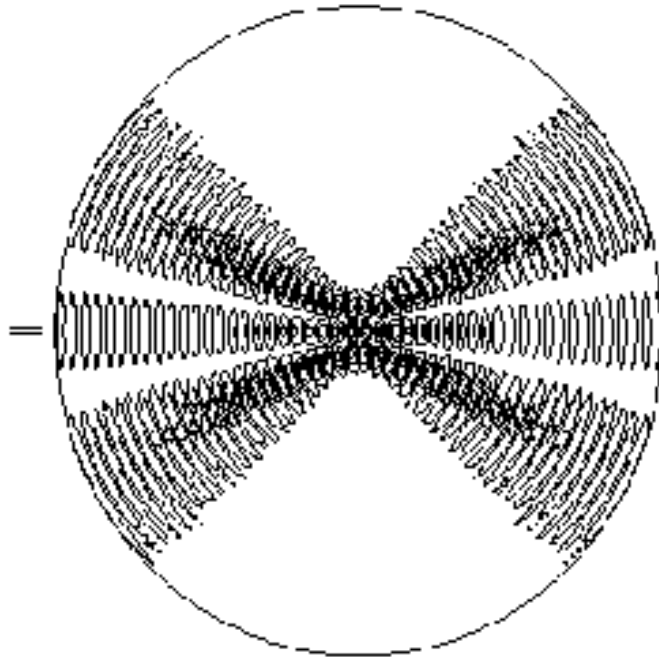


Figure 2.6: Contour plot of the numerical low angular momentum state  $n = 25$ ,  $m = 3$  for the short stadium with  $\epsilon = 0.01$ . The parallel lines on the left indicate the length and position of the straight segments of the boundary.

In a perfect circle the change of angle after one mapping  $\theta - \theta' = 2\pi p/q \equiv \Theta_{pq}$  for a  $(p, q)$ -resonant orbit. (By definition, the particle makes  $p$  times around the billiard after  $q$  mappings.) The angular momentum  $l_{pq} = (\text{sgn } p) k \cos(\Theta_{pq}/2)$ . For the perturbed circle we make an ansatz

$$\psi(\theta) = e^{il_{pq}\theta + ik[b f_1(\theta) + b^2 f_2(\theta) + \dots]}. \quad (2.18)$$

The function should also have a slowly varying prefactor but we disregard it for now. We retain terms to order  $kb^2$  in the phase of the  $T$ -operator and the lowest order term in the prefactor. The phase of  $T(\theta, \theta')$  and  $\psi(\theta')$  can be expanded in  $\delta\theta' = \theta' - \theta + \Theta_{pq}$ . We will see that  $\delta\theta' \sim b$ . Introducing the notation  $-d = L_0''(\Theta_{pq})$  for the second derivative of the unperturbed chord length (2.4) and  $W_{pq}(\theta) = L_2(\theta, \theta - \Theta_{pq})$  we can write the integral

$$\int d\theta' T(\theta, \theta') \psi(\theta') \simeq \int d\theta' \sqrt{\frac{kd}{2\pi i}} e^{i[kL_0(\Theta_{pq}) - \frac{kd}{2}\delta\theta'^2 + kb^2 W_{pq}(\theta) - \pi]} \times e^{il_{pq}(\theta - \Theta_{pq}) + ik[b f_1(\theta - \Theta_{pq}) + b f_1'(\theta - \Theta_{pq})\delta\theta' + b^2 f_2(\theta - \Theta_{pq})]} \quad (2.19)$$

where we have taken into account that  $l_{pq} = S_0'(\Theta_{pq})$ . The integral can be evaluated in the  $S\Phi$  approximation. The stationary point  $\delta\theta'_{\text{st}} = b f_1'(\theta - \Theta_{pq})/d \sim b$ .

After elementary manipulations equation  $\psi = T\psi$  becomes

$$e^{ik[b f_1(\theta) + b^2 f_2(\theta)]} = e^{ikL_0(\Theta_{pq}) - il_{pq}\Theta_{pq} + i\frac{\pi}{2} + ikb f_1(\theta - \Theta_{pq}) + ikb^2[f_2(\theta - \Theta_{pq}) + W_{pq}(\theta) + f_1'^2/2d]}. \quad (2.20)$$

We may try to proceed in the same fashion as in the  $(1, 2)$  resonance case. However the assumption  $\psi(\theta - \Theta_{pq}) = e^{-i\omega}\psi(\theta)$ , in general, is not self-consistent. Indeed, it would mean that  $f_1'$  has period  $\Theta_{pq}$  in this approximation and  $W_{pq}(\theta) + f_1'^2/2d = \text{const}$ . But  $W_{pq}(\theta)$ , in general, does not have period  $\Theta_{pq}$ , so the latter equation cannot be satisfied. The correct conditions would be

$$f_1(\theta) - f_1(\theta - \Theta_{pq}) = \text{const}, \quad (2.21)$$

$$f_2(\theta) - f_2(\theta - \Theta_{pq}) = W_{pq}(\theta) + f_1'^2/2d - E_m \quad (2.22)$$

where  $E_m$  is the constant to be determined. The first equation makes  $f_1'$   $\Theta_{pq}$ -periodic. The second equation defines  $f_2$  to compensate for the lack of periodicity in  $W_{pq}(\theta)$ . Thus it is essential to include  $f_2$  in the wavefunction when  $W_{pq}$  does not have period  $\Theta_{pq}$ .

Define a  $q$ -average of  $W_{pq}$

$$\bar{V}_q(\theta) = \frac{1}{q} \sum_{r=1}^q W_{pq}(\theta + r\Theta_{pq}). \quad (2.23)$$

$\bar{V}_q(\theta)$  has a period  $\Theta_{1q} = 2\pi/q$ . (This follows from the  $\Theta_{pq}$ -periodicity and the existence of an integer  $s$  such that  $s\Theta_{pq} = 2\pi N + \Theta_{1q}$ .) Performing the  $q$ -average on Eq. (2.22) we can determine

$$f_1'(\theta) = \pm \sqrt{2d [E_m - \bar{V}_q(\theta)]}. \quad (2.24)$$

Thus  $f_1'$  also has a period  $2\pi/q$ . This leaves us with equation

$$f_2(\theta) - f_2(\theta - \Theta_{pq}) = W_{pq}(\theta) - \bar{V}_q(\theta) \equiv V_{pq}(\theta) \quad (2.25)$$

that determines  $f_2$  up to a  $\Theta_{1q}$ -periodic (or  $q$ -periodic) function, which appears in the next order of the perturbation theory. This equation has an explicit solution

$$\tilde{f}_2(\theta) \equiv f_2 - \bar{f}_{2q} = -\frac{1}{q} \sum_{r=1}^{q-1} r V_{pq}(\theta - r\Theta_{pq}) \quad (2.26)$$

where  $\bar{f}_{2q}$  is a  $q$ -average. In the future we will, as a rule, leave out the tilde. If the perturbation is expanded in the Fourier series  $W_{pq}(\theta) = \sum_l \tilde{W}_l e^{il\theta}$  then  $\bar{V}_q(\theta) = \sum_l \tilde{W}_{ql} e^{iq_l\theta}$  and  $\tilde{f}_2(\theta) = \sum'_l (1 - e^{-il\Theta_{pq}})^{-1} \tilde{W}_l e^{il\theta}$ . The prime indicates that integers  $l$  divisible by  $q$  are not included in the sum.

Apart from function  $f_2$  the wavefunction  $\psi(\theta)$  is of WKB form for the potential  $\bar{V}_q(\theta)$  :

$$\psi_m(\theta) = [E_m - \bar{V}_q(\theta)]^{-1/4} e^{il_{pq}\theta \pm ik\sqrt{\epsilon} \int d\theta \sqrt{2d[E_m - \bar{V}_q(\theta)] + ik\epsilon f_2(\theta)}}. \quad (2.27)$$

It is shown in Sec. 2.5.1 that  $\psi(\theta)$  has a standard WKB prefactor  $(f_1')^{-1/2}$  in the lowest order (which has been added now by hand). This form is not valid near the turning points and is not convenient in the classically forbidden region. Hence it would be helpful to have a differential equation, similar to Eq. (2.10). Let

$$\psi(\theta) = e^{il_{pq}\theta + ikb^2 f_2(\theta)} \hat{\psi}(\theta). \quad (2.28)$$

Then the new function satisfies the equation  $\hat{\psi} = \hat{T}\hat{\psi}$  where the  $T$ -operator

$$\hat{T}(\theta, \theta') \simeq \sqrt{\frac{kd}{2\pi i}} e^{i[S_0(\Theta_{pq}) - \frac{kd}{2}\delta\theta'^2 - \pi]} e^{ikb^2 [W_{pq}(\theta) + f_2(\theta - \Theta_{pq}) - f_2(\theta)]}. \quad (2.29)$$

The second exponential is  $\exp [ikb^2\bar{V}_q(\theta)]$ . So, if  $k\epsilon |E_m - \bar{V}_q(\theta)| \ll 1$  we can repeat the argument in the previous section and derive a differential equation

$$\hat{\psi}'' + 2dk^2\epsilon [E_m - \bar{V}_q(\theta)] \hat{\psi} = 0. \quad (2.30)$$

This equation is valid either when  $k\epsilon \ll 1$  or near the turning points. If  $k\epsilon \sim 1$  and  $\theta$  is far from the turning points  $\hat{\psi}$  can be shown to satisfy this equation approximately by the direct substitution of the WKB form (2.27). Thus the first order wavefunction  $\hat{\psi}$  can *always* be determined from Eq. (2.30). An example of an eigenfunction for the (1, 3) resonance is shown in Fig. 2.7. Figure 2.8 depicts a two-dimensional wavefunction for the (1, 4) resonance.

## 2.2.4 Quantization conditions

The eigenenergies  $E_m$  are found after imposing the periodicity condition  $\psi_m(\theta + 2\pi) = \psi_m(\theta)$ . For  $\hat{\psi}(\theta)$  it translates to

$$\hat{\psi}(\theta + 2\pi) = e^{-i2\pi\delta} \hat{\psi}(\theta) \quad (2.31)$$

where  $\delta$  is the fractional part of  $l_{pq} \neq 0$ . (For negative  $l_{pq}$  we define  $[l_{pq}]$  as the closest integer from *above* and  $\delta = l_{pq} - [l_{pq}] < 0$ .) If  $\psi(\theta)$  has a WKB form we may again distinguish between the rotational [ $E_m > \max \bar{V}_q(\theta)$ ] and librational [ $E_m < \max \bar{V}_q(\theta)$ ] cases. In the former case the condition is

$$kb \int_0^{2\pi} d\theta \sqrt{2d [E_m - \bar{V}_q(\theta)]} = 2\pi(m \mp \delta) \quad (2.32)$$

where  $\delta$  is the fractional part of  $l_{pq}$ . The double sign reflects the two possibilities in Eq. (2.24). In the librational case, if the tunneling between the wells can be neglected,

$$kb \int_{\theta_{m-}}^{\theta_{m+}} d\theta \sqrt{2d [E_m - \bar{V}_q(\theta)]} = \pi \left( m + \frac{1}{2} \right). \quad (2.33)$$

The wavefunction  $\hat{\psi}$  within a well is given by Eq. (2.17) up to a phase. Assuming  $\bar{V}_q(\theta)$  has  $q$  wells, the phase shift between the wells  $\hat{\psi}(\theta + \Theta_{1q})/\hat{\psi}(\theta) = \exp(-i\delta\Theta_{1q})$  [cf. Eq. (2.31)]. Note that  $-\delta\Theta_{pq}/kb$  is the constant in Eq. (2.21).

The second quantization condition comes from Eq. (2.20). With the help of Eqs. (2.21) and (2.22) we find

$$\omega_m(k) \equiv kL_0(\Theta_{pq}) - [l_{pq}]\Theta_{pq} + k\epsilon E_m + \frac{\pi}{2} = 2\pi n, \quad l_{pq} \neq 0. \quad (2.34)$$



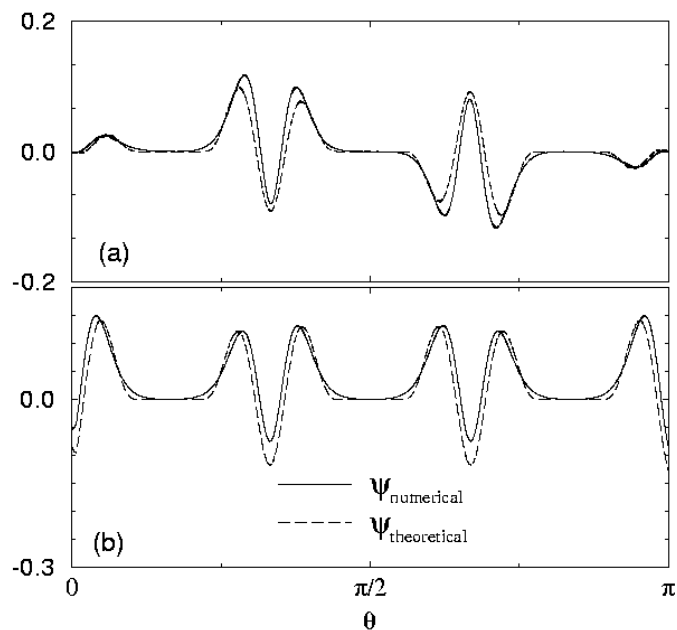


Figure 2.7: Numerical and theoretical surface of section wavefunctions for the (1, 3) resonance in the short stadium with  $k = 4032$ ,  $\epsilon = 6.79 \times 10^{-4}$ . The theoretical wavefunction is  $\psi = \cos(kbf_1) \sin(l\theta + kb^2 f_2)$ . The fast dependence on  $l\theta$  is removed by locally averaging (a)  $\psi \sin l\theta$  and (b)  $\psi \cos l\theta$ . The effective potential  $\bar{V}_3(\theta)$  has a nominal period  $2\pi/3$ , but there are two symmetric wells per period for this perturbation. The angular momentum  $l = k \cos \frac{\pi}{3}$  is integer, so the function  $\hat{\psi}(\theta)$  is  $2\pi/3$ -periodic (see Sec. 2.2.4). In the current example this function is the even combination of the second excited states in each well.

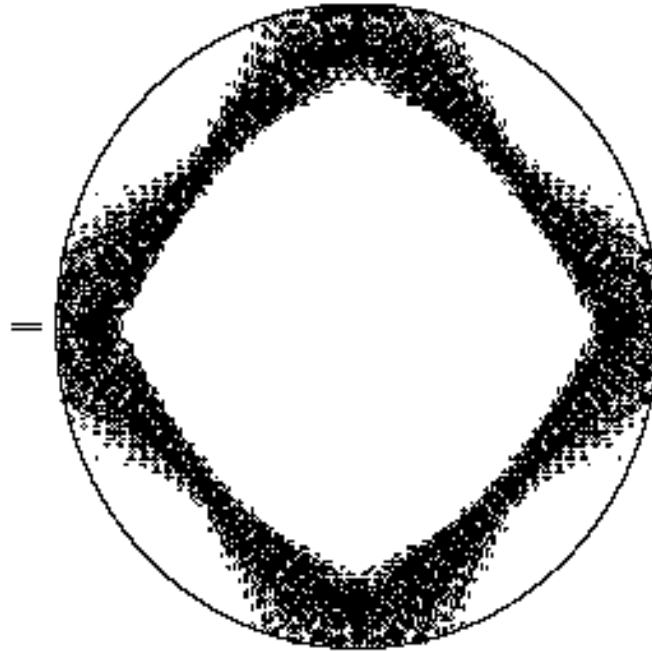


Figure 2.8: Contour plot of a numerically obtained state for the (1,4) resonance in the short stadium with  $k = 280.54$ ,  $\epsilon = 0.01$ . The parallel lines on the left indicate the length and position of the straight segments of the boundary.

The energy levels  $E_{nm} = k_{nm}^2$  are degenerate under  $l_{pq} \rightarrow -l_{pq}$ . This is a consequence of the time-reversal symmetry. The real degenerate eigenstates are the even and odd combinations of the states (2.27) with  $\pm p$ . Since  $l$  is large the states with  $\pm l$  do not overlap. However the overlap with the states from other resonances can create a transition between  $l$  and  $-l$ . We call it a *resonance assisted tunneling*. With this tunneling the states (2.27) are no longer the eigenstates, while their even and odd combinations are. The degeneracy between them will be removed. We will disregard this effect.

### 2.2.5 Third order theory: $k\epsilon^2 \ll 1 \sim k\epsilon^{3/2}$

If  $k\epsilon^{3/2} \gtrsim 1$  one has to keep terms to order  $kb^3$  in the ansatz (2.18) and  $T$ -operator. The additional terms in the phase of Eq. (2.19) are

$$k \left[ -\frac{1}{6} L_0'''(\Theta_{pq}) \delta\theta'^3 + b^2 \frac{\partial L_2(\theta, \theta - \Theta_{pq})}{\partial \theta'} \delta\theta' + \frac{b}{2} f_1''(\theta - \Theta_{pq}) \delta\theta'^2 + b^2 f_2'(\theta - \Theta_{pq}) \delta\theta' + b^3 f_3(\theta - \Theta_{pq}) \right]. \quad (2.35)$$

Although the stationary point  $\delta\theta'_{\text{st}} = bf_1'(\theta - \Theta_{pq})/d$  receives a  $b^2$ -order correction, it does not enter explicitly in the result. The above terms should be evaluated at  $\delta\theta'_{\text{st}}$  and included in the phase of Eq. (2.20). The balance of the  $kb^3$ -terms yields

$$f_3(\theta) - f_3(\theta - \Theta_{pq}) = -\frac{L_0'''(\Theta_{pq})f_1'^3}{6d^3} + \frac{f_1' [f_2' + \partial L_2/\partial \theta']}{d} + \frac{f_1'^2 f_1''}{2d^2} + c \quad (2.36)$$

where  $f_i'$ ,  $f_i''$ ,  $\partial L_2/\partial \theta'$  are evaluated at  $\theta' = \theta - \Theta_{pq}$  and  $c = \text{const}$ . Taking the  $q$ -average of both sides, we have an equation determining  $\bar{f}_{2q}$ , the  $q$ -periodic part of  $f_2$ ,

$$\bar{f}'_{2q} = \frac{L_0'''(\Theta_{pq})f_1'^2}{6d^2} - \frac{cd}{f_1'} + \frac{L_0'(\Theta_{pq})}{L_0(\Theta_{pq})} \bar{V}_q \quad (2.37)$$

where we used Eq. (2.5). This expression must have a vanishing angular average, since  $\bar{f}'_{2q}$  is the derivative of a periodic function, which determines  $c$ . Now  $f_3$  can be found from Eq. (2.36) up to a  $q$ -periodic function which is determined in the next order of the perturbation theory. Note that if  $f_1$  is double-valued, so is  $f_3$ .

### 2.2.6 Non-resonant case

The non-resonant tori that are not affected by the nearby resonances do not change their topology. They get perturbed proportionally to  $\epsilon$ . Unlike the resonant case,  $\sqrt{\epsilon}$  does not enter

the classical picture. As a consequence (see Sec. 2.3.1), the odd powers of  $b$  drop out of the expansion (2.18). The unperturbed state has an integer angular momentum  $l$ , and after one mapping the angle changes by a non-resonant amount  $\theta - \theta' = \Theta_l \equiv 2(\text{sgn } l) \cos^{-1} |l/k|$ .

We start with an ansatz  $\psi(\theta) = \exp[i l \theta + i k \epsilon f_2(\theta)]$  and proceed as in the resonant case. Similar to Eq. (2.20) we find

$$e^{i k \epsilon f_2(\theta)} = e^{i k L_0(\Theta_l) - i l \Theta_l + i \frac{\pi}{2} + i k \epsilon [f_2(\theta - \Theta_l) + W_l(\theta)]} \quad (2.38)$$

where  $W_l(\theta) = L_2(\theta, \theta - \Theta_l)$ . If we require

$$f_2(\theta) - f_2(\theta - \Theta_l) = W_l(\theta) \quad (2.39)$$

we find the quantization condition

$$k L_0(\Theta_l) - l \Theta_l = 2\pi \left( n - \frac{1}{4} \right). \quad (2.40)$$

Thus, at this order of the calculation, there is no shift in energy levels. (Note that the above expression is the Debye approximation to the roots of Bessel's function  $J_l(k)$  for large  $k$  and fixed  $l/k$ .) Expanding the perturbation in the Fourier series  $W_l(\theta) = \sum_r \tilde{W}_r e^{i r \theta}$  we find

$$f_2(\theta) = \sum_{r \neq 0} \frac{\tilde{W}_r e^{i r \theta}}{1 - e^{-i r \Theta_l}}. \quad (2.41)$$

Note that  $\tilde{W}_{r=0} = 0$  since, by definition, the perturbation has a vanishing angular average. Equation (2.41) would not be valid in a resonant case, when some denominators vanish, or if  $\Theta_l$  is close to a rational  $\Theta_{pq}$ . The same is true if  $\tilde{W}_r$  does not drop off with  $r$  sufficiently fast, since  $\exp(-i r \Theta_l)$  can be arbitrary close to 1 for some  $r$ . This is related to the *problem of small denominators* in classical mechanics [74, 52]. If the series does not converge, the resonant solution is needed. Figure 2.9 illustrates the wavefunction associated with the GM torus.

## 2.3 Comments and discussion

### 2.3.1 Classical interpretation

In Sec. 1.3 we discussed the relation between the  $T$ -operator and the surface of section map. The map  $(l', \theta') \mapsto (l, \theta)$  is given by the equations  $l' = -\partial S(\theta, \theta') / \partial \theta'$  and  $l = \partial S(\theta, \theta') / \partial \theta$ .

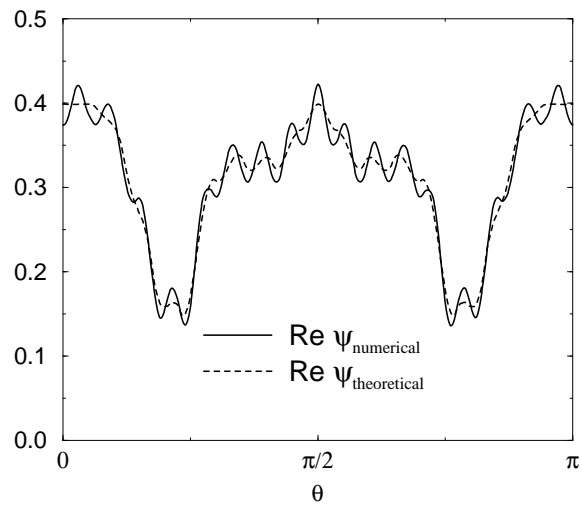


Figure 2.9: Numerical and theoretical surface of section wavefunctions for the non-resonant state on the golden mean torus. The system is a smoothed stadium with  $\epsilon = 10^{-4}$ ,  $\eta = 2 \times 10^{-2}$ . For this torus  $\Theta_l = \pi(\sqrt{5} - 1)$ . The factor  $e^{il\theta}$  has been removed and the real part of the wavefunction is shown.

We have shown that if a curve  $l'(\theta')$  is mapped into  $l(\theta)$  then the  $T$ -operator maps the wavefunction  $\psi'(\theta') \sim e^{i \int l'(\theta') d\theta'}$  into  $\psi(\theta) = T\psi'(\theta) \sim e^{i \int l(\theta) d\theta}$ . The eigenstates of Bogomolny's equation  $\psi = T\psi$  are invariant under the map. Hence the curve  $l = l_{\text{inv}}(\theta)$  associated with an eigenstate is mapped on itself. We call this curve an *invariant loop*. Comparing with Eq. (2.18) we conclude that our method gives a perturbation expansion for this loop

$$l_{\text{inv}}(\theta) = l_0 + k [bf'_1(\theta) + b^2 f'_2(\theta) + \dots] \quad (2.42)$$

and similar in the non-resonant case. Of course, this expansion can be derived by purely classical methods (see also Sec. 2.5.3). If we neglect terms of order  $kb^3$  and higher,

$$\tilde{l}_{\text{inv}} = l_0 \pm kb \sqrt{2d [E_m - \bar{V}_q(\theta)]} + kb^2 f'_2(\theta) \quad (2.43)$$

will be an approximation to the invariant loop. Under the Poincaré map it will be transformed into a new loop  $l_1$ . The area enclosed between the curves  $\tilde{l}_{\text{inv}}$  and  $l_1$  will be proportional to  $k\epsilon^{3/2}$ . If this area is smaller than  $2\pi\hbar$ , i.e.  $k\epsilon^{3/2} \ll 1$ , this approximation is good for the purposes of quantum mechanics. This is true even if no classical invariant loop exists.

Clearly,  $l_{\text{inv}}(\theta)$  is an intersection of an (approximate) invariant torus with the PSS. If we start with a point  $(l, \theta)$  and propagate it under the surface of section map its images will lie on an invariant loop going through this point. Fig. 2.1 shows some of the invariant loops. There are no invariant loops in a stochastic region near the separatrix, but if its typical area is less than  $2\pi\hbar$ , the separatrix will be an invariant curve for a semiclassical wavepacket. The same is true for the secondary resonances.

The three terms in Eq. (2.43) play different roles.  $l_0$  specifies the unperturbed torus. If this torus is close to a resonance a perturbation will transform its neighborhood into a resonant chain. The resonant islands have a size  $\sqrt{\epsilon}$  and are described by the  $q$ -periodic function  $f'_1 \propto \pm \sqrt{E_m - \bar{V}_q(\theta)}$ . The orbits are labeled by  $E_m$ , which is therefore an approximate constant of the classical motion. ( $E_m = \max \bar{V}_q$  for a separatrix.) The islands, in general, do not lie along a horizontal line. Instead, they form a wave of size  $\epsilon$ . This wave is given by the function  $f'_2$ , more precisely, by the non- $q$ -periodic part  $\tilde{f}'_2$  determined in the second order perturbation theory. The  $q$ -average  $\bar{f}'_{2q}$  distorts the shape of the islands but does not shift them with respect to each other. In principle, higher order corrections can be found. In the non-resonant case  $f'_1 = 0$ , and  $f'_2$  describes the distortion of the torus, which is of order  $\epsilon$ . In the special case of

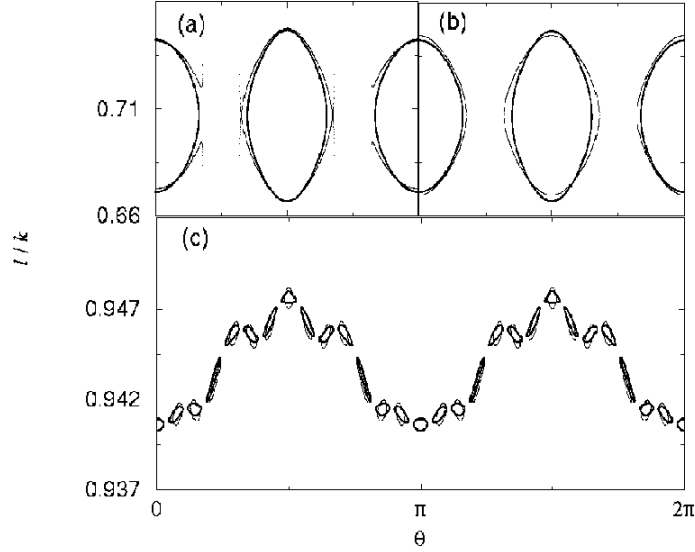


Figure 2.10: Exact and approximate invariant loops near the (a),(b) (1, 4) and (c) (1, 28) resonances in the smoothed stadium. The exact loops (thick line) are obtained by the propagation of the classical map. The approximate loops (thin line) are  $l_{\text{inv}}(\theta)$  that includes terms to order  $b^3$  in (a) and  $b^2$  in (b),(c). The parameters are  $\epsilon = 0.05$ ,  $\eta = 0.7$  in (a),(b), and  $\epsilon = 0.01$ ,  $\eta = 0.19$  in (c).

(1, 2) resonance the islands are not shifted by symmetry, so  $f'_2 = 0$ .

We calculated the invariant loops for the smoothed stadium from Eq. (2.43). For the (1, 2) resonance they are shown as discrete symbols in Fig. 2.2 (b). The orbits follow these curves closely and the deviation must be due to the higher order corrections. We can also formally calculate the loops for the short stadium [Fig. 2.2 (a)] although the orbits stay close to the loops only for a short time. Moreover, the expansion (2.42) breaks down in the higher orders, because  $\bar{V}_q(\theta)$  has a singular second derivative. Nevertheless, there are quantum states localized near these loops [Fig. 2.2 (c)]. Fig. 2.10 compares  $l_{\text{inv}}(\theta)$  with the orbits near the (1, 4) and (1, 28) resonances in the smoothed stadium. Figure 2.11 shows the same for the non-resonant GM torus.

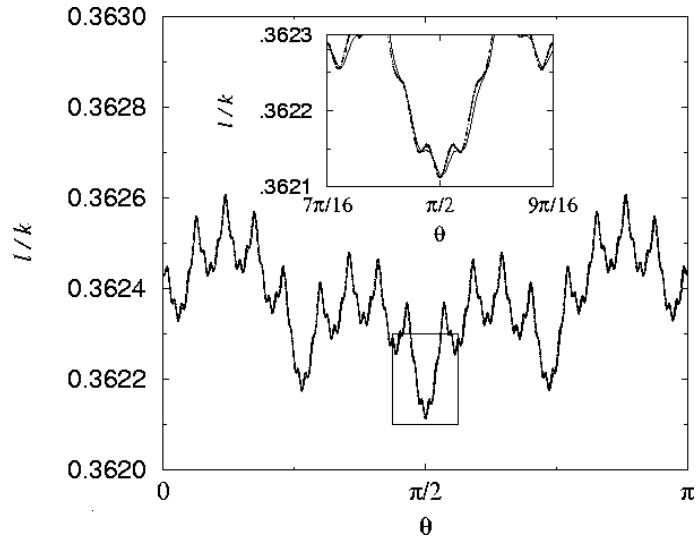


Figure 2.11: Exact and approximate golden mean torus for the smoothed stadium (parameters as in Fig. 2.9). The numerical classical map (dots, 20,000 iterations) is approximated by  $\cos \frac{1}{2}\Theta_l + \epsilon f'_2(\theta)$  (solid line). The inset enlarges a portion of the figure to demonstrate the degree of precision of the approximation. Presumably, this is the last torus to disappear as  $\eta$  is decreased.



### 2.3.2 Resonant or non-resonant?

When  $q$  becomes large the resonant islands become small (e.g. resonance (15, 32) in Fig. 2.1). When the area of the islands becomes smaller than  $2\pi\hbar$  the resonant structure is disregarded by the quantum state. Thus, on the bigger scale, the  $(p, q)$ -chain with large  $q$  looks similar to a perturbed non-resonant torus. This agrees with the intuitive, as well as the number-theoretical [47] notion that the irrational numbers can be approximated by rationals with large denominators with the increasing precision.

Clearly, the resonant solution is needed if the librational state  $E_m < \max \bar{V}_q$  exists. This requires [Eq. (2.33)]

$$\bar{V}_q > \frac{q^2}{k^2 \epsilon d}. \quad (2.44)$$

We assumed that the perturbation  $W_{pq}(\theta)$ , as well as  $\bar{V}_q$ , has vanishing angular average. As  $q$  increases,  $\bar{V}_q$ , the  $q$ -average of  $W_{pq}$ , becomes closer to the angular average and drops off. Another way to say it,  $\bar{V}_q$  is of order of the  $q$ th Fourier coefficient  $\tilde{W}_q$  of  $W_{pq}(\theta) = \sum_l \tilde{W}_l e^{il\theta}$ . But  $\tilde{W}_l$  decreases with  $l$ , usually exponentially for analytic perturbations or as  $l^{-s}$  if  $W_{pq}(\theta)$  has  $s - 2$  continuous derivatives. If  $\bar{V}_q \ll q^2/k^2 \epsilon d$  then  $kbf'_1 \approx \pm k\sqrt{2\epsilon d E_m}$  shifts the constant part of the angular momentum so the nontrivial expansion begins with  $k\epsilon f_2$  as in the non-resonant case.

Condition (2.44) also means that the area of a resonant island  $k\sqrt{\epsilon d \bar{V}_q}/q > 1$  as we implied above. Note that when  $k\sqrt{\epsilon} \ll 1$  all phase space of the system can be treated with the non-resonant perturbation theory in agreement with our earlier estimates.

The area of *all* resonances in the system can be estimated as  $\sum_{p,q} k\sqrt{\epsilon d \bar{V}_q} < k\sqrt{\epsilon d} \sum_q q\sqrt{\bar{V}_q}$ . So if  $\bar{V}_q$  drops off faster than  $q^{-4}$  (i.e. the perturbation has three continuous derivatives) the total affected area will vanish as  $\epsilon \rightarrow 0$ , as in the KAM theorem [52].

The perturbation  $\Delta R(\theta) = |\sin \theta| - 2/\pi$  introduced in Sec. 2.2.1 has a discontinuous derivative, so  $\bar{V}_q \sim q^{-2}$ . In this case the KAM theorem breaks down completely [24]. We expect our leading order solution, which does not include the derivatives, to be valid. Our theory contains the singular second derivatives of  $\Delta R$  in the  $k\epsilon^2$ -order. We assumed that  $k\epsilon^2$  is small. However, multiplied by an infinite  $\bar{V}_q''$  it may bring finite corrections. We call them the *diffraction corrections*. Figure 2.4 compares the theoretical and numerically exact wavefunctions in this case.

It is easy to show that if  $\Delta R(\theta)$  has only one Fourier harmonic, say  $\Delta R(\theta) = \cos(l\theta)$  for some integer  $l$ , then  $\bar{V}_q \neq 0$  only if  $q$  is a divisor of  $l$ . (See also Sec. 2.5.2.) For example,  $l = 1$  and  $l = 2$  are to first approximation a shifted circle and an integrable ellipse, respectively. Thus  $\Delta R$  can be transformed to a perturbation about an integrable system with perturbation parameter  $\epsilon^2$  rather than  $\epsilon$ . In the case of ellipse  $\bar{V}_2 \neq 0$  is the bouncing ball state which does not exist in a perfect circle. The states with the larger angular momentum are similar to the states in the circle.

### 2.3.3 Close to a large resonance

Another important question is whether a given unperturbed torus  $l$  (resonant or non-resonant) will be affected by a neighboring resonance  $l_{pq}$  once the perturbation is on. This is the case if the distance  $|l - l_{pq}| < k\sqrt{\epsilon d \bar{V}_q}$ , the size of the resonance. We can estimate  $|l - l_{pq}| \sim |\partial l / \partial \Delta \theta| |\Theta_l - \Theta_{pq}|$  where  $\Delta \theta$  is the change of angle after one mapping. Note that  $|\partial l / \partial \Delta \theta| = kd$  and  $|\Theta_l - \Theta_{pq}| > q^{-2}$ , which is a generic precision when a number is approximated by the rationals [47]. Thus if  $\bar{V}_q > d/\epsilon q^4$  the torus  $l$  may be affected by a  $(p, q)$  resonance. If  $\bar{V}_q$  drops off faster than  $q^{-4}$  only finite number of resonances may affect the torus.

If the torus *is* affected by a larger resonance, two cases are possible. If  $|l - l_{pq}|$  is sufficiently small, the topology of torus  $l$  will be changed, i.e. the torus will disappear and a new librational torus will appear inside the separatrix. In this case, obviously, torus  $l$  cannot be used as a starting point of the perturbation theory; instead, the expansion should be done near the resonant torus  $l_{pq}$ . On the other hand, if  $|l - l_{pq}|$  is large enough, so that the topology is not changed, torus  $l$  still exists outside the separatrix, although it may be strongly distorted. In this case torus  $l$  may be considered either as a rotational trajectory for the resonance  $(p, q)$  or the perturbation expansion can be done directly near the torus  $l$ . In fact, the larger  $|l - l_{pq}|$ , the better is the expansion near  $l$  and the worse is the expansion near  $l_{pq}$ . Note that  $l$  can be another resonance  $(p', q')$  with  $q' \gg q$ . Consider, for example, the resonance (15, 32) in Fig. 2.1. It is a secondary resonance for the large (1, 2) resonance. The perturbation expansion near the (1, 2) resonance yields only  $f_2$  part of the (15, 32) resonance, i.e. it cannot describe the loops. However, for small  $\epsilon$  the loops are small and will not be reflected in the quantum state anyway.

Suppose  $l$  is a non-resonant torus. The above discussion suggests that if  $l$  lies outside of the separatrix of a large resonance  $l_{pq}$ , we should be able to describe this torus by both the non-resonant perturbation theory for torus  $l$  and the resonant perturbation theory for torus  $l_{pq}$  to some approximation. For a rotational state far enough from the resonance we can assume  $|\bar{V}_q| \ll E_m$  and expand  $bf'_1 \simeq \pm\sqrt{2\epsilon d E_m} (1 - \bar{V}_q/2E_m)$ . We are going to show that

$$l_{pq} \pm k\sqrt{2\epsilon d E_m} (1 - \bar{V}_q/2E_m) + kb^2 f'_2 = l + kb^2 f'_{2l} \quad (2.45)$$

where  $f'_{2l}$  is a non-resonant function. The constant part of  $f'_1$  shifts the unperturbed angular momentum, so  $l_{pq} \pm k\sqrt{2\epsilon d E_m} \equiv l_{pq} + \delta l \simeq l$ . According to Eq. (2.41)

$$f'_{2l}(\theta) = \sum_{r \neq 0} ir \frac{L_0(\Theta_l) (1 + e^{-ir\Theta_l}) \Delta \tilde{R}_r e^{ir\theta}}{2(1 - e^{-ir\Theta_l})} \quad (2.46)$$

where  $\Delta \tilde{R}_r$  is a Fourier component of  $\Delta R(\theta)$ . We can expand Eq. (2.46) in  $\delta\Theta = \Theta_l - \Theta_{pq} \propto \sqrt{\epsilon}$ . The denominator becomes small when  $r$  is a multiple of  $q$ . We separate those terms. Then

$$f'_{2l}(\theta) \approx \tilde{f}'_2(\theta) + \sum_r \frac{L_0(\Theta_{pq}) + L'_0 \delta\Theta}{\delta\Theta} \Delta \tilde{R}_{rq} e^{irq\theta} \quad (2.47)$$

where  $\tilde{f}'_2(\theta)$  is the part of  $f'_2$  that vanishes under the  $q$ -average. The sum is  $(\delta\Theta^{-1} + L'_0/L_0) \bar{V}_q$ . With  $\delta\Theta^{-1} = -kd/\delta l + L'''_0/2L''_0 + O(\delta l)$  the leading term is  $\mp \bar{V}_q \sqrt{d/2\epsilon E_m}$ , which takes care of the respective term in Eq. (2.45), when multiplied by  $kb^2$ . The next order terms give  $\bar{f}'_{2q}$ , the  $q$ -average of  $f'_2$ , since, according to Eq. (2.37),

$$\bar{f}'_{2q} = \left[ \frac{L'_0(\Theta_{pq})}{L_0(\Theta_{pq})} + \frac{L'''_0(\Theta_{pq})}{2L''_0(\Theta_{pq})} \right] \bar{V}_q. \quad (2.48)$$

We thus confirmed that a rotational torus near a large resonance can be chosen as a starting point for the perturbation series in the semiclassical approximation.

### 2.3.4 Localization in angular momentum

As we explained in Sec. 2.3.1, the derivative of the phase of the eigenfunction  $\psi(\theta)$  approximates the invariant loop  $l_{\text{inv}}(\theta)$  in the PSS phase space [see Eq. (2.42)]. This suggests that the angular momentum spectrum of a given eigenstate is concentrated within the range of  $l$  covered by its invariant loop. Formally, we define the wavefunction in the angular momentum representation as

$$\psi_l = \int d\theta [E_m - \bar{V}_q(\theta)]^{-1/4} e^{i \int^\theta d\theta' l_{\text{inv}}(\theta') - l\theta}. \quad (2.49)$$

If  $k\sqrt{\epsilon}$  is large, the  $S\Phi$  can be employed. The stationary phase condition can be satisfied if  $l_{\text{inv}}(\theta) = l$  for some  $\theta$ . In particular, for a librational state near the (1, 2) resonance the spectrum range is  $0 \leq |l| < k\sqrt{\epsilon}\sqrt{\max(E_m - V)}$ . It has much overlap with zero angular momentum. In a higher resonance the range is centered near the resonant angular momentum  $l_{pq}$  and spreads by  $k\sqrt{\epsilon}\sqrt{2d\max(E_m - \bar{V}_q)}$  in both directions. In a non-resonant state the spectrum is highly localized near the unperturbed angular momentum, the spread being of order  $k\epsilon$ . The numerical examples are shown in Fig. 2.4.

Outside of the range of  $l_{\text{inv}}(\theta)$ , the angular momentum components  $|\psi_l|^2$  decay exponentially for smooth  $\bar{V}_q(\theta)$ . In this case the range of  $l_{\text{inv}}(\theta)$  defines the *localization length*. In the stadium case  $\Delta R(\theta) \sim |\sin \theta|$  (Sec. 2.2.1), on the other hand, they decay as a power law, that makes it necessary to define the localization length more precisely [25].

Note that  $\psi_l$  can be calculated by diagonalization of  $T$ -operator in the angular momentum representation. Consider the matrix elements  $T_{ll'} = (2\pi)^{-1} \int d\theta d\theta' T(\theta, \theta') e^{i(l'\theta' - l\theta)}$ . The stationary phase conditions require  $l = \partial S / \partial \theta$  and  $l' = -\partial S / \partial \theta'$  where the action  $S(\theta, \theta')$  is given by Eq. (2.3). It follows that for  $|l - l'| > k\epsilon$  the matrix elements are small, i.e.  $T_{ll'}$  is a band diagonal matrix.

### 2.3.5 Numerical computations

To verify our theory we conducted several numerical checks. Essentially, we compared the wavefunctions and energy levels obtained in Sec. 2.2 (“theoretical” solution) with the numerical solution of Bogomolny’s equation  $\psi = T\psi$ , which we presume to be semiclassically exact. The problem can be separated into two parts. First we solve a more general equation

$$e^{i\omega_m(k)}\psi = T(k)\psi \tag{2.50}$$

assuming  $k$  continuous (it follows from the semiclassical unitarity of  $T$ ). Then we can find the allowed  $k$ ’s from the quantization condition  $\omega_m(k) = 2\pi n$ . Unless we are interested in the energy quantization, we may consider only the general eigenvalue problem (2.50) with fixed  $k$ . This is done in some numerical examples to study the approximation of the wavefunctions.

Equation (2.50) can be solved both theoretically and numerically. The theory of Sec. 2.2 remains unchanged but one should not equate  $\omega_m(k)$  to  $2\pi n$  in Eq. (2.34). To solve the equation numerically [31] we choose an ansatz  $\psi(\theta)$  and evaluate a discrete function  $F(n) =$

$(T^n \psi)(\theta_0)$  at some  $\theta = \theta_0$ . We then find its Fourier image  $\bar{F}(\omega)$ , which consists of the peaks near the eigenphases  $\omega_m(k)$  (see below). We choose  $\omega_m$  of the highest peak. The eigenstate  $\psi_m(\theta) = \langle (e^{-i\omega_m T})^n \psi(\theta) \rangle_{n \rightarrow \infty}$  is the average over  $n$ .

To justify this method expand the ansatz  $\psi(\theta) = \sum_m c_m \psi_m(\theta)$  in the eigenstates of the  $T$ -operator. Then  $F(n) \approx \sum_m c_m e^{i\omega_m n} \psi_m(\theta_0)$ . The Fourier transform  $\bar{F}(\omega) = \sum_n F(n) e^{-i\omega n} \approx (2\pi)^{-1} \sum_m c_m \delta(\omega - \omega_m) \psi_m(\theta_0)$  has peaks at the eigennumbers  $\omega_m$ . If the ansatz is close to some eigenstate  $\psi_{m_0}(\theta)$ , the respective peak will have the largest weight (for a generic  $\theta_0$ ). In the combination  $(e^{-i\omega_{m_0} T})^n \psi(\theta) = c_{m_0} \psi_{m_0}(\theta) + \sum'_m c_m e^{i(\omega_m - \omega_{m_0})n} \psi_m(\theta)$  the sum over  $m \neq m_0$  disappears after the  $n$ -average is taken.

Figure 2.4 compares the theoretical (“WKB”) and numerical wavefunctions for the short stadium (Sec. 2.2.1). The librational and rotational states near the (1, 2) resonance are shown. The considerable difference in the bound state is due to the simplistic WKB solution of Eq. (2.10) with the condition that  $\psi(\theta)$  vanishes at the turning point. This one-dimensional equation can be solved, of course, numerically, but even the simple approach renders the main features of the state. Figure 2.2 (c) contains the Husimi plots of the numerical wavefunctions. In addition to the librational and rotational states, we show the state near the separatrix. This state has  $E_m$  just greater than the maximum  $V(\theta)$ , which means that the wavefunction has an excessive weight near an unstable periodic orbit (due to the WKB prefactor). This explains the observed “scars” of unstable orbits [42]. Note that scars do not appear in the previously developed perturbation theories that quantize the neighborhood of a stable orbit (minimum  $V$ ). It is necessary to know the potential  $V$  near its maximum, not minimum. Figure 2.7 shows the wavefunctions for the (1, 3) resonance. In this case we remove the fast dependence on  $l\theta$  by local averaging. The wavefunctions for the non-resonant GM torus in a smoothed stadium are shown in Fig. 2.9. The examples of the two-dimensional wave-functions are given in Figs. 2.5, 2.6, and 2.8.

The numerical and theoretical eigenphases modulo  $2\pi$ , as defined by Eq. (2.50), are compared in Table 2.1. We consider the states with different  $m$ , but all belonging to the lowest (1, 2) resonance in the short stadium billiard. The wavenumber  $k$  is fixed. One can see that the errors in  $\omega_{\text{theor}}$  are small compared with the average spacing,  $\omega_{m+1} - \omega_m$ , within the resonance.

The spacing is of order [cf. Eqs. (2.9) and (2.34)]

$$k\epsilon(E_{m+1} - E_m) \simeq \sqrt{\epsilon}. \quad (2.51)$$

The energy levels  $(k_{nm})^2$  are given by the condition  $\omega_m(k) = 2\pi n$ . Table 2.2 shows numerical and theoretical wavenumbers for fixed  $m$ . The error is much smaller than the differences

$$k_{n+1,m} - k_{n,m} \simeq \pi \quad \text{and} \quad k_{n,m+1} - k_{n,m} \simeq \sqrt{\epsilon} \quad (2.52)$$

given by Eq. (2.11). Note, however, that our theory gives the energy levels grouped by the resonances they belong to. In this example we have found the levels close to the lowest resonance. There are levels coming from other resonances (i.e the states with higher angular momentum) in the same energy range. The mean spacing of *all* levels in the billiard in terms of  $k$  is  $2/k$ , which is of the order of the errors committed. Nevertheless, the results are still useful since the interaction between the states belonging to different resonances is small.

### 2.3.6 Possible experiments

A number of experimental techniques could, in principle, be used to verify the theoretical results (see also Sec. 4.3). For example, using a scanning tunnel microscope (STM) individual iron atoms can be positioned on a copper surface to form a boundary of a two-dimensional domain called a quantum corral [27]. The two-dimensional electron gas on the surface will be partially confined within the corral, and the spatial images of the electron density standing waves can be produced with STM [43].

Another possible system would be a shallow container of liquid which is vibrated to produce standing surface waves [48, 1]. The dissipation may limit the selection of eigenstates that can be observed.

It is also feasible to utilize the analogy between a wavefunction and an electromagnetic wave in a resonator. Both the wavefunction in a billiard and the electric field in a cavity satisfy the Helmholtz equation with the Dirichlet conditions. A technique was developed [35] that allows to measure the spatial distribution of the magnitude of electric field in a microwave cavity.

$m$	$E_m + 4/\pi$	$\omega_{\text{num}}$	$\omega_{\text{theor}}$
1	0.2083	5.6199	5.6310
3	0.4321	5.7701	5.7680
5	0.6053	5.8726	5.8741
7	0.7544	5.9661	5.9654
9	0.8878	6.0465	6.0471
11	1.0097	6.1222	6.1218
13	1.1223	6.1904	6.1908
15	1.1272	6.2553	6.2550
17	1.3254	0.0317	0.0319
19	1.4175	0.0885	0.0884
21	1.5040	0.1411	0.1413
23	1.5852	0.1912	0.1911
25	1.6614	0.2376	0.2378
27	1.7327	0.2814	0.2814
29	1.7989	0.3217	0.3220
31	1.8599	0.3592	0.3593
33	1.9152	0.3924	0.3932
35	1.9638	0.4243	0.4229
37	2.0010	0.4461	0.4458

Table 2.1: Numerical ( $\omega_{\text{num}}$ ) and theoretical ( $\omega_{\text{theor}}$ ) eigenphases modulo  $2\pi$ , compared for states with different  $m$ , but all belonging to the same low angular momentum resonance.  $\Delta R$  corresponds to the stadium billiard. WKB “energy” parameter  $E_m - V_{\text{min}}$  is also given,  $k = 1000$  and  $\epsilon = 6.1 \times 10^{-4}$  are fixed.

$n$	$E_m + 4/\pi$	$k_{\text{num}}$	$k_{\text{theor}}$
319	1.0108	998.3207	998.3213
318	1.0128	995.1784	995.1789
317	1.0148	992.0358	992.0364
316	1.0169	988.8934	988.8940
315	1.0190	985.7509	985.7515
314	1.0210	982.6085	982.6090
313	1.0231	979.4660	979.4666
312	1.0252	976.3235	976.3241
311	1.0273	973.1810	973.1816
310	1.0294	970.0387	970.0392

Table 2.2: Energies  $k$  with different quantum numbers  $n$ , but same  $m = 11$ , computed numerically and found solving Eq. (2.34).  $\epsilon$  as in Table 2.1.

## 2.4 Two-dimensional wavefunctions

Although the surface of section wavefunction  $\psi(\theta)$  together with the quantization conditions contain most information about the state, it might be occasionally necessary to reconstruct the actual two-dimensional wavefunction  $\Psi(r, \theta)$  in the billiard. The procedure is straight-forward and involves evaluation of the integral (1.33) by the  $S\Phi$ .

We start with the PSS wavefunction (or one of its branches)

$$\psi(\theta) = \frac{1}{\sqrt{f_1'(\theta)}} e^{il_{pq}\theta + ik[bf_1(\theta) + b^2 f_2(\theta)]} \quad (2.53)$$

where  $b = \sqrt{\epsilon}$ . Without worrying about normalization, and thus leaving out constant factors, we write the Green function (1.34)

$$\tilde{G}(\mathbf{r}, \theta') = \left| \frac{\partial^2 L(\mathbf{r}, \theta')}{\partial r_\perp \partial \theta'} \right|^{1/2} e^{ikL(\mathbf{r}, \theta')} \quad (2.54)$$

where  $L(\mathbf{r}, \theta')$  is the length of a direct orbit between point  $\theta'$  on the boundary and point  $\mathbf{r} = (r, \theta)$  inside the billiard. In the unperturbed billiard there are two such orbits of angular



momentum  $l_{pq}$  for any given  $\mathbf{r}$  (Fig. 2.12). They start at the points

$$\theta'_{1,2} = \theta - \frac{\Theta_{pq}}{2} \pm \cos^{-1} \left( \frac{l_{pq}}{kr} \right) \quad (2.55)$$

on the boundary. These points will satisfy the lowest order stationary phase condition in the integral  $\int d\theta' \tilde{G}(\mathbf{r}; \theta') \psi(\theta')$ . We therefore can expand the phase of the integrand in  $\delta\theta' = \theta' - \theta'_{1,2} \sim b$ . We keep terms up to  $b^2$ . In the prefactor we keep only the lowest order. It can be shown that at these points

$$\frac{\partial^2 L}{\partial r_{\perp} \partial \theta'} = -\frac{\gamma(1)}{L_{1,2}^{(0)}} \quad (2.56)$$

where

$$L_{1,2}^{(0)} = L^{(0)}(\mathbf{r}, \theta'_{1,2}) = \gamma(1) \mp \gamma(r) \quad (2.57)$$

is the length of the orbits for an unperturbed circle and

$$\gamma(r) = \sqrt{r^2 - (l_{pq}/k)^2}. \quad (2.58)$$

Integrating over  $\delta\theta'$  near the two stationary points we find the two-dimensional wavefunction (up to a constant factor)

$$\Psi(\mathbf{r}) = \sum_{1,2} \frac{\psi(\theta'_{1,2})}{\sqrt{k\gamma(r)}} e^{ikL_{1,2}^{(0)} + ikb^2 \left[ \gamma(1)\Delta R(\theta'_{1,2}) \mp \frac{f_1'^2(\theta'_{1,2})L_{1,2}^{(0)}}{2\gamma(1)\gamma(r)} \right] \pm i\frac{\pi}{4}}, \quad r > \frac{l_{pq}}{k}, \quad (2.59)$$

$$\Psi(\mathbf{r}) \approx 0, \quad r < \frac{l_{pq}}{k}. \quad (2.60)$$

Note that the theory breaks down when  $r \rightarrow (l_{pq}/k)$ . This is easy to understand in the case of a perfect circle. Indeed,  $r = l/k$  is a caustic for the trajectories with angular momentum  $l$ . The semiclassical approximation normally fails near caustics. There are no classical trajectories in the region  $r < l/k$ , which means that the wavefunction should be exponentially small there. This is the case for the Bessel function  $J_l(kr)$  for  $r < l/k$  and  $l \gg 1$  [41].

The explicit form of wavefunction (2.59) is rather cumbersome in the general case. It simplifies significantly for the  $l = 0$  resonance. In this case  $\theta'_1 = \theta$  and  $\theta'_2 = \theta - \pi$  and the wavefunction becomes

$$\Psi(\mathbf{r}) = \frac{\cos \Gamma}{\sqrt{kr}} \frac{\exp ikbf_1(\theta)}{\sqrt{f_1'(\theta)}}, \quad (2.61)$$

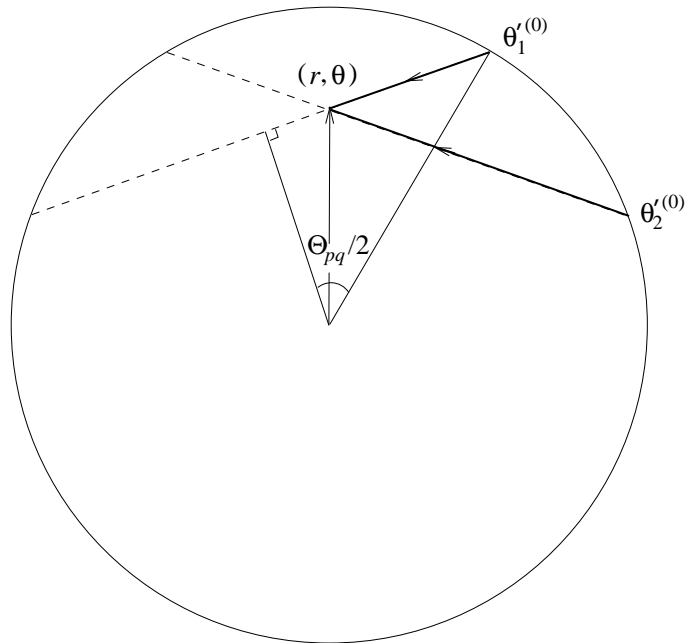


Figure 2.12: Two orbits with angular momentum  $l_{pq} = (\text{sgn})k \cos(\Theta_{pq}/2)$  in the circular billiard arriving at point  $(r, \theta)$  from points  $\theta_{1,2}^{(0)}$  on the boundary.

$$\Gamma \equiv kr + kb^2 \left[ \frac{f_1'^2}{2r} - \frac{\Delta R(\theta) - \Delta R(\theta - \pi)}{2} \right] - \pi \left( \frac{m}{2} + \frac{1}{4} \right). \quad (2.62)$$

We assumed that  $\omega_m = \pi m$  in Eq. (2.11) and dropped all constant factors. The non- $\pi$ -periodic correction to the phase  $kb^2 \tilde{f}_2(\theta) = 0$  for the lowest resonance and the  $\pi$ -periodic  $kb^2 \bar{f}_2(\theta)$  can be included in the phase, if needed. Note that the first factor in Eq. (2.61) is the Debye expansion [41] for a linear combination of Bessel's functions  $\alpha(\theta) J_l(kr) + \beta(\theta) N_l(kr)$  with  $l \equiv kb f_1'$  when

$$kr \gg l \gg 1. \quad (2.63)$$

This relation will reemerge in Sec. 5.4 where we solve the same problem by the Born-Oppenheimer approximation. Equation (2.63) sets the limits of *our* theory, as well. Indeed, if  $\mathbf{r}$  is close to the center of the billiard, the stationary phase trajectory connecting this point with the boundary is not well-defined.

It is instructive to show that the two-dimensional wavefunction (2.59) satisfies Dirichlet's conditions on the boundary. When we substitute  $r = 1 + b^2 \Delta R(\theta)$ , we find

$$\theta_1^{(0)} \cong \theta + \frac{b^2 \Delta R(\theta) l_{pq}}{\gamma(1) k}, \quad \theta_2^{(0)} \cong \theta - \Theta_{pq} - \frac{b^2 \Delta R(\theta) l_{pq}}{\gamma(1) k}, \quad (2.64)$$

$$\gamma(r) \cong \gamma(1) + \frac{b^2 \Delta R(\theta)}{\gamma(1)}, \quad (2.65)$$

$$L_1^{(0)} \cong -\frac{b^2 \Delta R(\theta)}{\gamma(1)}, \quad L_2^{(0)} \cong 2\gamma(1) + \frac{b^2 \Delta R(\theta)}{\gamma(1)}. \quad (2.66)$$

We use these expressions in Eq. (2.59) keeping terms up to order  $b^2$  in the phase and the lowest order in the prefactor. Note that the wavefunction  $\Psi(\mathbf{r}) \propto \cos[(\phi_1 - \phi_2)/2]$ , where  $\phi_i$  are the phases of the two terms in Eq. (2.59). Using Eqs. (2.21),<sup>2</sup> (2.22), and (2.34) one can show that the cosine argument is  $\pi/2 - \pi n$ , completing the proof.

The examples of the two-dimensional wavefunctions in the short stadium are shown in Figs. 2.5, 2.6, and 2.8.

## 2.5 Additional remarks

---

<sup>2</sup>The constant in this equation is  $-\delta \Theta_{pq}/kb$ , where  $\delta$  is the fractional part of  $l_{pq}$ , as explained in Sec. 2.2.4

### 2.5.1 The prefactor

It was noted in Sec. 2.2.3 that the PSS wavefunction  $\psi(\theta)$  has a standard WKB prefactor  $[f'_1(\theta)]^{-1/2}$  if  $k\epsilon |E_m - \bar{V}_q(\theta)| \ll 1$ . Now we lift this restriction. We solve Bogomolny's equation

$$\psi(\theta) = \int d\theta' T(\theta, \theta') \psi(\theta') \quad (2.67)$$

with the ansatz in general form

$$\psi(\theta) = \exp \left[ il_{pq}\theta + ik \sum_{n=1}^{\infty} b^n f_n(\theta) \right] \quad (2.68)$$

where  $b = \sqrt{\epsilon}$ . We will be interested in the imaginary part of the phase. To evaluate the integral (2.67) by  $S\Phi$  we expand the phase of the integrand in  $\delta\theta' = \theta' - \theta + \Theta_{pq}$ . This phase is

$$\phi(\theta, \theta') = kL_0(\theta, \theta') + l_{pq}\theta + k \sum_{n=1}^{\infty} b^n F_n(\theta, \theta') \quad (2.69)$$

where  $F_n(\theta, \theta') = L_n(\theta, \theta') + f_n(\theta)$ . Here  $L_n(\theta, \theta')$  is the term in the expansion of the chord length in Eq. (2.3),  $L(\theta, \theta') = \sum_{n=0}^{\infty} b^n L_n(\theta, \theta')$ ,  $L_n = 0$  for odd  $n$ .

The integral (2.67) is equal to

$$\left[ 1 + \left( \sum_{n=1}^{\infty} b^n F_n''/L_0'' \right) \right]^{-1/2} \exp i \left[ \phi(\theta, \theta - \Theta_{pq}) - k \frac{(\sum_{n=1}^{\infty} b^n F_n')^2}{L_0'' + \sum_{n=1}^{\infty} b^n F_n''} + \frac{\pi}{2} \right] \quad (2.70)$$

where all functions are evaluated at  $\theta' = \theta + \Theta_{pq}$  and all the derivatives are with respect to  $\theta'$ .

The prefactor can be moved to the exponent by the transformation

$$\left[ 1 + \left( \sum_{n=1}^{\infty} b^n F_n''/L_0'' \right) \right]^{-1/2} = \exp \left[ -\frac{bf_1''}{2L_0''} \right] + O(b^2). \quad (2.71)$$

It adds the imaginary component to the phase in Eq. (2.70). This phase should be equal to the phase in the *l.h.s.* of Eq. (2.67). The imaginary part of the resulting equation is

$$\text{Im} \left\{ k \sum_{n=1}^{\infty} b^n [f_n(\theta) - f_n(\theta - \Theta_{pq})] + k \frac{(\sum_{n=1}^{\infty} b^n F_n')^2}{L_0'' + \sum_{n=1}^{\infty} b^n F_n''} \right\} = \frac{bf_1''}{2L_0''} + O(b^2). \quad (2.72)$$

We need to keep terms only to the order  $b$ . Suppose we can choose  $n_0$  such that  $kb^{n_0+1} \sim b$ . Let us make a self-consistent assumption that there is no variable imaginary part in  $f_n(\theta)$  for  $n < n_0$ . Collecting terms of order  $kb^{n_0+1}$  we can write

$$\text{Im} \left[ f_{n_0+1}(\theta) - f_{n_0+1}(\theta - \Theta_{pq}) + \frac{f_1' f_{n_0}'}{L_0''} \right] = \frac{f_1''}{2kb^{n_0} L_0''}. \quad (2.73)$$

After the  $q$ -average we obtain the equation

$$kb^{n_0} \text{Im} \bar{f}'_{n_0} = \frac{f_1''}{2f_1'} = \left( \ln \sqrt{f_1'} \right)' \quad (2.74)$$

which means that the prefactor in function  $\psi(\theta)$  is  $e^{-\ln \sqrt{f_1'} + O(b^2)} = 1/\sqrt{f_1'} + O(b^2)$ . Note that  $\text{Im} f_{n_0}$  is  $q$ -periodic since, according to Eq. (2.72),  $\text{Im} [f_{n_0}(\theta) - f_{n_0}(\theta - \Theta_{pq})] = 0$ .

## 2.5.2 Fourier expanded perturbation

Consider a system described by the perturbed Hamiltonian (2.1). Suppose the perturbation is expanded in Fourier series

$$H_2(\mathbf{I}, \theta) = \sum_{\mathbf{m}} H_{\mathbf{m}}(\mathbf{I}) e^{i\mathbf{m}\cdot\theta}. \quad (2.75)$$

It is known in the classical perturbation theory [74] that each Fourier component produces a resonance when  $\mathbf{I}$  satisfies the equation

$$\omega(\mathbf{I}) \cdot \mathbf{m} = 0 \quad (2.76)$$

where  $\omega(\mathbf{I}) = \partial H_0(\mathbf{I}) / \partial \mathbf{I}$  are the unperturbed frequencies. Below we show that the semiclassical theory agrees with this condition.

Suppose the perturbation consists of one component  $H_{\mathbf{m}}(\mathbf{I}) e^{i(m_1\theta_1 + m_2\theta_2)}$ . We choose the surface of section  $\theta_2 = 0$ , as in Sec. 2.1. We show that the effective potential for the  $(p, q)$  resonance  $\bar{V}_q(\theta_1) = 0$  unless  $\omega_1/\omega_2 = p/q = -m_2/m_1$ . The perturbed action  $S_2(\theta, \theta'; E) = -\int H_2 dt$ , where the integral is taken over the unperturbed trajectory between two consecutive crossings of the PSS at  $\theta_1 = \theta'$  and  $\theta_1 = \theta$ . With the substitution  $\theta_1 = \theta' + \omega_1 t$  and  $\theta_2 = \omega_2 t$  we find

$$S_2(\theta, \theta'; E) = -\frac{H_{\mathbf{m}} e^{im_1\theta'}}{\omega_2} \int_0^{2\pi} \exp \left[ i \left( m_1 \frac{\omega_1}{\omega_2} + m_2 \right) \theta_2 \right] d\theta_2. \quad (2.77)$$

Note that  $H_{\mathbf{m}}(\mathbf{I})$  and  $\omega_i(\mathbf{I})$  depend on  $\theta - \theta'$  and  $E$ . The effective potential

$$\bar{V}_q(\theta) = \langle S_2(\theta, \theta - \Theta_{pq}; E) \rangle_q \propto \sum_{r=0}^{q-1} e^{2\pi i m_1 r p/q} = 0 \quad (2.78)$$

unless  $m_1 p/q \equiv l$  is integer. But in this case  $\int_0^{2\pi} \exp \left[ i \left( m_1 \frac{\omega_1}{\omega_2} + m_2 \right) \theta_2 \right] d\theta_2 = 0$ , except when  $l = -m_2$ , i.e.  $\omega \cdot \mathbf{m} = 0$ . In the latter case  $\bar{V}_q(\theta) = -\frac{2\pi}{\omega_2} H_{\mathbf{m}} e^{im_1\theta}$ . Note that the current definition of  $\bar{V}_q(\theta)$  differs from one in Sec. 2.2.3 by a factor of  $k$ .

### 2.5.3 Direct quantization of classical perturbation theory

In Sec. 2.3.1 we have mentioned that some results of the classical perturbation theory follow from our semiclassical theory. In fact, the connection between the two theories is even closer. In this section we are going to show how one could develop the semiclassical theory in the action-angle variables solely on the grounds of the classical *resonant* perturbation theory, without employing the  $T$ -operator formalism.

#### First order theory

We begin with the classical Hamiltonian (2.1) keeping terms to order  $\epsilon$ . We will quantize the orbits near the  $(p, q)$  resonance, for which the ratio of unperturbed frequencies  $\omega_1/\omega_2 = p/q$ . Following the recipe [52], we make a canonical transformation to the rotating frame  $(\mathbf{I}, \theta) \rightarrow (\hat{\mathbf{I}}, \hat{\theta})$  defined by the equations

$$I_1 = q\hat{I}_1, \quad I_2 = \hat{I}_2 - p\hat{I}_1, \quad (2.79)$$

$$\hat{\theta}_1 = q\theta_1 - p\theta_2, \quad \hat{\theta}_2 = \theta_2. \quad (2.80)$$

The new Hamiltonian is  $\hat{H}(\hat{\mathbf{I}}, \hat{\theta}) = H(\mathbf{I}(\hat{\mathbf{I}}), \theta(\hat{\theta}))$ . Like the original Hamiltonian, it can be expanded in the perturbation series

$$\hat{H}(\hat{\mathbf{I}}, \hat{\theta}) = \hat{H}_0(\hat{\mathbf{I}}) + \epsilon\hat{H}_2(\hat{\mathbf{I}}, \hat{\theta}). \quad (2.81)$$

The new variable  $\hat{\theta}_1$  is “slow”, i.e.  $\dot{\hat{\theta}}_1 \simeq q\omega_1 - p\omega_2 \ll \dot{\hat{\theta}}_2$ . It describes the slow deviation from the resonance. Under this condition one can make an *infinitesimal* canonical transformation  $(\hat{\mathbf{I}}, \hat{\theta}) \rightarrow (\bar{\mathbf{I}}, \bar{\theta}) = (\hat{\mathbf{I}}, \hat{\theta}) + O(\epsilon)$  that would eliminate the  $\hat{\theta}_2$ -dependence from the Hamiltonian. The transformed Hamiltonian has the form

$$\bar{H}(\hat{I}_1, \hat{\theta}_1; \hat{I}_2) = \hat{H}_0(\hat{\mathbf{I}}) + \epsilon\bar{H}_2(\hat{I}_1, \hat{\theta}_1; \hat{I}_2) \quad (2.82)$$

where the perturbed part is simply the average of  $\hat{H}_2$  over  $\hat{\theta}_2$ ,

$$\bar{H}_2(\hat{I}_1, \hat{\theta}_1; \hat{I}_2) = \frac{1}{2\pi q} \int_0^{2\pi q} \hat{H}_2(\hat{\mathbf{I}}, \hat{\theta}) d\hat{\theta}_2. \quad (2.83)$$

(When  $\hat{\theta}_1$  is fixed, the period of  $\hat{H}_2$  in variable  $\hat{\theta}_2$  is  $2\pi q$ .) At this stage we neglect the difference between the “hatted” and “barred” variables.

Now the problem becomes essentially one-dimensional.  $\hat{I}_2 = \hat{I}_{20} = \text{const}$  is an integral of motion. We define  $\hat{I}_{10}$  by the resonance condition

$$\left. \frac{\partial \hat{H}_0}{\partial \hat{I}_1} \right|_{\hat{I}_1 = \hat{I}_{10}} = 0. \quad (2.84)$$

(The meaning of this definition will become clear later, when we transform back to the original variables.) The energy conservation  $\bar{H} = E$  requires

$$\frac{\hat{H}_0''}{2} (\Delta \hat{I}_1)^2 + \epsilon \bar{H}_2(\hat{\mathbf{I}}_0, \hat{\theta}_1) = E - E_0. \quad (2.85)$$

Here  $\Delta \hat{I}_1 = \hat{I}_1 - \hat{I}_{10}$ ,  $E_0 = \hat{H}_0(\hat{\mathbf{I}}_0)$ , and  $\hat{H}_0'' = (\partial^2 \hat{H}_0 / \partial \hat{I}_1^2)_{\hat{\mathbf{I}} = \hat{\mathbf{I}}_0}$ . Remarkably, Eq. (2.85) is similar to the energy conservation law for a one-dimensional particle of mass  $\hat{H}_0''$  with momentum  $\Delta \hat{I}_1$  moving in a potential  $\epsilon \bar{H}_2(\hat{\mathbf{I}}_0, \hat{\theta}_1)$ . We will quantize it by changing the variables to the appropriate operators, but first we will express the constant parameters in terms of the original actions  $\mathbf{I}_0$ .

To begin with, note that

$$\frac{\partial \hat{H}_0}{\partial \hat{I}_1} = q\omega_1(\mathbf{I}) - p\omega_2(\mathbf{I}) \quad (2.86)$$

so that condition (2.84) means that  $\hat{\mathbf{I}}_0$  is a resonant torus. To calculate the second derivative, it is convenient to express  $(\partial / \partial \hat{I}_1)_{\hat{I}_2}$  in terms of  $(\partial / \partial I_1)_E$ . Using the notation from Sec. 1.7,  $I_2 = g_E(I_1)$  and  $\alpha(\mathbf{I}) = \omega_1(\mathbf{I}) / \omega_2(\mathbf{I}) = -g'_E(I_1)$ , we can write

$$\frac{1}{q} \left( \frac{\partial}{\partial \hat{I}_1} \right)_{\hat{I}_2} = \left( \frac{\partial}{\partial I_1} \right)_{I_2} - \alpha(\mathbf{I}) \left( \frac{\partial}{\partial I_2} \right)_{I_1} = \left( \frac{\partial}{\partial I_1} \right)_E. \quad (2.87)$$

Then the second derivative becomes

$$\hat{H}_0'' = q \left( \frac{\partial \omega_2(q\alpha - p)}{\partial I_1} \right)_E = -q^2 \omega_2 g''_E \Big|_{\mathbf{I} = \mathbf{I}_0} \quad (2.88)$$

where we took into account that  $q\alpha - p = 0$  at the resonance. If the PSS is chosen at  $\theta_2 = 0$ , we can express  $\hat{H}_0''$  in terms of the unperturbed action (2.2). We have shown in Sec. 1.7 that  $S_0''(\Theta_{pq}) = -(2\pi g''_E)^{-1}$ , therefore

$$\hat{H}_0'' = \frac{q^2 \omega_2}{2\pi S_0''(\Theta_{pq})}. \quad (2.89)$$

Now let us take care of the potential term in Eq. (2.85). Returning to the original variables we write

$$\bar{H}_2(\hat{\mathbf{I}}_0, \hat{\theta}_1) = \frac{\omega_2}{2\pi q} \int_0^{2\pi q / \omega_2} H_2 \left( \mathbf{I}_0, \theta_1 = \frac{\hat{\theta}_1}{q} + \omega_1 t, \theta_2 = \omega_2 t \right) dt. \quad (2.90)$$

Note that the correction to the action between two crossings of the surface of section  $S_2(\theta_1, \theta_1 - \Theta_{pq}) = -\int_0^{2\pi/\omega_2} H_2 dt$  where the integral is taken along the unperturbed orbit. If we define the effective potential as a  $q$ -average  $\bar{V}_q(\theta_1) = \langle S_2(\theta_1, \theta_1 - \Theta_{pq}) \rangle_q$ , we find that

$$\bar{H}_2(\hat{\mathbf{I}}_0, \hat{\theta}_1) = -\frac{\omega_2}{2\pi} \bar{V}_q(\theta_1 = \hat{\theta}_1/q). \quad (2.91)$$

Equation (2.85) can be transformed to the Schrödinger equation by changing  $\Delta \hat{I}_1 \rightarrow -i\partial/\partial \hat{\theta}_1$ . With the help of Eqs. (2.89) and (2.91), we have

$$\frac{1}{2S_0''(\Theta_{pq})} \frac{\partial^2 \hat{\psi}}{\partial (\hat{\theta}_1/q)^2} + \epsilon \bar{V}_q(\hat{\theta}_1/q) \hat{\psi} = \epsilon \mathcal{E} \hat{\psi} \quad (2.92)$$

where

$$\epsilon \mathcal{E} = -(2\pi/\omega_2)(E - E_0). \quad (2.93)$$

It is easy to construct the complete wavefunction, which is trivial in  $\hat{\theta}_2$ ,

$$\Psi(\theta_1, \theta_2) = \hat{\psi}\left(\frac{\hat{\theta}_1}{q}\right) e^{i\hat{\mathbf{I}}_0 \cdot \hat{\theta}} = \hat{\psi}\left(\theta_1 - \frac{p}{q}\theta_2\right) e^{i\mathbf{I}_0 \cdot \theta}. \quad (2.94)$$

Setting  $\theta_2 = 0$  we obtain the one-dimensional wavefunction that would also follow from the first order perturbation theory based on the  $T$ -operator. In fact, Eq. (2.92) is similar to Eq. (2.30) when  $\theta_1 = \hat{\theta}_1/q$ . Thus both theories are equivalent to this order.

### Quantization conditions

The quantization conditions follow from the requirement that  $\Psi(\theta_1, \theta_2)$  be  $2\pi$ -periodic in both variables up to the Maslov phases. With

$$\hat{\psi}(\theta + 2\pi) = \hat{\psi}(\theta) \exp(-i2\pi\delta), \quad (2.95)$$

where  $0 \leq \delta < 1$  is to be determined, we obtain two equations,

$$I_{10} = l + \nu_l + \delta, \quad (2.96)$$

$$I_{20} = n + \nu_n - \frac{p}{q}\delta. \quad (2.97)$$

Here  $l$  and  $n$  are integer and  $\nu_l$  and  $\nu_n$  are the Maslov phases. Since  $I_{10}$  and  $I_{20}$  are related by the resonance condition (2.84), the above equations allow us to express  $\delta$ ,  $I_{10}$ , and  $I_{20}$  in terms of  $l$  and  $n$ . Note that  $l$  and  $n$  are not independent. Usually  $l, n \gg \delta$ , so they are related



by the resonance condition on  $I_{10}$  and  $I_{20}$ . In the perturbed circle, for example,  $l$  is an integer part of  $l_{pq}$ .

The Schrödinger equation (2.92) with Eq. (2.95) as the boundary condition provides the quantized “energy” levels  $\mathcal{E}_m$ . The total energy

$$E = H_0(\mathbf{I}_0) - \epsilon \mathcal{E}_m \frac{\omega_2(\mathbf{I}_0)}{2\pi} \quad (2.98)$$

is found from Eq. (2.93).

Let us compare this result with the quantization condition given by the  $T$ -operator [cf. Eq. (2.34)],

$$S_0(\Theta_{pq}, E) - (l + \nu_l) \Theta_{pq} + \epsilon \mathcal{E}_m = 2\pi(n + \nu_n). \quad (2.99)$$

Here  $S_0(\Theta_{pq}, E)$  is the action for an unperturbed system with energy  $E$  between two crossings of the PSS  $\theta_2 = 0$  with the difference in  $\theta_1$  equal  $\Theta_{pq}$ . By inverting the function  $S_0$  one finds the energy

$$E = H_0[\Delta\theta_1 = \Theta_{pq}, S = (l + \nu_l) \Theta_{pq} + 2\pi(n + \nu_n) - \epsilon \mathcal{E}_m]. \quad (2.100)$$

It can be shown that  $(\partial H_0 / \partial S)_{\Delta\theta_1} = \omega_2 / 2\pi$ . Hence expanding the above equation in  $\epsilon$  we obtain Eq. (2.98), taking into account that  $H_0(\mathbf{I}_0) = H_0[\Delta\theta_1 = \Theta_{pq}, S = \Theta_{pq} I_{10} + 2\pi I_{20}]$ .

## Second order theory

To find the next order correction to the wavefunction (2.94) we need to take into account the difference between the coordinates  $(\hat{\mathbf{I}}, \hat{\theta})$  and  $(\bar{\mathbf{I}}, \bar{\theta})$  defined above. In particular,  $\Delta \hat{I}_1$  in Eq. (2.85) should be changed to

$$\Delta \bar{I}_1 = \Delta \hat{I}_1 - \epsilon \frac{\partial F}{\partial \hat{\theta}_1} \quad (2.101)$$

where the function  $F(\hat{\mathbf{I}}_0, \hat{\theta})$  can be determined from the equation [52]

$$\omega_2 \frac{\partial F}{\partial \hat{\theta}_2} \cong \bar{H}_2(\hat{\mathbf{I}}_0, \hat{\theta}_1) - \hat{H}_2(\hat{\mathbf{I}}_0, \hat{\theta}). \quad (2.102)$$

The solution of the Schrödinger equation will be modified by a factor  $\exp(i\epsilon F)$ .

The two-dimensional wavefunction becomes

$$\Psi(\theta_1, \theta_2) = \hat{\psi} \left( \frac{\hat{\theta}_1}{q} \right) e^{i\hat{\mathbf{I}}_0 \cdot \hat{\theta} + i\epsilon F(\hat{\mathbf{I}}_0, \hat{\theta})}. \quad (2.103)$$

Function  $F$  should satisfy Eq. (2.102) and have period  $2\pi$  in  $\theta_1$  and  $\theta_2$ . Hence the energy quantization does not change. Explicitly,

$$F(\hat{\theta}_1, \hat{\theta}_2) = \frac{1}{\omega_2} \int_0^{\hat{\theta}_2} [\bar{H}_2(\hat{\theta}_1) - \hat{H}_2(\hat{\theta}_1, \hat{\theta}'_2)] d\hat{\theta}'_2 + f_2 \left( \theta_1 = \frac{\hat{\theta}_1}{q} \right) \quad (2.104)$$

where we dropped argument  $\hat{\mathbf{I}}_0$  to shorten notation. The function  $f_2(\theta_1)$  comes from the  $T$ -operator theory. It is the second order term in the phase of the PSS wavefunction  $\psi(\theta_1) = \hat{\psi}(\theta_1) \exp[iI_{10}\theta_1 + i\epsilon f_2(\theta_1)]$  and it should satisfy the equation

$$\begin{aligned} f_2(\theta_1 + \Theta_{pq}) - f_2(\theta_1) &= S_2(\theta_1 + \Theta_{pq}, \theta_1) - \bar{V}_q(\theta_1) \\ &= \frac{1}{\omega_2} \int_0^{2\pi} [\bar{H}_2(\hat{\theta}_1) - \hat{H}_2(\hat{\theta}_1, \hat{\theta}'_2)]_{\hat{\theta}_1=q\theta_1} d\hat{\theta}'_2. \end{aligned} \quad (2.105)$$

The  $2\pi$ -periodicity in  $\theta_1$  for  $F(\hat{\theta})$  is trivial. To show that it is  $2\pi$ -periodic in  $\theta_2$  consider

$$\begin{aligned} &\int_0^{\hat{\theta}_2+2\pi} \hat{H}_2(\hat{\theta}_1 - 2\pi p, \hat{\theta}'_2) d\hat{\theta}'_2 = \int_0^{\hat{\theta}_2+2\pi} \hat{H}_2(\hat{\theta}_1, \hat{\theta}'_2 - 2\pi) d\hat{\theta}'_2 \\ &= \int_0^{\hat{\theta}_2} \hat{H}_2(\hat{\theta}_1, \hat{\theta}'_2) d\hat{\theta}'_2 + \int_{-2\pi}^0 \hat{H}_2(\hat{\theta}_1, \hat{\theta}'_2) d\hat{\theta}'_2. \end{aligned} \quad (2.106)$$

Then it follows from Eq. (2.105) that  $F(\hat{\theta}_1 - 2\pi p, \hat{\theta}_2 + 2\pi) = F(\hat{\theta}_1, \hat{\theta}_2)$ , which is the desired result.

Note that  $F(\hat{\theta})$  is defined up to an arbitrary function  $F_1(\hat{\theta}_1)$ . This function is constant along the unperturbed resonant trajectory. This trajectory crosses the PSS  $\theta_2 = 0$  at  $q$  points separated by angle  $\Delta\theta_1 = 2\pi/q$ . Since  $F_1(\hat{\theta}_1)$  must be single-valued on the torus  $(\theta_1, \theta_2)$ , it has to be  $2\pi$ -periodic in  $\hat{\theta}_1$ .

The above results are in agreement with the  $T$ -operator perturbation theory. To see this set  $\hat{\theta}_2 = 0$ . Then  $F(q\theta_1, 0) = f_2(\theta_1)$ , defined up to a  $2\pi/q$ -periodic function  $F_1(q\theta_1)$ .

In conclusion, we have shown that the semiclassical resonant perturbation theory can be constructed on the basis of the classical theory without employing the  $T$ -operator. Both theories are equivalent, at least to the second order. The theory discussed in this section automatically gives the two-dimensional wavefunction. Unfortunately, the use of action-angle variables is rather important. The  $T$ -operator method can be more convenient in practice, since it is not restricted to a specific set of coordinates. Still, even here the unperturbed action should depend on the difference of the surface of section coordinates, which, in effect, limits the choice to the coordinates that are similar to action-angle.

### 2.5.4 Perturbed spherical billiard

It is easy to generalize our theory in the case of low angular momentum resonance in a perturbed spherical billiard. The billiard is a three-dimensional cavity with the boundary  $r(\theta, \varphi) = 1 + \epsilon \Delta R(\theta, \varphi)$ . We choose the PSS to coincide with the boundary, which is now two-dimensional, as well as the surface of section wavefunction  $\psi(\theta, \varphi)$ .

Following the method of Sec. 2.2.2 we expand the  $T$ -operator near  $\theta' = \pi - \theta$ ,  $\varphi' = \varphi - \pi$ . With the notation  $\mathbf{r} = (\theta, \varphi)$  and  $\mathbf{r}' = (\theta', \varphi')$  it becomes

$$T(\mathbf{r}, \mathbf{r}') \simeq -\frac{k \sin \theta}{4\pi i} \exp \left[ i2k \left( 1 - \frac{\delta\theta'^2}{8} - \frac{\delta\varphi'^2}{8} \sin^2 \theta \right) \right] [1 + ik\epsilon V(\mathbf{r})] \quad (2.107)$$

where the effective potential  $V(\mathbf{r}) = \Delta R(\mathbf{r}) + \Delta R(-\mathbf{r})$ . The wavefunction is also expanded up to the quadratic terms. The integral  $\int T(\mathbf{r}, \mathbf{r}') \psi(\mathbf{r}') d(\delta\theta') d(\delta\varphi')$  is evaluated in the  $S\Phi$  approximation. It should be equal to  $\psi(\mathbf{r})$ :

$$e^{i2k} \left\{ \psi(-\mathbf{r}) [1 + ik\epsilon V(\mathbf{r})] + \frac{1}{ik} \left[ \frac{\partial^2 \psi}{\partial \theta^2} + \frac{1}{\sin^2 \theta} \frac{\partial^2 \psi}{\partial \varphi^2} \right] \right\} = \psi(\mathbf{r}). \quad (2.108)$$

Substitute  $\psi(-\mathbf{r}) = e^{-i\omega} \psi(\mathbf{r})$  where  $\omega = 2k + k\epsilon E_{lm}$ . Expanding in  $k\epsilon$  we obtain the differential equation

$$-\left[ \frac{\partial^2 \psi}{\partial \theta^2} + \frac{1}{\sin^2 \theta} \frac{\partial^2 \psi}{\partial \varphi^2} \right] + k^2 \epsilon [V(\mathbf{r}) - E_{lm}] \psi = 0. \quad (2.109)$$

Solving this equation we find possible  $E_{lm}$ 's. Since  $V(\mathbf{r})$  is symmetric the resulting wavefunctions can be made symmetric or antisymmetric. Hence the quantization condition for  $k$  is

$$2k + k\epsilon E_{lm} = 2\pi n + \omega_{lm} \quad (2.110)$$

where  $\omega_{lm} = 0$  or  $\pi$ .

The problem of low angular momentum resonance can also be solved by the Born-Oppenheimer approximation (Sec. 5.4). So far we have not succeeded in treating high angular momentum resonances.

## 2.6 Conclusions

In this chapter we developed the semiclassical resonant perturbation theory. The essence of the theory is to quantize the classical motion near the resonances. The Poincaré surface of section method and its semiclassical analogue, Bogomolny's  $T$ -operator, effectively reduce

the dimensionality of the problem. The number of terms entering the perturbation series is determined by relationship between the parameters  $k$  and  $\epsilon$ . It would be impractical to use this theory if one needs to find *all* states in a certain energy range. Here the states are classified by the regions of phase space (resonances) they belong to. Each resonance is treated separately. We have found the expressions for the PSS wavefunctions and the energy levels within any given resonance. For two-dimensional systems the wavefunctions are the solutions of one-dimensional Schrödinger equation. So, as soon as the effective potential is known, it is easy to predict how the states will look like, before a numerical solution is obtained. The effective potential contains information about all orbits on a perturbed torus, not just the neighborhood of a stable orbit. This, in particular, explains scars near unstable periodic orbits.

It should be noted that the states described by our theory are not necessarily close to the true eigenmodes of the system. The states associated with one resonance can mix appreciably with nearly degenerate states of other resonances. Although the mixing can, in principle, be estimated and the proper eigenmodes can be constructed, it is hard to do it systematically. This observation, however, does not completely invalidate the theory. While the approximate states are not stationary, they may exist for a long time before leaking to other degenerate states. Such states are called the *quasimodes* [3].

There are a number of other methods that deal with perturbed integrable systems. The quantization of the Birkhoff-Gustavson normal form [15, 38, 68] can be considered complementary to the present method. Birkhoff-Gustavson is applied to the systems that are, essentially, perturbed harmonic oscillators. Our theory works for strongly anharmonic systems, as was remarked earlier. In addition, the Birkhoff-Gustavson method requires numerous algebraic transformations, which in practice makes it numerical. The adiabatic methods based on the Born-Oppenheimer approximation (BOA) will be discussed in Ch. 5. These methods are equivalent to our perturbation theory in certain cases. The BOA is rather straightforward and easy to understand since it is applied directly to the Schrödinger equation. It does not require the surface of section and automatically produces the two-dimensional wavefunction. Unfortunately, its application is limited to the cases where a slowly changing parameter can be found. For example, only the low angular momentum resonance in the perturbed circle can be studied by the BOA, while the perturbation theory does all of them.

## Chapter 3

# Rectangular billiard and other systems

In the previous chapter we developed the resonant perturbation theory for a perturbed circular billiard. Now we apply this theory to the perturbed rectangular billiard. In the second half of the chapter we consider examples of the systems without an explicit small parameter. It is sometimes possible to tailor the  $T$ -operator approach to these systems on the case-by-case basis in order to study certain classes of states, like bouncing ball or whispering gallery modes. The surface of section method can also be used for the scattering problems.

### 3.1 Rectangular billiard — general case

This section has mostly an auxiliary purpose. We consider a rectangular billiard with slightly perturbed sides. A number of particular cases of this model has been studied such as the tilted billiard, the long stadium, or the square in magnetic field. We will use the general results of this chapter when discussing these examples. The last case is particularly interesting since the perturbation here is the magnetic field (that breaks the time-reversal symmetry) rather than the shape of the boundaries. A separate chapter is devoted to this example.

#### 3.1.1 Classification of trajectories

Consider a rectangle defined by its vertices  $(0, 0)$ ,  $(X, 0)$ ,  $(X, Y)$ , and  $(0, Y)$ , where  $X, Y > 0$ . The boundary shape, starting with the lower boundary and going clockwise, is described by

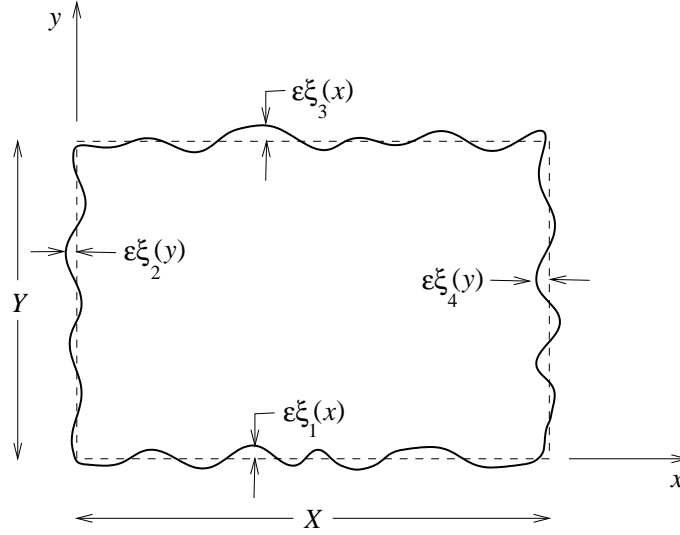


Figure 3.1: Perturbed rectangular billiard.

the functions (Fig. 3.1)

$$\begin{aligned}
 y &= \epsilon \xi_1(x), & 0 < x < 1, \\
 x &= \epsilon \xi_2(y), & 0 < y < 1, \\
 y &= Y - \epsilon \xi_3(x), & 0 < x < 1, \\
 x &= X - \epsilon \xi_4(y), & 0 < y < 1.
 \end{aligned} \tag{3.1}$$

In the following we assume  $\epsilon \ll 1$ , while  $|\xi_i| \sim |\xi'_i| \sim X \sim Y \sim 1$ . The averages  $\langle \xi_i \rangle = 0$ . Note that, by definition,  $\xi_i > 0$  inside the unperturbed billiard. All the conclusions concerning the relationship between the dimensionless wavenumber  $k$  and the perturbation parameter  $\epsilon$  made for the circle billiard remain in force. In particular, if  $ke^{3/2} \ll 1$ , it suffices to continue the perturbation expansion up to the second order (assuming there are no extremely large higher derivatives of  $\xi_i$ ).

We choose the lower boundary of the billiard as the Poincaré surface of section (PSS). Thus, an orbit might bounce off three other walls several times between the two consecutive mappings. We will classify the orbits according to their topology in the unperturbed billiard. But, first, we introduce an equivalent representation for the trajectories, using the method of

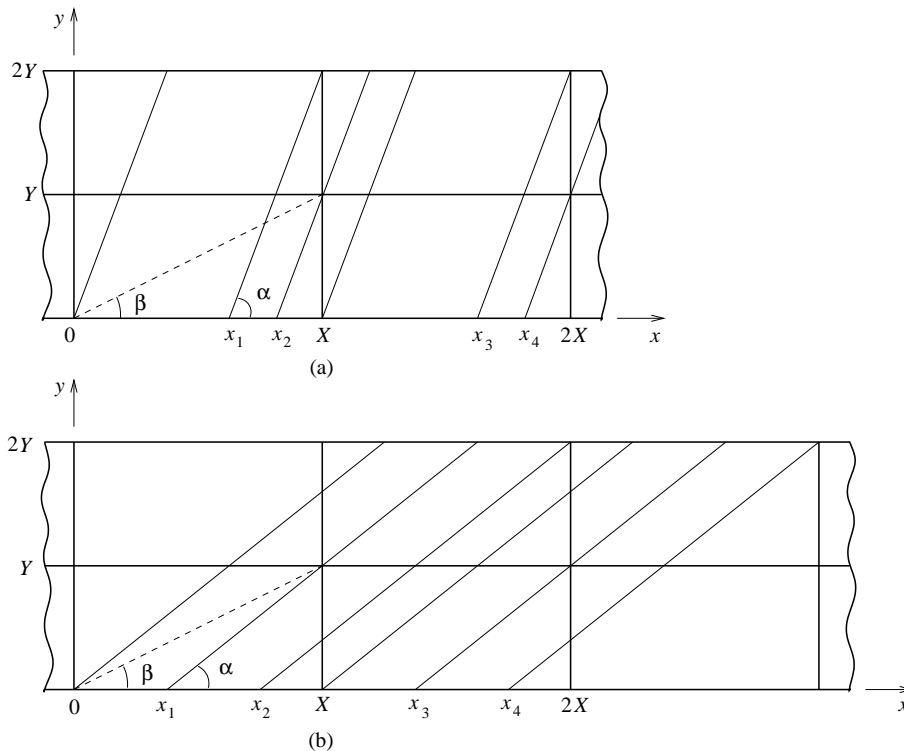


Figure 3.2: Method of images for the rectangular billiard. (a)  $\tan \alpha > 2 \tan \beta$ , (b)  $\tan \beta < \tan \alpha < 2 \tan \beta$ , where  $\alpha$  is the angle that the orbits make with the  $x$  axis,  $\tan \beta = Y/X$ . The orbits starting within the intervals defined by points  $x_i$  and the vertices reflect from the same sequences of the walls.

images. Assuming for the moment there is no perturbation, we reflect the billiard about its upper side and attach the image to the original. Then we reflect the resulting billiard about its right side to obtain a  $2X \times 2Y$  billiard. After that we continue this billiard periodically in  $x$ -direction. Thus, we have an infinite strip of width  $2Y$  (Fig. 3.2). The PSS  $y = 0$  is identified with  $y = 2Y$ . All orbits go from the bottom to the top.

Suppose an orbit makes angle  $\alpha$  with the  $x$ -axis. We can always assume  $0 < \alpha < \pi/2$ , i.e. the  $x$ -projection of the momentum  $p_x > 0$ , in this extended scheme. The region  $X < x < 2X$  is responsible for the negative  $p_x$  in the original billiard. Similarly,  $Y < y < 2Y$  represents the negative  $p_y$ . With these definitions the extended unperturbed billiard has the topology of

a torus, and the coordinates and momenta are similar to the action-angle variables.

We will consider only the orbits with  $\tan \alpha \geq \tan \beta = Y/X$ , where  $\beta$  is the angle between the  $x$ -axis and the diagonal. In the opposite case we can switch the  $x$ - and  $y$ -directions. The trajectories can be divided in two classes depending on whether  $\tan \alpha$  is greater (class I) or less (class II) than  $2 \tan \beta$ . Each family of orbits with given  $\alpha$  divides the stretch of PSS from 0 to  $2X$  into six intervals between the points  $0 < x_1 < x_2 < X < x_3 < x_4 < 2X$ . Orbits starting within the same interval reflect from the same sequence of walls as they propagate. Although the borders of these intervals depend on  $\alpha$ , the sequences of walls remain the same within the class. Points  $x_i$  are defined in Fig. 3.2 (a) for class I and (b) for class II. Analytic expressions can also be written down. For example,  $x_1 = X - 2Y/\tan \alpha$  for class I. The orbits beginning in the interval  $(0, x_1)$  reflect off side 3 (as defined in Fig. 3.1) before returning to the PSS. For the orbits beginning in  $(x_1, x_2)$  these are sides 3 and 4, etc.

### 3.1.2 Perturbation theory

We begin with constructing the  $T$ -operator for the system,

$$T(x, x') = \sqrt{\frac{k}{2\pi i} \left| \frac{\partial^2 L}{\partial x \partial x'} \right|} e^{ikL(x, x') - i\frac{\pi}{2}\nu(x, x')}. \quad (3.2)$$

$\nu(x, x')$  is the Maslov index for the orbit that goes from point  $x'$  to point  $x$  on the PSS. It increases by 2 on each reflection (in the original billiard). Note that each trajectory reflects off the upper and lower boundaries once, which changes the phase by  $2\pi$ . Thus, one may count in  $\nu(x, x')$  only reflections from the side walls. As was explained in Sec. 1.6, the Maslov phase remains, even when we work in the extended scheme.  $L(x, x')$  is the length of the orbit. With the intent to calculate the two-dimensional wavefunction later, we first find  $\mathcal{L}(x, y; x')$ , the length of the orbit that starts at  $x'$  on the PSS and ends at point  $(x, y)$  inside the billiard.

We argue that the shift of the point of reflection *along* the boundary due to the perturbation can be neglected when calculating the length. Here is what we mean by that. Consider, for example, the right wall. It is parametrized by  $y$  [see Eq. (3.1) for wall 4]. Suppose an orbit with fixed end points reflects at point  $y_0$  in an unperturbed billiard. If there is a perturbation, the orbit with the same end points will reflect at point  $y_0 + \Delta y$  where the length is extremal, that is  $\partial L/\partial y = 0$ . Since  $|\xi'_4| \sim 1$ , the shift  $\Delta y \sim \epsilon$ . The correction to the length, however, is  $\frac{1}{2} (\partial^2 L/\partial y^2) (\Delta y)^2 \sim \epsilon^2$  and can be neglected at this order of the calculation. As a result, all



the corrections will depend on functions  $\xi_i$  evaluated at the reflection points for unperturbed trajectories.

It is convenient to express the corrections to the length  $\mathcal{L}(x, y; x')$  in terms of auxiliary functions  $\eta_i(x, y; \alpha)$ ,  $i = 1, \dots, 4$ , where  $\tan \alpha = y/(x - x')$ . To define them, consider the trajectory from family  $\alpha$  that arrives at point  $(x, y)$  of the extended billiard. On its way this trajectory may hit the  $i^{\text{th}}$  wall. In this case  $\eta_i$  is equal to the value of  $\xi_i$  at the point of reflection. Otherwise,  $\eta_i = 0$ . For example, for class I trajectories, when  $0 \leq x \leq 2X$  and  $0 \leq y \leq 2Y$ ,

$$\eta_2(x, y; \alpha) = \begin{cases} 0, & 0 \leq y \leq x \tan \alpha \leq 2X \tan \alpha, \\ \xi_2(y - x \tan \alpha), & x \tan \alpha \leq y \leq Y + x \tan \alpha, \\ \xi_2(2Y + x \tan \alpha - y), & Y + x \tan \alpha \leq y \leq 2Y. \end{cases} \quad (3.3)$$

$\eta_i$ 's have period  $2X$  in  $x$ . Note that  $\eta_2$  is discontinuous at wall 2, similar for other  $\eta_i$ 's. What complicates things even more, the extended scheme is only *approximate* in the perturbed billiard, in which the domains may slightly overlap near the boundaries.  $\eta_i$  is double valued near the  $i^{\text{th}}$  wall where  $\xi_i < 0$ . It is equal there either  $\xi_i$  or 0, depending on which sheet the point is located. Equation (3.3) can still be used in the boundary regions, but the inequalities are incorrect there.

Now the length becomes

$$\begin{aligned} \mathcal{L}(x, y; x') = & \\ & \sqrt{\{x - x' - 2\epsilon[\eta_2(x, y) + \eta_4(x, y)]\}^2 + \{y - \epsilon[\eta_1(x, y) + 2\eta_3(x, y)]\}^2} = \\ & \mathcal{L}_0(y, \alpha) + \epsilon \mathcal{L}_2(x, y; \alpha) \end{aligned} \quad (3.4)$$

where

$$\mathcal{L}_0(y, \alpha) = \frac{y}{\sin \alpha}, \quad \mathcal{L}_2(x, y; \alpha) = -2 \cos \alpha (\eta_2 + \eta_4) - \sin \alpha (\eta_1 + 2\eta_3). \quad (3.5)$$

When the end point is on the surface of section, i.e. substituting  $y = 2Y - \epsilon \xi_1(x) = 2Y - \epsilon \eta_1(x, 0)$ , we find the length that enters the  $T$ -operator

$$L(x, x') = \frac{2Y}{\sin \alpha} + \epsilon L_2(x, \alpha) \quad (3.6)$$

where  $\tan \alpha = 2Y/(x - x')$  and

$$L_2(x, \alpha) = -2 \cos \alpha [\eta_2(x, 2Y) + \eta_4(x, 2Y)]$$

$$-\sin \alpha [\eta_1(x, 0) + \eta_1(x, 2Y) + 2\eta_3(x, 2Y)]. \quad (3.7)$$

We will be interested in the states near a  $(p, q)$  resonance. The resonant trajectory maps point  $x'$  to  $x = x' + x_{pq}$  on the upper part of the PSS, where  $x_{pq} = (p/q)2X$ . Hence we expand the phase of  $T$ -operator in  $\Delta x' = x' - x + x_{pq} \sim \sqrt{\epsilon}$ . By assumption, only the case when  $p \leq q$  is considered. The solution of Bogomolny's equation  $\psi = T\psi$  has the form [cf. Eq. (2.28)]

$$\psi(x) = \hat{\psi}(x) e^{i[p_x x + k\epsilon f_2(x) + g(x)]}. \quad (3.8)$$

Here  $p_x$  satisfies the resonance condition  $p_x/p_y = x_{pq}/2Y$  or  $p_x = k/\sqrt{1 + \left(\frac{qY}{pX}\right)^2}$ . The step-function  $g(x)$  compensates for the change in the Maslov phase each time the orbit crosses a domain boundary at  $x = 0, \pm X, \pm 2X, \dots$ . It satisfies the condition [cf. Eq. (1.60)]

$$g(x) - g(x - x_{pq}) = -\frac{\pi}{2}\nu(x, x - x_{pq}) \quad (3.9)$$

that has a solution

$$g(x) = -\pi [x/X]_{\text{int}} \quad (3.10)$$

where  $[\dots]_{\text{int}}$  is an integer part. Function  $\hat{\psi}(x)$  satisfies the Schrödinger equation

$$\hat{\psi}'' + 2dk^2\epsilon [E_m - \bar{V}_q(x)] \hat{\psi} = 0, \quad (3.11)$$

where  $d = (\sin \alpha)^3 / 2Y$ , with the effective potential

$$\bar{V}_q(x) = -\langle L_2(x, \alpha) \rangle_q. \quad (3.12)$$

The angle  $\alpha$  has the resonant value:  $\tan \alpha_{pq} = qY/pX$ . Note that  $d$  and  $\bar{V}_q$  are defined with the opposite sign from the circular billiard. When the walls are deformed towards outside of the billiard, the potential tends to decrease, thus supporting a localized state. In the circular billiard, on the other hand, the states concentrate where the billiard is deformed inwards.

The Schrödinger equation should be solved with the boundary condition  $\hat{\psi}(x + 2X) = \hat{\psi}(x) e^{-i2\pi\delta}$ , where  $\delta$  is the fractional part of  $2Xp_x/2\pi$ . This condition makes  $\psi(x)$  periodic with period  $2X$ . Once  $E_m$ 's are known, the total energy can be found from the second quantization condition

$$\frac{2Yk}{\sin \alpha} - 2\pi \frac{p}{q} \left[ \frac{2Xp_x}{2\pi} \right]_{\text{int}} - k\epsilon E_m = 2\pi n. \quad (3.13)$$

The part of  $f_2(x)$  that vanishes under  $q$ -average is

$$\tilde{f}_2(x) = \frac{1}{q} \sum_{r=1}^{q-1} r \left[ \langle L_2(x, \alpha) \rangle_q - L_2(x - rx_{pq}, \alpha) \right]. \quad (3.14)$$

The  $q$ -periodic part can be found from the equation similar to Eq. (2.37), but this time it will include the derivative of the perturbation, since  $L_2$  is not of the special form (2.5).

### 3.1.3 Two-dimensional wavefunction

The wavefunction  $\Psi(\mathbf{r}) = \int dx' \tilde{G}(\mathbf{r}, x') \psi(x')$ , where the integral is evaluated in the stationary phase approximation (S $\Phi$ ). The kernel

$$\tilde{G}(\mathbf{r}, x') = \frac{1}{2\sqrt{2\pi}} \left| \frac{\partial^2 \mathcal{L}(\mathbf{r}; x')}{\partial r_\perp \partial x'} \right|^{1/2} e^{ik\mathcal{L}(\mathbf{r}; x') - i\frac{\pi}{2}\nu(\mathbf{r}; x')} \quad (3.15)$$

where  $r_\perp$  is the direction perpendicular to the trajectory at point  $\mathbf{r}$ . The Maslov phase  $\nu(\mathbf{r}; x')$  changes by 2 on every boundary. The lowest order stationary phase condition selects one point

$$x'(\mathbf{r}) = x - y \cot \alpha_{pq} \quad (3.16)$$

indicating that only one classical trajectory contributes to the integral. This is the trajectory that approximately makes angle  $\alpha_{pq}$  with axis  $x$  and arrives at point  $\mathbf{r}$ . Keeping terms to order  $\epsilon$  in the phase and dropping the constant factors we find the two-dimensional wavefunction

$$\Psi(x, y) = \varphi(x, y) e^{ig(x') - i\frac{\pi}{2}\nu(\mathbf{r}; x')} \quad (3.17)$$

where

$$\varphi(x, y) = \hat{\psi}(x') e^{i\mathbf{p}\cdot\mathbf{r} + ik\epsilon \{ f_2(x') - \frac{y}{2Y} [E_m - \bar{V}_q(x')] + \mathcal{L}_2(\mathbf{r}; \alpha_{pq}) \}} \quad (3.18)$$

and  $x'$  is given by Eq. (3.16).  $\Psi(x, y)$  has period  $2X$  in  $x$ -direction.

Each point in the original  $X \times Y$  domain has four images in the extended billiard (up to a translation by  $2X$ ). Hence the physical wavefunction  $\Psi_{\text{ph}}(x, y)$  is the sum of four respective terms  $\Psi(x, y)$  (Fig. 3.3). The combination  $g(x') - \frac{\pi}{2}\nu(\mathbf{r}; x')$  is constant within one domain but differs by  $\pi$  between neighboring domains. Therefore the complete wavefunction is

$$\Psi_{\text{ph}}(x, y) = \varphi(x, y) - \varphi(x, 2Y - y) - \varphi(2X - x, y) + \varphi(2X - x, 2Y - y). \quad (3.19)$$

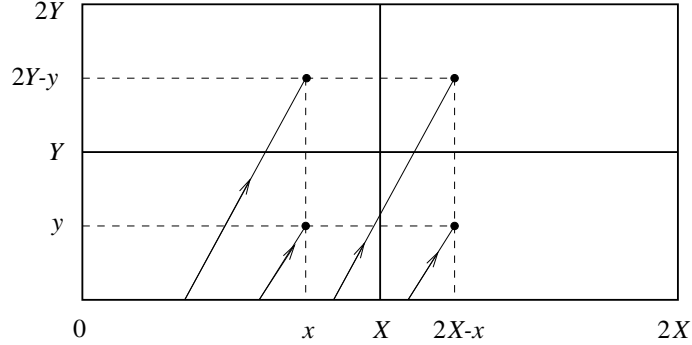


Figure 3.3: Four classical orbits that contribute to the wavefunction in a rectangle.

This function vanishes on the physical boundary of the billiard to order  $\epsilon$ . Consider, for example, the left border where  $x = \epsilon \xi_2(y)$ . In the first term of Eq. (3.19)  $x' \simeq -y \cot \alpha$ . In the third term  $x' \simeq 2X - y \cot \alpha$ . The phase difference between these terms is  $p_x [2\epsilon \xi_2(y) - 2X] + 2\pi\delta - 2k\epsilon \cos \alpha [\eta_2(0^+, y) - \eta_2(2X^-, y)]$ , which is a multiple of  $2\pi$ . [The last term comes from  $k\epsilon \mathcal{L}_2$ ;  $\eta_2(0^+, y) = \xi_2(y)$  and  $\eta_2(2X^-, y) = 0$ ]. Thus the first and third terms in Eq. (3.19) cancel. The second and fourth terms cancel as well. Similarly, the wavefunction vanishes on the other sides of the rectangle. In particular, in order for it to vanish on the lower side, the quantization condition (3.13) must be satisfied.

Setting  $\epsilon = 0$ , we find the familiar result for an unperturbed billiard:  $\Psi_{\text{ph}}(x, y) \propto \sin(\pi m x/X) \sin(\pi n y/Y)$  and  $k_{mn} = \sqrt{(\pi m/X)^2 + (\pi n/Y)^2}$ . For generic  $X$  and  $Y$  the resonance condition  $p_x/p_y = pX/qY$  is incompatible with the quantized momenta  $p_x = \pi m/X$  and  $p_y = \pi n/Y$  for any integer  $p$  and  $q$ . This is of no surprise because the resonances are irrelevant for the quantum unperturbed billiard.

### 3.1.4 Example: tilted square

We illustrate the results of previous sections with the example of tilted square. This is a trapezoid resulted from tilting one side of the square by a small amount. This billiard was studied in a different context [44], but no specific states were mentioned. For definitiveness, suppose the vertices of the trapezoid are located at points  $(0, 0)$ ,  $(0, 1)$ ,  $(1, 1)$ , and  $(1, \epsilon)$ . The

lower side  $y = \epsilon x$ ,  $0 \leq x \leq 1$ , is chosen as the PSS. We will be interested in the states near (1, 1) resonance, which are characterized by the diamond shaped classical orbits. The PSS wavefunction  $\psi(x) = \exp(i\kappa x) \hat{\psi}(x)$ , where  $\kappa = k/\sqrt{2}$ , indicates that the unperturbed orbits make angle  $\alpha = 45^\circ$  with the sides of the square. Note that, as in any (1, 1) resonance, function  $f_2$  appears only in the third order theory.

The perturbed part  $\hat{\psi}(x)$  satisfies the Schrödinger equation (3.11) with the effective potential in the extended scheme  $V(x) = \sqrt{2}|x|$  ( $|x| \leq 1$ ).  $V(x)$  is repeated with period 2. The requirement for  $\psi(x)$  to be of period 2 makes  $\hat{\psi}(x+2) = e^{i2\kappa} \hat{\psi}(x)$ . Equation (3.11) is a piece-wise Airy equation. For the well-localized states deep inside the wells the solutions are approximately

$$\hat{\psi}_m(x) = \text{Ai} \left[ \left( \frac{\sqrt{2}}{\mathcal{L}} k^2 \epsilon \right)^{1/3} x - z_m \right], \quad 0 \leq x \leq 1, \quad (3.20)$$

where  $\mathcal{L} = \sqrt{8}$  is the length of the unperturbed orbit,  $z_m$  is an extremum (zero) of  $\text{Ai}(-z)$  for even (odd)  $m$  and  $\hat{\psi}_m(-x) = (-1)^m \hat{\psi}_m(x)$ . The eigenenergy  $E_m = z_m (2\mathcal{L}/k^2\epsilon)^{1/3}$  and the total energy

$$E_{nm} = k^2 \simeq \left( \frac{2\pi n}{\mathcal{L}} \right)^2 \left[ 1 + z_m \left( \frac{2\epsilon}{\pi n} \right)^{2/3} \right]. \quad (3.21)$$

A state can be considered deep inside the well if  $E_m \ll \max V(x)$ , i.e.  $z_m \ll (\sqrt{2}k^2\epsilon/\mathcal{L})^{1/3}$ .

Figure 3.4 shows the lowest surface of section state  $\hat{\psi}_0(x)$ . It is localized near  $x = 0$ , which for the (1, 1) resonance means that the two-dimensional state is concentrated along the diagonal  $y = x$ . To check this one looks at the two-dimensional wavefunction in the physical domain that has the form

$$\begin{aligned} \Psi(x, y) = & e^{i\kappa(x+y) + ik\epsilon\sqrt{2}[-yE_m + (y-1)V(x-y)]} \hat{\psi}_m(x-y) \\ & + e^{i\kappa(-x-y) + ik\epsilon\sqrt{2}[yE_m + (1-y)V(x-y)]} \hat{\psi}_m(-x+y) \\ & - e^{i\kappa(-x+y) + ik\epsilon\sqrt{2}[-yE_m + (y-1)V(x+y)]} \hat{\psi}_m(-x-y) \\ & - e^{i\kappa(x-y) + ik\epsilon\sqrt{2}[yE_m + (1-y)V(x+y)]} \hat{\psi}_m(x+y), \quad 0 \leq x, y \leq 1. \end{aligned} \quad (3.22)$$

In Figs. 3.5 and 3.6 we plotted a simplified version of this function where we neglected terms of order  $k\epsilon$  and set  $\kappa = \pi n/2$ . To make the resulting function satisfy the boundary conditions we made a substitution  $y \rightarrow (y - \epsilon x)/(1 - \epsilon x)$ , which does not change the order of approximation. The reduced function keeps the gross features of the exact function. The cross-section of the

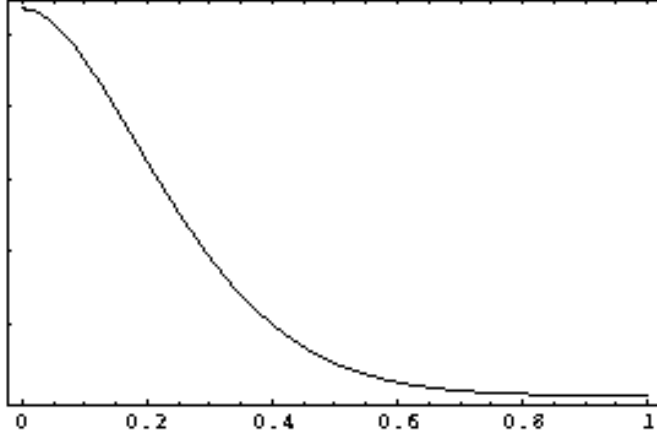


Figure 3.4: Function  $\hat{\psi}_0(x)$  for the tilted square with  $\epsilon = 0.03$ , state  $n = 50$ ,  $m = 0$ .

state along the diagonal

$$\Psi(x, x) \simeq \begin{cases} \hat{\psi}_m(2x) - \hat{\psi}_m(0) \cos(\pi n x), & m \text{ even} \\ 0, & m \text{ odd} \end{cases} \quad (0 \leq x \leq 1) \quad (3.23)$$

is shown in Fig. 3.7 for a numerical wavefunction, as well as the section across another diagonal  $y = 1 - x$

$$\Psi(x, 1 - x) \simeq \begin{cases} \hat{\psi}_m(2x - 1), & m, n \text{ both even or both odd} \\ 0, & \text{otherwise} \end{cases}, \quad (3.24)$$

both numerical and theoretical. The line  $y = 1 - x$  is the diagonal of the unperturbed square, not the trapezoid. It crosses its boundary at  $x = 1/(1 + \epsilon)$  which explains the cut-off in the figure.

Note that the neglect of the  $k\epsilon$  order terms in  $\kappa$  leads to the symmetries  $\hat{\psi}_m(-x) = (-1)^m \hat{\psi}_m(x)$  and  $\hat{\psi}_m(x + 2) = (-1)^n \hat{\psi}_m(x)$  for *all*  $x \in (-\infty, +\infty)$ . This is consistent with the fact that the potential  $V(x)$  is even at  $x = 0$  and  $x = 1$  and the Schrödinger equation (3.11) is solved with the real boundary condition. In general, however, the complex condition  $\hat{\psi}(x + 2) = e^{i2\kappa} \hat{\psi}(x)$  leaves a weaker symmetry  $\hat{\psi}_m(-x) = (-1)^m \hat{\psi}_m^*(x)$ .

We have shown that even with a small perturbation of the side of the square the strongly perturbed localized states can exist, as long as  $k\sqrt{\epsilon} \gg 1$ . By constructing an effective potential

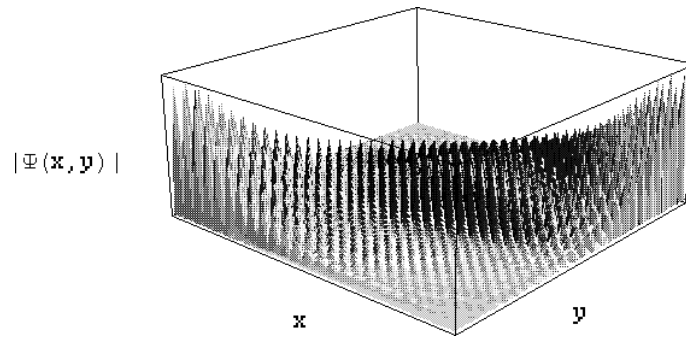


Figure 3.5: The absolute value of the theoretical wavefunction to order  $k\sqrt{\epsilon}$  in the tilted square is plotted for the parameters of Fig. 3.4.

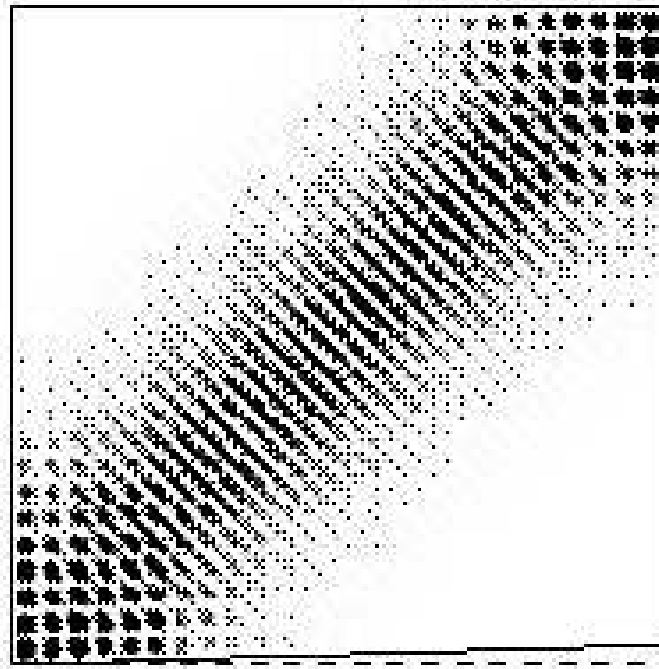


Figure 3.6: Density plot for the wavefunction of Fig. 3.5. The dashed line is  $y = 0$ .

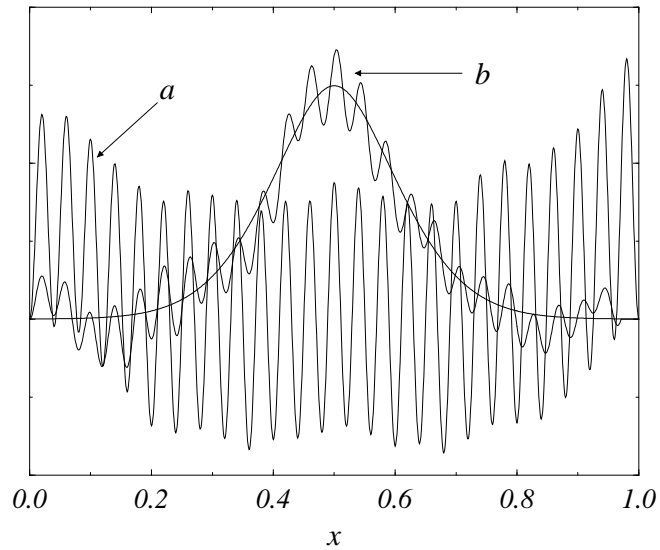


Figure 3.7: The cross-section of the numerical wavefunction for the state of Figs. 3.4-3.6 along the diagonals. (a)  $\Psi(x, x)$ , (b)  $\Psi(x, 1 - x)$ . The theoretical wavefunction, which is smoother, is also shown in (b). The diagonal of the unperturbed square  $y = 1 - x$  crosses the boundary at  $x = 1/(1 + \epsilon)$ , which explains the cut-off in (b).



it is easy to see that there are also states concentrated along the side  $x = 0$  corresponding to  $(0, 1)$  resonance. We will study these states using the Born-Oppenheimer approximation when we revisit this billiard in Sec. 5.2. It is also clear that there are no diagonal states in the symmetric trapezoid with sides  $x = 0, 1, y = \epsilon x, 1 - \epsilon x$ , but there are states near  $x = 0$ . For the parallelogram billiard with sides  $x = 0, 1, y = \epsilon x, 1 + \epsilon x$  there are states along the long diagonal but no states near the edges.

## 3.2 Billiards without small parameter

In some cases the perturbation theory that we developed can be applied to a system that is not a small perturbation of an integrable system. However, this system may possess certain states that are close to the states in an integrable system. Then these states could be studied using the perturbation theory where the small parameter would depend on the state itself.

As a first example, consider the ice cream cone billiard (Fig. 3.8), which is a unit circle for  $\pi > |\theta| > \beta$  and a triangular shaped region for  $|\theta| < \beta$ . For the surface of section states that are concentrated in the circular region the perturbation theory for the circle can be used. The perturbation of the boundary,  $\Delta R(\theta) = 1/\cos(\beta - \theta)$  for  $|\theta| < \beta$  and zero elsewhere, grows as  $\theta$  goes into the triangular region. Consequently, the effective potential  $\bar{V}_q(\theta)$  is large near  $\theta = 0$ , repeated with period  $2\pi/q$ . The PSS wavefunction obeys the Schrödinger equation (2.30) with  $\epsilon = 1$ . Clearly, the state will not significantly penetrate the non-circular region as long as  $E_m \ll \max \bar{V}_q = q^{-1} \sin(\Theta_{pq}/2) / \cos \beta$  ( $2\pi/q > 2\beta$ ). This defines the small parameter that depends on  $E_m$ . For example, the states of the low angular momentum resonance with small  $E_m$  are concentrated near the diameter at  $\theta = \pm\pi/2$ . There is also an upper limit on the denominator  $q$ : the potential becomes shallower when  $2\pi/q$  is smaller than  $2\beta$ .

Another example are the “bouncing ball” (BB) states in a stadium billiard [5, 6, 75, 46]. The billiard has the straight segments of length  $2a$  and the endcaps of radius 1, and we can reduce the billiard to its upper half by symmetry (Fig. 3.9). We are looking for the states that have low momentum parallel to the sides and large perpendicular momentum. If such states are concentrated outside of the endcaps, they will not be too different from the localized  $(0, 1)$ -states in a perturbed infinite channel or a long rectangle. The deviation of the upper boundary from the straight line is described by the function  $\xi(x) = 0, |x| < a, \xi(x) \approx (|x| - a)^2/2$ ,

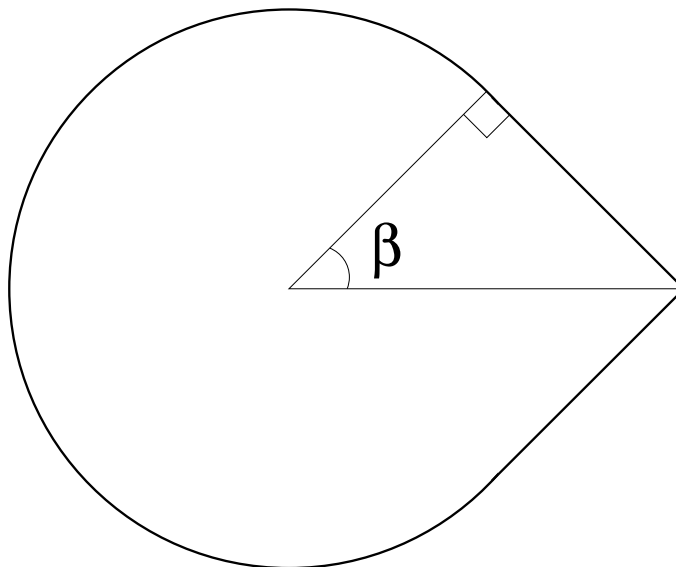


Figure 3.8: Ice-cream cone billiard.

$|x| > a$ . The effective potential  $V(x) = 2\xi(x)$  is multiplied by a large factor of  $k^2$  in the Schrödinger equation, thus it is almost a square well with  $V \rightarrow \infty$  for  $|x| > a$ . Therefore the states are contained in the straight region if  $E_m \ll 1$ . Since  $E_m \sim (m/ka)^2$ , the billiard should be longer than  $m/k$  to apply the method. (The opposite case is a perturbed circle.) The ratio of the parallel and perpendicular momenta  $p_x/p_y \approx \sqrt{E_m}$  is small, as expected. Since we consider only half of the billiard, we need to find the states with both Dirichlet's and Neumann's conditions on the lower boundary. In the latter case the  $T$ -operator has an additional Maslov phase  $\pm\pi$ , which should be added to the quantization condition (3.13). The theoretical state  $n = 10$ ,  $m = 1$  is shown in Fig. 3.10. The similar results for the BB states can be obtained by the Born-Oppenheimer approximation [6]. The theory can be generalized, of course, to include the perturbation of the boundary of the stadium. For example, the radii of the endcaps can be slightly different so that the straight segments are tilted [64]. Then, from what we know, the BB states will be shifted towards the wider end (Fig. 3.11). When the sides are strongly tilted we have an ice cream cone billiard (Fig. 3.12).

Kudrolli *et al.* [48] observed the surface wave patterns in a Bunimovich stadium filled with

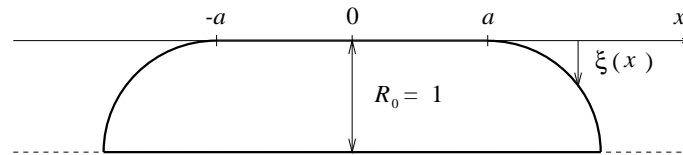


Figure 3.9: The Bunimovich stadium with the straight sides of length  $2a$  and the endcaps of radius  $R_0 = 1$  reduced to the upper half by symmetry. The deviation of the upper boundary from the straight line is  $\xi(x)$ .

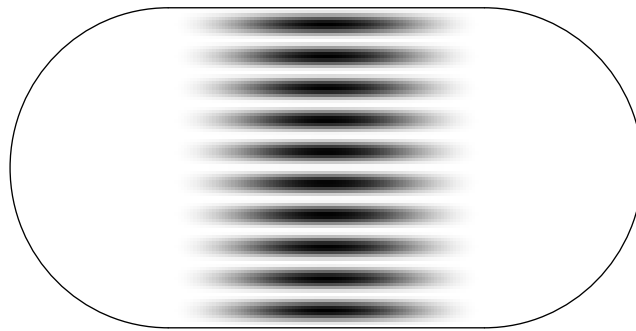


Figure 3.10: Square of the theoretical wavefunction for the bouncing ball state  $n = 10$ ,  $m = 1$  in the Bunimovich stadium.

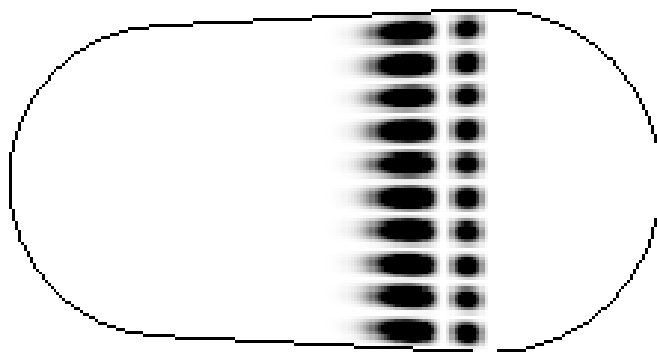


Figure 3.11: Bouncing ball state in the slanted stadium. The radii differ by  $\Delta R/R = 0.1$ . The quantum numbers are  $n = 10$ ,  $m = 2$ .

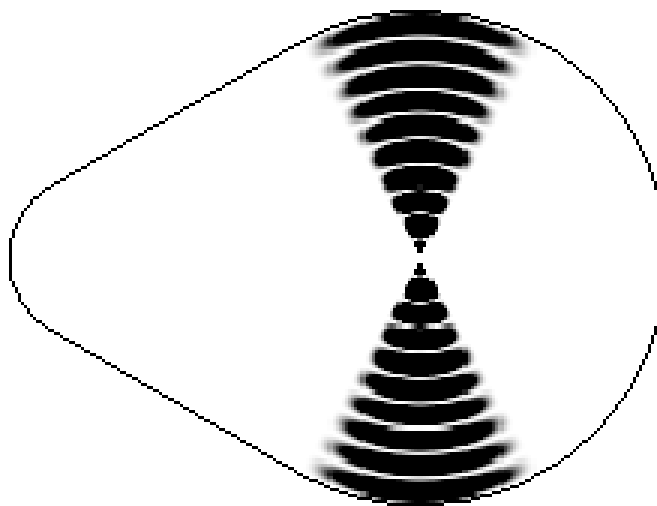


Figure 3.12: Localized state in the “baseball” stadium. The cap radii are  $R_1 = (1/\sqrt{20})\ell$ ,  $R_2 = (3/\sqrt{20})\ell$ , where  $\ell$  is the distance between them. If treated as a perturbed circle the quantum numbers are  $n = 10$ ,  $m = 1$ . The theoretical wavefunction is inaccurate near the center of the billiard (cf. Sec. 2.4).

liquid. The modes were excited by oscillating the container vertically with an appropriate frequency. Only three types of all possible modes were actually observed, including the BB mode. It was argued [1] that the whispering gallery mode and the excitations of other types do not appear due to strong boundary dissipation.

The notion of BB states can be generalized to the states near a short periodic orbit that connects opposite sides in a generic billiard [56, 23] (Fig. 3.13). Assume constant radii of curvature  $R_1$  and  $R_2$  in the neighborhoods of the points joined by the periodic orbit. Then the length of a nearby chord in terms of the local coordinates along the boundary is

$$L(s_1, s_2) \cong d - \frac{s_1^2}{2R_1} - \frac{s_2^2}{2R_2} + \frac{(s_1 - s_2)^2}{2d} \quad (3.25)$$

where  $2d$  is the length of the periodic orbit and  $s_1$  and  $s_2$  measure the distance from the periodic orbit along the boundary with counterclockwise and clockwise positive direction, respectively (see Fig. 3.13). Let the PSS coincide with the boundary. We define the PSS wavefunctions locally on each side and assume that they are well localized. Then we need to solve a couple of Bogomolny's equations

$$\begin{aligned} \psi_1(s_1) &= \int T(s_1, s_2) \psi_2(s_2) ds_2, \\ \psi_2(s_2) &= \int T(s_2, s_1) \psi_1(s_1) ds_1. \end{aligned} \quad (3.26)$$

The formula [37]

$$\int_{-\infty}^{\infty} e^{-(x-y)^2} H_m(ax) dx = \sqrt{\pi} (1-a^2)^{m/2} H_m\left(\frac{ay}{\sqrt{1-a^2}}\right) \quad (3.27)$$

suggests looking for the solution in the form

$$\psi_i(s_i) = \sqrt{\alpha_i} \exp\left(-\frac{k}{2d}\alpha_i s_i^2\right) H_m\left(\sqrt{\frac{k}{d}}\beta_i s_i\right) \quad (i = 1, 2) \quad (3.28)$$

where  $H_m(x)$  is a Hermite's polynomial. The constants  $\alpha_i$  and  $\beta_i$  are determined after substituting the ansatz in the Bogomolny equations. They are

$$\begin{aligned} \alpha_1 &= \sqrt{\frac{\frac{d}{R_1} - 1}{\frac{d}{R_2} - 1} \left[1 - \left(\frac{d}{R_1} - 1\right) \left(\frac{d}{R_2} - 1\right)\right]}, \\ \beta_1 &= \sqrt{\frac{\frac{d}{R_1} - 1}{\frac{d}{R_2} - 1}} \alpha_1 \end{aligned} \quad (3.29)$$

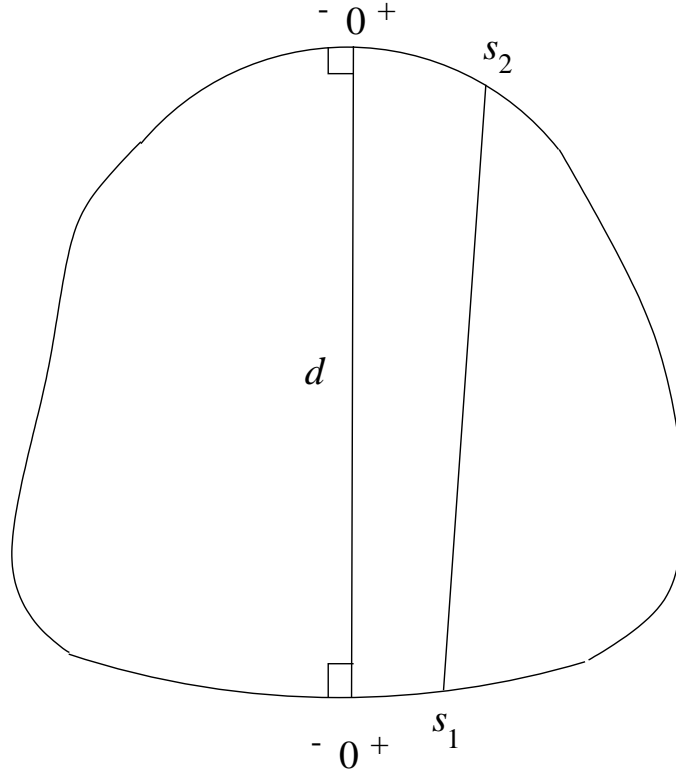


Figure 3.13: Short periodic orbit of length  $2d$  and a nearby orbit between points  $s_1$  and  $s_2$  in a generic billiard. The positive and negative directions are indicated.

and similar for  $\alpha_2$  and  $\beta_2$ . This approach is valid only if  $0 < \left(\frac{d}{R_1} - 1\right) \left(\frac{d}{R_2} - 1\right) < 1$ . Also the localization lengths  $\sqrt{d/k\alpha_i}$  should be smaller than the characteristic scale of the boundary, including  $R_i$ . The quantization condition is

$$kd = \pi \left( 2n + \frac{m}{2} + \frac{5}{4} \right) + \varphi (2m + 1) \quad (3.30)$$

where

$$\varphi = \frac{1}{2} \operatorname{sgn} \left( \frac{d}{R_i} - 1 \right) \arcsin \sqrt{\left( \frac{d}{R_1} - 1 \right) \left( \frac{d}{R_2} - 1 \right)}. \quad (3.31)$$

In the case of equal radii  $R_1 = R_2 = R$  we have the same functions with  $\alpha = \beta = \sqrt{\frac{d}{R} \left( 2 - \frac{d}{R} \right)}$  on each side. The phase  $\varphi = \frac{1}{2} \arcsin \left( \frac{d}{R} - 1 \right)$ . Note that when  $d = 2R$  the

state is delocalized, as expected for a perfect circle. Coincidentally, we have the correct WKB quantization in this limit, although the theory obviously fails. In the confocal case  $d = R_1 = R_2$  the solution is  $\psi(s) = \exp(-\frac{k}{2d}s^2) H_m\left(\sqrt{\frac{k}{d}}s\right)$  with the quantization condition  $kd = \pi\left(2n + \frac{m}{2} + \frac{5}{4}\right)$ .

### 3.3 Whispering gallery modes

A wide range of billiards can support the states that are concentrated close to the boundary and called the *whispering gallery* modes (WGMs). This effect was first discussed by G. B. Airy and Lord Rayleigh [66], and Keller and Rubinow [46] obtained the quantization conditions. Apart from the trivial cases the WGMs should be regarded as quasimodes (see Sec. 2.6). The WGMs in the asymmetric resonant optical cavities with emission have a long life-time and might be useful in lasers [58]. There is a recent experimental observation of the chaos-assisted tunneling between the WGMs in a superconducting microwave cavity [29], as well as of the excitation of WGMs by a vortex in a Josephson junction [77].

The standard problem can be solved by various analytical methods giving essentially the same leading order result. Among them the ray method by Keller and Rubinow, the parabolic equation and the etalon methods are reviewed in Ref. [4]; the Born-Oppenheimer approximation is discussed in Sec. 5.5; and the  $T$ -operator is used in this section. All these methods are based on the adiabatic assumption that the curvature of the boundary is slowly varying (the estimate is given below) and never vanishes. Under these conditions a classical (non-periodic) orbit is proven [50] to have a caustic and an adiabatic invariant, meaning that the invariant tori can be constructed in the perturbation theory. If a boundary has at least one point of zero curvature, there are trajectories infinitely close to the boundary that reverse themselves and thus do not have a caustic [55]. A wider variety of classical whispering gallery trajectories is found in a magnetic billiard [69]. It should be noted, however, that the existence of classical tori is a sufficient but not necessary condition for a quantum state to exist. For example, Fig. 3.14 shows a state localized near the boundary in a short stadium billiard. We discuss a possible way to deal with such systems in Sec. 3.4.

To apply the Bogomolny's equation method we need to find the length of the chord between two points on the boundary. The classical trajectory stays close to the boundary, so, typically,

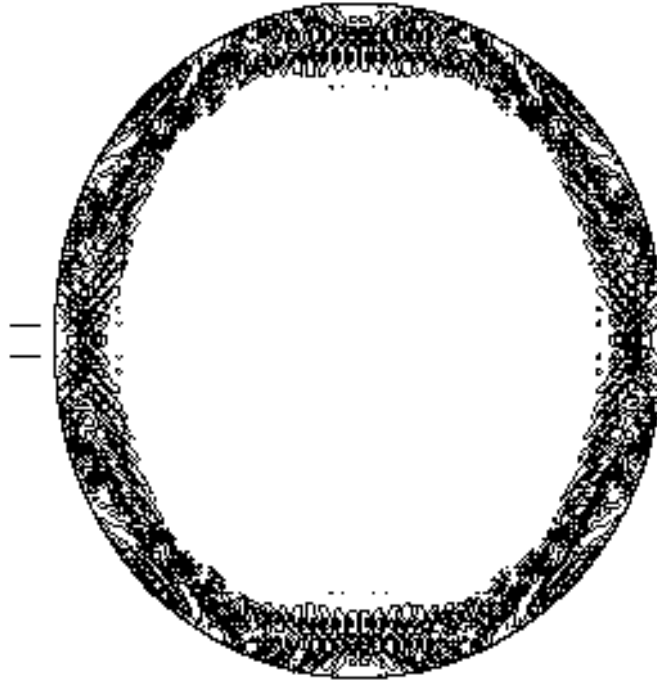


Figure 3.14: Contour plot of the whispering gallery mode in the short stadium with  $\epsilon = 0.05$  (see Sec. 2.2.1). The numerically obtained wavefunction with  $k = 242.7611$  is shown. There are no caustics in this case and almost no classical orbits that stay close to the boundary for a long time. The parallel lines on the left indicate the length and position of the straight segments of the boundary.



the two points will be close to each other and the boundary between them can be approximated by an arc of a circle. Let  $s$  be the distance along the boundary. It can be shown that the chord length

$$\begin{aligned} L(s, s') &= |s - s'| - \frac{|s - s'|^3}{24 [R(\frac{s+s'}{2})]^2} + O(|s - s'|^5) \\ &\cong |s - s'| - \frac{|s - s'|^3}{24 [R(s)]^2} - \frac{|s - s'|^4 R'(s)}{24 [R(s)]^3} \end{aligned} \quad (3.32)$$

where  $R(s)$  is the radius of curvature. Although the best estimate for the radius is at the middle-point, it is more convenient to express it locally at point  $s$ . We make an ansatz for the wavefunction

$$\psi(s) = C(s)e^{ik[s-f(s)]}. \quad (3.33)$$

The wavefunction can be found using the first two terms in Eq. (3.32). One can show that the inclusion of the (small) third term in this form does not result in the  $R'/R$ -order correction in the wavefunction. Using the stationary phase approximation ( $S\Phi$ ) in  $\int T\psi ds$  we find

$$f'(s) = \left[ \frac{3\sqrt{2}\pi(n-1/4)}{4kR(s)} \right]^{2/3} \quad (3.34)$$

and the prefactor [78]

$$C(s) \propto R^{-1/3}(s) \propto \sqrt{f'(s)}. \quad (3.35)$$

The quantization condition comes from the periodicity of  $\psi(s)$  over the perimeter of the boundary  $\mathcal{L}$ ,

$$k[\mathcal{L} - f(\mathcal{L}) + f(0)] = 2\pi m. \quad (3.36)$$

Quantum number  $m$  indicates the momentum along the boundary and  $n$  reflects the motion in the perpendicular direction.

The last term in Eq. (3.32) is small if

$$|s - s'|_{\text{st}} \frac{|R'|}{R} \ll 1 \quad (3.37)$$

where the  $S\Phi$  value  $|s - s'|_{\text{st}} = \sqrt{8f'R} \sim n^{1/3}R^{2/3}k^{-1/3}$  is a typical hop the classical orbit makes near point  $s$ . Condition (3.37) becomes

$$|R'| \ll (kR/n)^{1/3} \quad (3.38)$$

thus restricting the pace of variation of the curvature.

It is convenient to describe the motion in two dimensions in the  $(\rho, s)$  coordinates where  $\rho$  is the distance from the boundary positive inside the billiard. These coordinates are well-defined close to the boundary, where  $\rho \ll R(s)$ . The two-dimensional function can be found by the standard technique,

$$\Psi(\rho, s) = \int \tilde{G}(\rho, s; s') \psi(s') ds' \quad (3.39)$$

where  $\tilde{G}(\rho, s; s') \propto \exp[ikL(\rho, s; s')]$ . The distance  $L(\rho, s; s')$  between point  $s'$  on the boundary and point  $(\rho, s)$  inside the billiard is shown in Fig. 3.15. As in the case of a circle (Sec. 2.4), there are two classical orbits (for fixed  $m$  and  $n$ ) arriving at point  $(\rho, s)$  that satisfy the  $S\Phi$  condition. They leave the boundary at points

$$s'_{1,2} = s - \sqrt{2}R \left( \sqrt{f'} \pm \sqrt{f' - \frac{\rho}{R}} \right). \quad (3.40)$$

When we sum the contributions from these two stationary points we get the wavefunction

$$\Psi(\rho, s) = \frac{\psi(s)}{(f' - \frac{\rho}{R})^{1/4}} \cos \left[ \frac{2\sqrt{2}}{3} kR \left( f' - \frac{\rho}{R} \right)^{3/2} - \frac{\pi}{4} \right]. \quad (3.41)$$

The function is defined in the classically allowed region  $\rho < f'R$ . Clearly,  $\rho = f'R$  is an equation for the caustic. Note that  $\Psi(\rho, s)$  vanishes on the boundary, when  $\rho = 0$ .

The  $\rho$ -dependent part of  $\Psi(\rho, s)$  is an asymptotic form of the Airy function [41]  $\text{Ai}(-z)$  for  $z = 2^{1/3}(kR)^{2/3}(f' - \rho/R) \gg 1$ , i.e. not too close to the caustic. Function (3.41) can be rewritten approximately as

$$\Psi(\rho, s) = (kR)^{-1/6} \text{Ai} \left( \frac{2^{1/3}k^{2/3}}{R^{1/3}} \rho - z_n \right) \exp \left[ i \int l(s) ds/R \right] \quad (3.42)$$

where  $l(s) = kR(1 - f')$  is an angular momentum about the local center of curvature and  $z_n$  is the  $n$ th root of  $\text{Ai}(-z)$ . Alternatively, the Airy function can be expressed in terms of the Bessel function  $J_{l(s)}[k(R - \rho)]$  with variable index  $l(s) \gg 1$ . Hence, Eq. (3.42) can be interpreted locally as an eigenfunction for a circle of radius  $R(s)$ . We will return to this point in Sec. 5.5 where the Bessel function will follow directly from the Born-Oppenheimer approximation.

### 3.4 Scattering problem

As was mentioned in the previous section, the billiards that do not support classical whispering gallery orbits may still have the quantum states that are localized near the boundary (perhaps

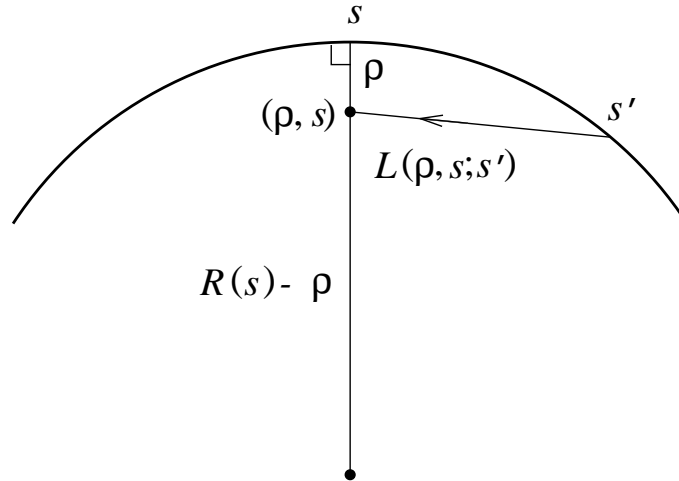


Figure 3.15: Classical orbit of length  $L(\rho, s; s')$  from point  $s'$  on the boundary to point  $(\rho, s)$  inside the billiard. The radius of curvature at point  $s$  is  $R(s)$ .

for finite energy). The candidates for this behavior are the boundaries that have short regions of zero, or even negative, curvature. These regions act like scatterers on the whispering gallery waves that can still exist along the remaining parts of the boundary. The scattering mixes the waves with different transverse quantum numbers  $n$  defined in the previous section. As a consequence, the proper stationary states (or, strictly speaking, quasimodes [3]) are the linear combinations of states with different  $n$ 's. If only a limited number of  $n$ 's contribute to an eigenstate, this eigenstate can be localized near the boundary, and thus look like a whispering gallery mode.

We illustrate these ideas with a model of a boundary that has one point of zero curvature. The work is still in progress. Specifically, we assume that the curvature in the neighborhood of this point, say  $s = 0$ , can be described by the simplest analytic expression

$$\frac{1}{R(s)} = \frac{\mu s^2}{2} \quad (3.43)$$

where  $\mu$  is a dimensional parameter. [In the Cartesian coordinates this boundary is locally  $y(x) = (\mu/4!)x^4$  where zero curvature is at  $x = 0$ .] The boundary is assumed closed in a regular fashion for  $|s|$  greater than all relevant scales.

### 3.4.1 Classical theory

Suppose a classical whispering gallery orbit is incident on the singular region from  $s < 0$ . This orbit generates a map in the phase space of the boundary  $(\epsilon, s)$ , where  $\epsilon$  is a (small) angle between the orbit and the boundary at the point of reflection  $s$ . In order to derive the map equations, we introduce, following the recipe in Ref. [4], the local Cartesian coordinates with the origin at a reflection point  $s_i$ . The  $x$  axis touches the boundary such that  $x$  increases with  $s$  and the  $y$  axis points inside the boundary.

Now we can write the parametric equation of the boundary

$$\begin{aligned} x(s) &= \int_{s_i}^s \cos \left[ \int_{s_i}^{s'} \frac{d\xi}{R(\xi)} \right] ds' = s - s_i + O(s^7 \mu^2), \\ y(s) &= \int_{s_i}^s \sin \left[ \int_{s_i}^{s'} \frac{d\xi}{R(\xi)} \right] ds' \\ &= \frac{\mu}{6} \left[ \frac{1}{4} (s^4 - s_i^4) - s_i^3 (s - s_i) \right] + O(s^{10} \mu^3). \end{aligned} \quad (3.44)$$

From this we find the angle of reflection

$$\begin{aligned} \epsilon_i &\approx \tan \epsilon_i = \frac{y(s_{i+1})}{x(s_{i+1})} \\ &= \frac{\mu}{24} [s_{i+1}^3 + s_{i+1}^2 s_i + s_{i+1} s_i^2 - 3s_i^3] + O(s^9 \mu^3) \end{aligned} \quad (3.45)$$

where  $s_{i+1}$  is the next reflection point. Another equation results from the elementary geometry

$$\epsilon_{i+1} + \epsilon_i = \int_{s_i}^{s_{i+1}} \frac{ds}{R(s)} = \frac{\mu}{6} [s_{i+1}^3 - s_i^3]. \quad (3.46)$$

Equations (3.45) and (3.46) provide the approximate classical map. The first is the cubic equation for  $s_{i+1}$ . Once  $s_{i+1}$  is known, it can be used in the second equation to obtain  $\epsilon_{i+1}$ .

Far from the region of small curvature, where

$$|\Delta s_i| \equiv |s_{i+1} - s_i| \ll s_i, \quad (3.47)$$

we can expand the map equations in  $\Delta s_i$  to express

$$\Delta \epsilon_i \equiv \epsilon_{i+1} - \epsilon_i \approx \frac{\mu}{6} s_i \Delta s_i^2 \approx \frac{2}{3} \epsilon_i \frac{\Delta s_i}{s_i}. \quad (3.48)$$

Treating this as a differential equation we deduce that  $\epsilon(s) \propto s^{2/3} \propto R^{-1/3}(s)$ . This confirms the well-known result that

$$I = \epsilon R^{1/3} \quad (3.49)$$

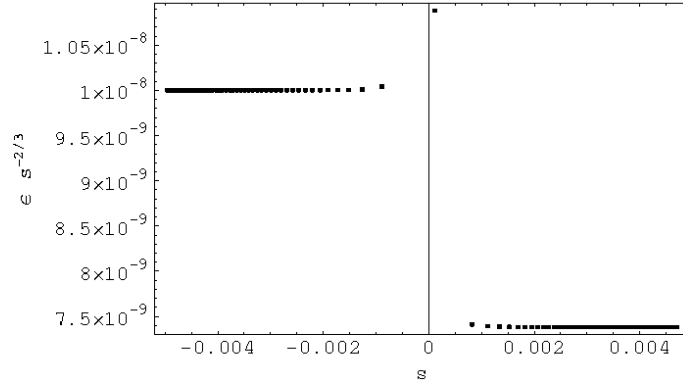


Figure 3.16:  $\epsilon s^{-2/3}$  at the bounce points  $s_i$  for a classical orbit ( $\mu = 1$ ). The quantity is constant outside of the singular region near  $s = 0$ .

is an adiabatic invariant asymptotically for  $\epsilon \rightarrow 0$  if  $R$  is bounded.

In the present case, however, the adiabatic invariant is broken when the trajectory enters the region of small curvature (however small the initial  $\epsilon$  may be). Figure 3.16 shows the quantity  $\epsilon_i s_i^{-2/3}$ , which is proportional to  $I$ , for a certain orbit passing through the singular region. Clearly, it is almost constant on the approach, then it changes significantly within a couple of bounces, after which it stays constant again but at a different value. This observation agrees with Eq. (3.47) that estimates the size of the critical region as two jumps (i.e. only one reflection point of any orbit lies in the critical region for this orbit). The critical region thus depends on the orbit. Explicitly, the size of the jump outside of the critical region is  $\Delta s(s) \simeq \epsilon(s)R(s) \sim I/(\mu s^2)^{2/3}$ . Taking  $s \sim \Delta s$  we estimate the size of the critical region as

$$|\Delta s| \sim I^{3/7}/\mu^{2/7}. \quad (3.50)$$

This estimate will reemerge in the semiclassical regime.

Now consider a family of orbits with the same  $I$  that are incident on the singular region from one side. We are interested in the “spectrum” of  $I$ ’s after the orbits pass through this region. The final values of  $I$ ’s for such family are shown in Fig. 3.17. We chose an arbitrary orbit with a an initial adiabatic invariant  $I_0$ , shown as a horizontal line. Then we started 100 orbits equidistantly from the interval  $(s_0, s_1)$ , i.e. between the first two bounces of the original

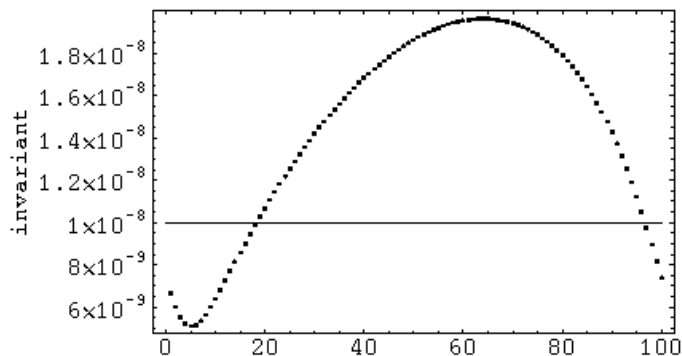


Figure 3.17: Values of adiabatic invariant  $I$  for 100 orbits after they pass the singular region. The orbits had the same initial  $I$  indicated by the horizontal line.

orbit, with the initial  $\epsilon = I_0 R^{-1/3}$ . The figure shows the final  $I$  vs. the orbit number.

Clearly, there is a considerable spread in the final values, and thus the family and the caustic associated with it no longer exist beyond the  $s = 0$  region.<sup>1</sup> In fact, numerically, the maximal and minimal final values of  $I$  are related to the initial value  $I_0$  by

$$I_{\max}/I_0 \approx 1.96, \quad I_{\min}/I_0 \approx 0.51. \quad (3.51)$$

This agrees with the relation

$$I_{\max}/I_0 = I_0/I_{\min}, \quad (3.52)$$

which is proven below. These results are important for the scattering theory in the next section.

It should be pointed out that the right hand sides of Eq. (3.51) are valid for any  $\mu$  and any sufficiently small  $I_0$ . This follows from the scaling properties of the equations of motion (3.45) and (3.46). For any trajectory  $(\epsilon_i, s_i)$  there is a trajectory  $(\epsilon'_i, s'_i) = (\epsilon_i, s_i/\alpha)$  that satisfies the equations of motion in a billiard with a new parameter  $\mu' = \alpha^3 \mu$ . The new adiabatic invariant

<sup>1</sup>A generic orbit going around the generic billiard will have a certain statistical probability to increase  $I$  on each return to the  $s = 0$  region, i.e. it will make a kind of random walk in  $I$ -space. After some time it will eventually diffuse in the large  $I$  region, where the map equations are no longer valid. Thus there is no classical localization near the boundary for a generic orbit.

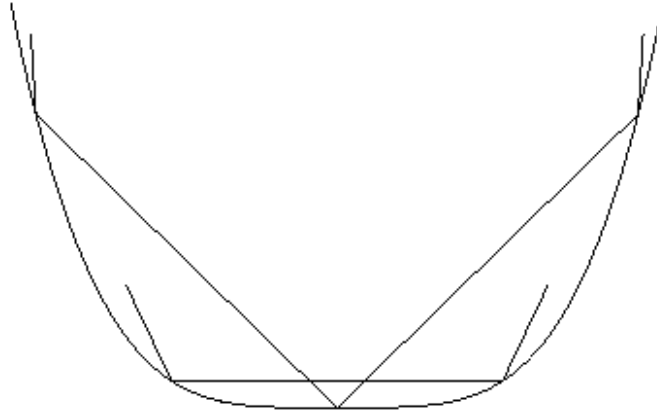


Figure 3.18: Two orbits that preserve the adiabatic invariant.

$I' = I/\alpha^{1/3} \propto I$ . This proves the  $\mu$ -independence. Likewise, an orbit  $(\alpha\epsilon_i, \alpha^{1/3}s_i)$  satisfies the equations of motion with the same  $\mu$ , but has the adiabatic invariant  $\alpha^{7/9}I$ . This shows the independence of  $I_0$ .

Now we can justify Eq. (3.52). Suppose an orbit starts with  $I_0$  and ends up with  $I_1 = I_{\max}(I_0) = \eta I_0$  where  $\eta \approx 1.96$ . Since there are time-reversal and  $s \rightarrow -s$  symmetries, we can start an orbit with  $I_1$  that ends up with  $I_0 = \eta^{-1}I_1$ . We claim that  $I_0 = I_{\min}(I_1)$ . Indeed, if there is a final  $I_2 < I_0$  then we can start an orbit with  $I_2$  that ends up with  $I_1$  and  $I_1/I_2 > \eta$ . But this contradicts the relation  $I_{\max}(I)/I = \eta$ , which is true for any  $I$  according to the previous paragraph. We thus showed that  $I_{\min}(I_1) = \eta^{-1}I_1$ , which, again, must be true for any  $I_1$ . This completes the proof of Eq. (3.52).

Finally, we see from Fig. 3.17 that there are two trajectories that preserve adiabatic invariant. These are the two orbits symmetric under  $s \rightarrow -s$ . One bounces at  $s = 0$ , another at  $s_{i+1} = -s_i$  for some  $i$  (Fig. 3.18).

### 3.4.2 Semiclassical theory

The destruction of caustic prevents us from applying the standard quantization procedure, for example, the ray method. On the other hand, the whispering gallery mode is well-defined

outside the small curvature region. So, before looking for the stationary states inside a closed boundary, we may first consider the scattering problem of determining the amplitudes of transitions between the modes due to the flat region.

Suppose a mode with a transverse quantum number  $n$  is incident from  $s = -\infty$ . Its surface of section wavefunction  $\psi_n(s)$  is given by Eq. (3.33). With the open boundary the energy  $k^2$  is not quantized. It is conserved throughout the motion serving as an external parameter. According to the Eqs. (3.37) and (3.38) the whispering gallery mode is well-defined for

$$|s| \gg |s - s'|_{\text{st}} \sim (n/\mu^2 k)^{1/7}. \quad (3.53)$$

Since the stationary phase quantity  $|s - s'|_{\text{st}}$  corresponds to the size of the classical jump, we find that the strong inequality is similar to the classical condition (3.47). In fact, the second estimate is associated with another classical equation (3.50). To show this, we note that, since the phase of  $\psi_n(s)$  is a projection of the semiclassical momentum onto the boundary, there is a relation  $\cos \epsilon \simeq 1 - f'_n$ . Here  $\epsilon$  is the earlier defined angle between the classical orbit and the boundary at the reflection point  $s$ , and  $f'_n$  is given by Eq. (3.34). Then the adiabatic invariant can be expressed in terms of the quantum quantities as

$$I = I_n(k) \simeq \sqrt{2f'_n} R^{1/3} = \frac{2^{1/3} \sqrt{z_n}}{k^{1/3}} \quad (3.54)$$

where  $z_n \approx [\frac{3}{2}\pi(n - \frac{1}{4})]^{2/3}$  is the  $n$ th root of  $\text{Ai}(-z)$  for large  $n$ . This connects Eqs. (3.53) and (3.50). We see that the  $n$ th transverse mode is related to the classical family with the adiabatic invariant  $I_n$ .

As we know, the whispering gallery wavefunction  $\psi_n(s)$  is not valid near  $s = 0$ . It will be scattered into a number of transverse modes that are well-defined for sufficiently large positive  $s$ . We are interested in the transition amplitude between  $\psi_n(s < 0)$  and  $\psi_{n'}(s > 0)$ . In order to apply the  $T$ -operator technique to the scattering problem, the surface of section can be divided into an external (SSE) and internal (SSI) pieces [34], such that  $\psi_n$  and  $\psi_{n'}$  are well-defined on the SSE. From the previous discussion we conclude that the size of SSI is of order of two classical jumps. We will give an explicit definition later, but for now we assume only that the classical orbit that belongs to the family  $I_n$  before the scattering and to the family  $I_{n'}$  after the scattering makes *one and only one* bounce within the SSI. (In principle, we could extend the SSI to two or more bounces, which would make the theory more precise and also more



complicated.)

Suppose that the SSI is an interval  $(-s_n, s_{n'})$ . The transfer operator between point  $s < -s_n$  and point  $s' > s_{n'}$  is

$$T^2(s', s) \simeq \int_{-s_n}^{s_{n'}} ds'' T(s', s'') T(s'', s) \simeq \left[ \frac{k}{2\pi i} \left| \frac{\partial^2 L}{\partial s' \partial s} \right| \right]^{1/2} e^{ikL(s', s)} \quad (3.55)$$

where  $L(s', s)$  is the length of the classical orbit between  $s$  and  $s'$  that makes one bounce within the SSI. Note that this expression is valid only for the given  $n$  and  $n'$  in the  $S\Phi$ , because we did not include the orbits from other families that have a different number of bounces in the SSI. The scattering amplitude

$$S_{n'n} = (T^2)_{n'n} = \int_{-\infty}^{-s_n} ds \int_{s_{n'}}^{\infty} ds' \psi_{n'}^*(s') T^2(s', s) \psi_n(s). \quad (3.56)$$

When we evaluate this integral by the  $S\Phi$ , only those  $s$  and  $s'$  that belong to a certain classical orbit are selected. Namely, this is the orbit that belongs to the family  $I_n(k)$  before the scattering and  $I_{n'}(k)$  after the scattering. The stationary points  $s_{\text{st}}$  and  $s'_{\text{st}}$  are the points of the last bounce before the SSI and the first bounce after the SSI, respectively. We conclude from Eq. (3.51) and Fig. 3.17 that, given  $n$ , the stationary points exist for those  $n'$  that satisfy  $0.51I_n(k) < I_{n'}(k) < 1.96I_n(k)$ , or, according to Eq. (3.54),

$$0.26z_n < z_{n'} < 3.84z_n, \quad (3.57)$$

moreover, they come in pairs. Equation (3.57) shows that within the  $S\Phi$  an incident mode scatters into a limited number of modes. For example, if  $n = 1$  (the lowest mode) then  $n' = 1, \dots, 5$ .

Clearly, if the  $n \rightarrow n'$  transition is possible then the  $n' \rightarrow n$  transition is also possible because of the symmetry. The same conclusion follows from Eq. (3.57),<sup>2</sup> based on the classical property (3.52), which is a consequence of the same symmetries. In addition, the probabilities of these transitions must be the same. This is ensured by the unitarity of the scattering matrix (3.56). In the  $S\Phi$  the  $T$ -operator is unitary and so is  $S_{n'n}$ .

The  $S\Phi$  result is independent of the limits of integration  $s_n$  and  $s_{n'}$ . In order to go beyond the  $S\Phi$ , one should, first of all, improve the transfer operator to have it include orbits with a different number of bounces. The boundaries of the SSI can be defined by the orbit in Fig.

---

<sup>2</sup>0.26 = 1/3.84

3.18 that does *not* bounce at  $s = 0$ . Let  $s_n$  be the reflection point of this orbit that is the closest to the origin. From the map equations we find

$$s_n \approx (36I_n^3 \mu^{-2})^{1/7} \approx [108\pi(n - 1/4)k^{-1}\mu^{-2}]^{1/7} \quad (3.58)$$

[cf. Eq. (3.53)]. With this definition the  $S\Phi$  orbit makes one bounce within the SSI.

If the boundary is closed, i.e. the states  $\psi_n(s)$  are defined on  $s_{n'} < s < -s_n$ , then one can consider the propagator  $(\Lambda \cdot S)_{n'n}$  around the circumference. Here  $\Lambda_{n'n}$  is a diagonal unitary matrix that accounts for the phase change outside of the singular region. Its elements are just  $e^{ik[\mathcal{L}_n - f_n(\mathcal{L}_n) + f_n(0)]}$  where  $\mathcal{L}_n$  is the length of the regular part of the boundary for the state  $\psi_n(s) \sim e^{ik[s - f_n(s)]}$ . The product  $(\Lambda \cdot S)_{n'n}$  can be diagonalized. Its eigenvalues will be of the form  $e^{i\lambda_j(k)}$ . Since  $S_{n'n} \approx 0$  for  $n$  and  $n'$  outside of the range (3.57), we presume that the new eigenmodes will, in general, include the number of original modes within this range (although this qualitative statement should be verified). The wavenumber  $k$  is quantized by the condition  $\lambda_j(k) = 2\pi n$ . So, if a billiard boundary contains a point of zero curvature, the whispering gallery modes may still exist (Fig. 3.14) but they are no longer simple Airy function type solutions. These conclusions need to be verified by the direct numerical computations, which are in the plans for the future.

## 3.5 Conclusions

In this chapter we considered several examples when the perturbation theory can be applied. The perturbed rectangular billiard, like the perturbed circle, is one of the few systems where the *unperturbed* action depends only on the difference of their *natural* coordinates. It is straightforward to build the perturbation theory in its general form in this case without changing to the action-angle variables. As we know, a perturbed system may possess the eigenstates that are localized near the (semiclassically) stable periodic orbits. We have an example of such state localized near the long diagonal in a tilted square. To have a strong localization, the perturbation of the boundary  $\delta L$  must be much greater than  $\lambda^2/L$ , where  $\lambda$  is the wavelength.

We have discussed a number of non-perturbative cases in which the  $T$ -operator method can be used to derive the analytic expressions for the wavefunctions and energy levels. These include the localized states in the ice-cream cone billiard, the bouncing ball states in a stadium

and near a period-2 orbit, the whispering gallery modes. Moreover, the theory allows to include an additional perturbation to such systems, for example, to tilt the sides of the stadium.

The standard whispering gallery modes result from the quantization of classical families of orbits that are localized near the boundary. The families lie on the invariant tori that exist for the smooth boundaries with positive curvature in the limit of small sliding angle. When the boundary contains a point or a short interval of zero curvature, the classical tori do not exist but the localized quantum states are still possible. The bound state problem involves finding the scattering amplitudes, which is another area where the semiclassical surface of section method can be used.

## Chapter 4

# Square billiard in magnetic field

In this chapter we consider a square billiard where the perturbation is caused not by the boundary, but by the magnetic flux perpendicular to its plane. We concentrate on two particular cases: a uniform magnetic field and an Aharonov-Bohm flux line (ABFL). The latter system is purely quantal — the famous Aharonov-Bohm effect [2] results from the phase interference and has no classical analogue. We will be interested precisely in the effect of phase interference on the eigenstates in the billiard, and therefore even in the uniform field case will neglect the Lorentz force (below we estimate the field where it can be done). We know from the previous chapters that a relatively small non-integrable perturbation of an integrable square makes it possible for the strongly localized states to exist (Figs. 3.5, 3.6). This is still the case when the perturbation is the magnetic flux [57], and these states will be the primary focus of our discussion.

Although we confine our attention to the weakly non-integrable billiard, the ergodic behavior of the system for larger fields can be of interest. As in the Sinai billiard, the magnetic field imposes its circular symmetry on the square, which leads to chaos. Classically, depending on the field, mixed and chaotic regimes are possible [8]. Quantally, one is interested in the energy level statistics. The energy level distribution in a strongly chaotic billiard depends on the symmetries of the system, in particular, the time-reversal symmetry. The magnetic field breaks this symmetry, and, in general, the statistics will be different from the non-magnetic chaotic billiard [12]. (The square in uniform field still has an antiunitary symmetry, however.) The spectral statistics of a rectangular billiard with the ABFL at the center is discussed in Refs. [28, 65].

The measurements of the orbital magnetic susceptibility in the array of GaAs ballistic squares [51] motivated a certain amount of theoretical activity in the last few years [67]. The trace formula is a powerful semiclassical approach that allows one to express the density of states (and thus the susceptibility) in terms of the actions of the periodic orbits. For the relevant temperatures only the short orbits need to be taken into account. In the weak field regime, when the perturbed Berry-Tabor trace formula can be used, our perturbation theory also allows to find the susceptibility.

The main reason to use the perturbation theory, however, is to predict and give the approximate expressions for the wavefunctions. Even the relatively simple analytical formulas produce the states with the non-trivial probability and current distributions. It is possible to have current loops of opposite sense within one state. For a given field one finds the states with the overall current ranging from paramagnetic to diamagnetic, including those with the small overall current but strong local currents nearly canceling each other.

## 4.1 Uniform field

### 4.1.1 Limits of applicability

A free particle of charge  $e$  moves in the uniform field  $B$  along a circular orbit of cyclotron radius  $R_c = mcv/eB$  where  $v$  is its speed. If confined by the square boundary the orbit will consist of the respective arcs. We are interested in the regime when the Lorentz force can be neglected in the lowest order and the orbits are made up of nearly straight segments. This means that  $\epsilon = L/R_c$ , where  $L$  is the side of the square, is a small parameter. In this case the classical momentum  $mv \gg eA/c$ , where  $A$  is the vector potential, so one can approximate  $mv \simeq \hbar k$  in the semiclassical picture. Then we can express  $\epsilon = 2\pi\phi/\phi_0 kL$ , where  $\phi = BL^2$  is the flux through the billiard and  $\phi_0 = hc/e$  is the flux quantum. We shall see that  $\epsilon$  is the small parameter of the perturbation theory.

In the units  $\hbar = c = e = L = 1$  we have  $\epsilon = B/k \ll 1$  where the dimensionless field  $B = \phi = 2\pi\phi/\phi_0$ . Without loss of generality we assume  $B > 0$ . In the semiclassical approximation we take the wavenumber  $k \gg 1$ . As explained in the beginning of Ch. 2, the resonant perturbation theory is required when  $k\sqrt{\epsilon} = \sqrt{kB} \gtrsim 1$ , i.e. when the magnetic field is relatively large. The

upper boundary for  $B$  is given by the number of terms kept in the perturbation series and by the smoothness of the perturbation (which determines the onset of diffraction). If the terms of order no higher than  $M$  are kept then  $kb^{M+1} \ll 1$  where  $b = \sqrt{\epsilon}$ . To keep the diffraction effects small we limit  $kb^4 \ll 1$  (see the next section), but if we do not go higher than the second order then the stricter condition  $kb^3 \ll 1$  must be imposed. Note that if  $k$  is fixed then  $B$  may not be too big, if  $B$  is fixed then  $k$  should be large enough, and if  $\epsilon$  is fixed then the energy is bounded. With the ABFL the diffraction is stronger, and  $kb^2 \ll 1$  in that case.

### 4.1.2 Effective potential and eigenstates

As far as the formal theory is concerned, the square in magnetic field is similar to the square with the perturbed boundary (Sec. 3.1).<sup>1</sup> Again we use the method of images reflecting the square about its boundaries. The magnetic field has opposite signs in the adjacent squares and the orbits are curved differently (Fig. 4.1). Note that we chose the origin at the center of the square. The Poincaré surface of section (PSS) is the bottom side  $y = -1/2$  identified with  $y = 3/2$ . We will be interested in the states near resonances (periodic orbits) since they differ the most from the states of the unperturbed billiard. Figure 4.1, for example, shows a trajectory near the  $(1, 1)$  resonance. This trajectory is paramagnetic, the square boundaries make it circulate in the opposite direction from a free particle in the field.

The action along the orbit in the extended scheme is

$$S(x, x') = k\sqrt{4 + (x - x')^2} + \Phi(x, x') \quad (4.1)$$

where  $\Phi = (e/c) \int \mathbf{A} \cdot d\mathbf{r}$ . The curvature of the orbit can be neglected because it makes a correction of  $\epsilon^2$ . We will primarily consider the  $(1, 1)$  resonance since, as will become clear, it is the most important. In this case the PSS wavefunction has the form  $\psi(x) = e^{i\kappa x} \hat{\psi}_m(x)$  where  $\kappa = k \cos 45^\circ = k/\sqrt{2}$ . The slower varying function  $\hat{\psi}_m(x)$  satisfies the Schrödinger equation

$$\hat{\psi}_m'' + [E_m - V(x)] \hat{\psi}_m = 0. \quad (4.2)$$

The effective potential  $V(x) = -k\Phi(x, x-2)/\mathcal{L}$  is proportional to the perturbed part of the action evaluated along the unperturbed orbit of length  $\mathcal{L} = \sqrt{8}$ . Note that  $\Phi(x, x-2)$  is just

<sup>1</sup>The same lowest order results are given by the channeling method (Sec. 5.3).

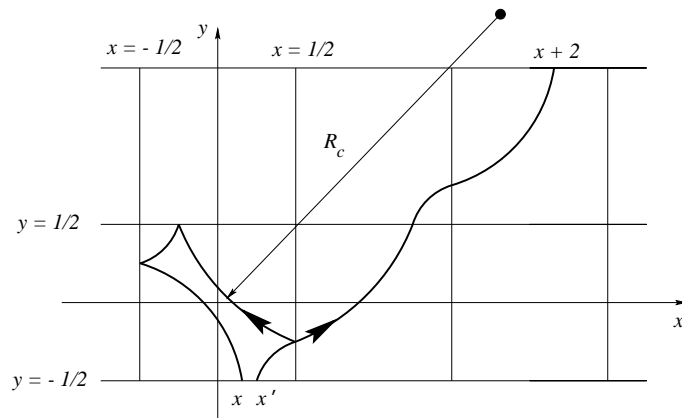


Figure 4.1: Method of images for the square in magnetic field. The magnetic field has different signs in the adjacent squares and the orbits are curved differently.  $R_c$  is the cyclotron radius. The curvature is exaggerated for clarity. The Poincaré surface of section is  $y = -1/2$  identified with  $y = 3/2$ . The orbit shown is close to the  $(1, 1)$  periodic orbit. It goes from  $x'$  to  $x + 2$  identified with point  $x$  in the original square. The square causes the particle to circulate in the paramagnetic sense, which is opposite to the direction of a free orbit in the field.

the flux enclosed by the unperturbed periodic orbit in the original square, equal  $B$  times the area of the loop with the positive sign for counter-clockwise orbits. The potential is then

$$V(x) = \begin{cases} -Bk \left( \frac{1}{2} - 2x^2 \right) / \mathcal{L}, & x \in \left[ -\frac{1}{2}, \frac{1}{2} \right] \\ Bk \left[ \frac{1}{2} - 2(x+1)^2 \right] / \mathcal{L}, & x \in \left[ \frac{1}{2}, \frac{3}{2} \right] \end{cases} \quad (4.3)$$

with the periodicity  $V(x+2) = V(x)$ . The potential is proportional to  $k^2\epsilon$ , which justifies the use of  $\epsilon$  as a small parameter.  $V(x)$  consists of alternating parabolic wells and barriers of height  $Bk/2$  joined smoothly at  $x = \pm 1/2$ , where the potential is odd. Note that the potential for the tilted square of Sec. 3.1.4 for the same resonance is even on the boundary because of the time-reversal symmetry.

The potential  $V(x)$  has a discontinuous second derivative at  $x = \pm 1/2$  due to the diffraction from the corners. It will bring a step-function to the  $kb^4$ -order of the perturbation theory. Since the perturbation expansion takes place in the *phase* of Bogomolny's equation, the discontinuity allows to shift the pieces of  $V''(x)$  independently by integer number of  $2\pi$ . This is the reason for the condition  $kb^4 \ll 1$ . (By the same token, we must require  $kb^3 \ll 1$  in the tilted square.)

The potential is negative for the trajectories leaving the PSS with the positive velocity projection  $v_x$ . These trajectories go counter-clockwise around the square. The minimum at  $x = 0$  indicates a stable periodic orbit. In its neighborhood the potential is of the harmonic oscillator type, so for the low-lying states the energies are approximately given by

$$E_m = -\frac{1}{2} \frac{Bk}{\mathcal{L}} + \left( m + \frac{1}{2} \right) \sqrt{\frac{8Bk}{\mathcal{L}}}. \quad (4.4)$$

The formula holds for  $m \ll \sqrt{Bk/\mathcal{L}}$ . The lowest wavefunction  $\hat{\psi}_0(x) = e^{-\sqrt{\frac{Bk}{2\mathcal{L}}}x^2}$  is localized near  $x = 0$ . The two-dimensional state is localized near the stable periodic orbit (Fig. 4.4). Not surprisingly, it maintains the paramagnetic current, as explained below. The wavefunctions with higher  $m$ 's penetrate into the region  $1/2 < |x| < 1$  more and more. Hence these states include the diamagnetic orbits. The states with large  $m$  are diamagnetic. The maximum at  $x = 1$  marks an unstable periodic orbit, which is almost a time-reversed stable orbit. Our method accounts for the scars of unstable orbits (Sec. 2.3.5), i.e. the states with  $E_m \approx V_{\max}$  (Fig. 4.11).

In general, Eq. (4.2) should be solved with the periodic condition  $\psi(x+2) = \psi(x)$ . It is



accompanied by the quantization

$$k_{nm} = 2\pi n/\mathcal{L} + E_m(k)/k \quad (4.5)$$

that follows from Bogomolny's equation. Thus  $n$  is roughly the number of wavelengths along the periodic orbit. In the first approximation  $k$  in the *r.h.s.* can be replaced by  $2\pi n/\mathcal{L}$ . Note that  $E_m/k$  weakly depends on  $n$  [cf. Eq. (4.4)]. The energy

$$E_{nm} = k^2 = (2\pi n/\mathcal{L})^2 + 2E_m \quad (4.6)$$

depends on  $B$  only via  $E_m$ .

The two-dimensional wavefunction could be found similarly to the tilted square (Sec. 3.1.4). But here we do it by another method that takes into account the symmetries of the problem. The PSS wavefunction  $\psi(x) = e^{i\kappa x}\hat{\psi}_m(x)$  can be propagated with the Green's function (3.15) to give a two-dimensional wavefunction

$$\Psi_0(x, y) = e^{i\kappa(x+y)}\hat{\psi}_m\left(x - y - \frac{1}{2}\right) \quad (4.7)$$

where we ignored the terms of order  $k\epsilon$  in the phase. In this approximation  $\kappa = \pi n/2$  and  $\hat{\psi}_m(x)$  solves the Schrödinger equation with the boundary condition  $\hat{\psi}_m(x+2) = (-1)^n \hat{\psi}_m(x)$ . By symmetry, there are three more states with the same energy obtained from  $\Psi_0$  by  $90^\circ$  rotations. For example,  $\Psi_1(x, y) = \mathcal{R}\Psi_0(x, y) = \Psi_0(y, -x)$  where  $\mathcal{R} : (x, y) \rightarrow (y, -x)$  is a rotation operator. The gauge is chosen to make the Hamiltonian invariant under  $\mathcal{R}$ . The eigenstates in the physical domain will be the linear combinations of  $\Psi_i$ 's that are also the eigenvectors of  $\mathcal{R}$  with the eigenvalues  $i^{-r}$ ,  $r = 0, \dots, 3$ . The eigenfunction of symmetry  $r$  is

$$\Psi_{(r)}(x, y) = \left(\sum_{s=0}^3 i^{rs}\mathcal{R}^s\right) e^{i\kappa(x+y)}\hat{\psi}_m\left(x - y - \frac{1}{2}\right). \quad (4.8)$$

The eigenstate symmetry  $r$  depends on the quantum numbers  $n$  and  $m$ . By the boundary condition  $\Psi_{(r)}(x, -1/2)$  has to vanish. The  $s = 0, 3$  terms are proportional to  $e^{i\kappa x}$  and must cancel each other. This implies  $\hat{\psi}_m(-x) = -i^{-3r}e^{-i\kappa}\hat{\psi}_m(x)$ . Since the potential  $V(x)$  is even and  $\hat{\psi}_m$  satisfies real boundary conditions we can choose  $\hat{\psi}_m(-x) = (-1)^m \hat{\psi}_m(x)$ . Then  $n$  is related to  $m$  and  $r$  as

$$n \bmod 4 = [2(1 - m \bmod 2) + r] \bmod 4. \quad (4.9)$$

For fixed  $m$  the successive values of  $n$  cycle through the representations of  $\mathcal{R}$ . Note that  $\hat{\psi}_m(x+2) = (-1)^r \hat{\psi}_m(x)$ .

These results are easy to generalize to the other resonances  $(p, q)$ . In the weak field approximation the orbits with even  $pq$  do not enclose any flux. These orbits can be subdivided into  $pq$  smaller loops, half of which are positive, and half are negative, so the total flux is zero. (If the curvature is taken into account, there will be a small flux). In particular, the bouncing ball  $(0, 1)$  orbits are non-magnetic, and  $(1, 1)$  is the lowest resonance that responds to the magnetic field. If  $pq$  is odd, the effective potential is

$$V_{pq}(x) = \frac{q}{p} \left[ \frac{\mathcal{L}_{11}}{\mathcal{L}_{pq}} \right]^3 V \left[ q \left( x + \frac{1}{2} \right) - \frac{1}{2} \right] \quad (4.10)$$

where  $\mathcal{L}_{pq} = 2\sqrt{p^2 + q^2}$  and  $V$  is given by Eq. (4.3). The potential has a period  $2/q$ . If  $kB \ll pq\mathcal{L}_{pq}^3$ , the potential does not support localized states and can be ignored. The PSS states should satisfy the boundary condition  $\hat{\psi}_m(x+2) = e^{-i2\pi\delta} \hat{\psi}_m(x)$  where  $\delta$  is the fractional part of  $np/(p^2 + q^2)$ . The energy is

$$k_{nm}^2 \approx (2\pi n/\mathcal{L}_{pq})^2 + \left( 1 + \frac{p^2}{q^2} \right) E_m^{(q)} \quad (4.11)$$

where we have to distinguish between  $E_m^{(q)}$  for the resonance  $(p, q)$  and  $E_m^{(p)} = (p/q)^2 E_m^{(q)}$  for the resonance  $(q, p)$ . These resonances produce nearly uncoupled states with the same energy that are related by a  $90^\circ$  rotation. The splitting of the levels is negligible unless these resonances are close in the phase space. The latter occurs when  $p/q$  is close to 1 so that the tunneling can be assisted by the  $(1, 1)$  resonance, but not too close to have  $(p, q)$  and  $(q, p)$  resonances destroyed by the  $(1, 1)$  resonance.

### 4.1.3 Magnetic response

The magnetic susceptibility at high temperatures is dominated by the Landau term coming from the smooth part of the density of states. At low temperatures the oscillatory corrections become large as the Fermi wavenumber  $k_F$  increases. This contribution to the susceptibility can be found using the trace formula [67], which does not require the knowledge of the wavefunctions or the spectrum. When the magnetic field is weak enough, the resonant perturbation theory can be used to calculate the share of a particular resonance in the susceptibility. This method is related to the perturbed Berry-Tabor formula (Sec. 6.4).

We start with a grand potential for a system of non-interacting electrons

$$\Omega(T, \mu, B) = -k_B T \sum_a \ln \left[ 1 + e^{-(E_a - \mu)/k_B T} \right] \quad (4.12)$$

where  $\mu$  is the chemical potential and the sum is over the single-electron states. If we are interested in the part of the susceptibility coming from the (1, 1) resonance, we include in the sum the subset of states given by Eq. (4.6). The magnetization  $\mathcal{M} = -\partial\Omega/\partial B$  is

$$\mathcal{M}(T, \mu, B) = - \sum_{nm} \frac{\partial E_{nm}}{\partial B} f_D [E_{nm}(B)]. \quad (4.13)$$

Here  $f_D$  is the Fermi-Dirac distribution function. The sum over  $n$  can be done using the Poisson sum formula. The result is

$$\mathcal{M}(T, \mu, B) = - \sum_m \sum_{s=1}^{\infty} \alpha_m \frac{\mathcal{L} k_B T / 2k_F}{\sinh(\pi s \mathcal{L} k_B T / 2k_F)} \sin \left[ \mathcal{L} s \left( k_F - \frac{E_m}{k_F} \right) \right] \quad (4.14)$$

where  $\alpha_m = \partial E_m / \partial B$  evaluated at  $k = k_F$ . For the other resonances  $(p, q)$  one should substitute  $E_m \rightarrow \left(1 + \frac{p^2}{q^2}\right) E_m^{(q)} / 2$  if  $pq$  is odd; the resonances with even  $pq$  are non-magnetic. The magnetization decreases exponentially as  $\mathcal{L}$  becomes large. Therefore the (1, 1) resonance gives the strongest magnetic response. If we neglect the higher resonances, we do not need to keep the terms with  $s > 1$  either. In the trace formula approach  $s$  gives the number of repetitions of the primitive periodic orbit. The susceptibility is given by  $\chi = \partial\mathcal{M}/\partial B$ . It is exponentially suppressed for high temperature giving place to the Landau susceptibility that decays as a power law. Since  $\chi$  is proportional  $k_F^{3/2}$  ( $k_F$  coming from  $\alpha_m$  and of order  $\sqrt{k_F}$  terms in the sum over  $m$ ) it is greater than the  $k_F$  independent Landau term at low temperature, which is of order of one in our units. In the experiment [51] the temperature was about 10 level spacings, i.e.  $k_B T \simeq 20\pi$ . The squares contained  $2 \div 6 \times 10^4$  electrons which makes  $k_F \simeq 300 \div 600$ . Then  $\pi s \mathcal{L} k_B T / 2k_F \simeq 0.5 \div 1$ , and the exponential suppression is not too strong. If an experiment is conducted on an array of squares the result should be averaged over the distribution of sizes. Because of the oscillating sine factor the result will be reduced. Reference [67] provides the corrections.

The magnetization depends on the response of individual states  $\alpha_m$ . Note that  $\partial E_m / \partial \hat{B} = \partial \langle H \rangle_m / \partial \hat{B} = \left\langle \hat{\psi}_m \left| \hat{V} \right| \hat{\psi}_m \right\rangle$  where  $\hat{B} = Bk/2\mathcal{L}$ ,  $\hat{V}(x) = V(x)/\hat{B}$ , and  $H$  is the effective

Hamiltonian in the Schrödinger equation (4.2). Semiclassically,

$$\frac{\partial E_m}{\partial \hat{B}} = \frac{\int dx \hat{V}(x) [\hat{E} - \hat{V}(x)]^{-1/2}}{\int dx [\hat{E} - \hat{V}(x)]^{-1/2}}. \quad (4.15)$$

If  $\hat{E} = E_m/B$  is treated as a continuous variable, the values of  $\partial E_m/\partial \hat{B}$  as a function of  $\hat{E}$  will fall on a continuous curve independent of  $B$  (Fig. 4.2). The integration is between the turning points. The states with low  $m$ 's have negative  $\alpha_m$  and thus are paramagnetic. The wavefunction has more weight in the region  $x \in [-\frac{1}{2}, \frac{1}{2}]$  which is classically identified with the counter-clockwise orbits and where  $\hat{V}$  is negative. The states with higher  $m$ 's are diamagnetic. In this case the weight shifts towards the turning points located in the region  $|x| \in [\frac{1}{2}, 1]$  where  $\hat{V}$  is positive. If  $\hat{E} = \hat{V}_{\max}$ , the curve has a cusp. The simple WKB formula fails in this case. The wavefunction is large near the unstable periodic orbit, which is strongly diamagnetic. As  $m$  gets even bigger, the wavefunction becomes more uniformly distributed in  $x$  with slightly higher weight near  $x = 1$ . So the states remain diamagnetic but their magnetization goes down.

The quantized transverse “energy” is approximately given by the Bohr-Sommerfeld condition

$$\int dx \sqrt{\hat{E}_m - \hat{V}(x)} = \pi \left( m + \frac{1}{2} \right) / \sqrt{\hat{B}}. \quad (4.16)$$

The number of transverse modes in the resonant island, that can be estimated as  $0.6\sqrt{\hat{B}}$ , depends on  $\hat{B}$ . In the example of Fig. 4.2  $k \approx 142$  and  $B = 25$ , and there are 15 states inside the well. With these parameters we have two special states:  $m = 14$  which is close to the diamagnetic maximum and  $m = 10$  which is almost non-magnetic.

#### 4.1.4 Visual representation of eigenstates

As we learned in the previous sections, the square in magnetic field can support the eigenstates with different degree of localization and a wide range of magnetic properties. Here we show some examples of the wavefunctions and current distributions calculated using the perturbation theory (referred to as “theoretical” results) and compared with the numerical solution of the Schrödinger equation in the square (“numerical” results). We restricted our attention to the states of the (1, 1) resonance that are invariant under the 90° rotation, i.e. having the symmetry

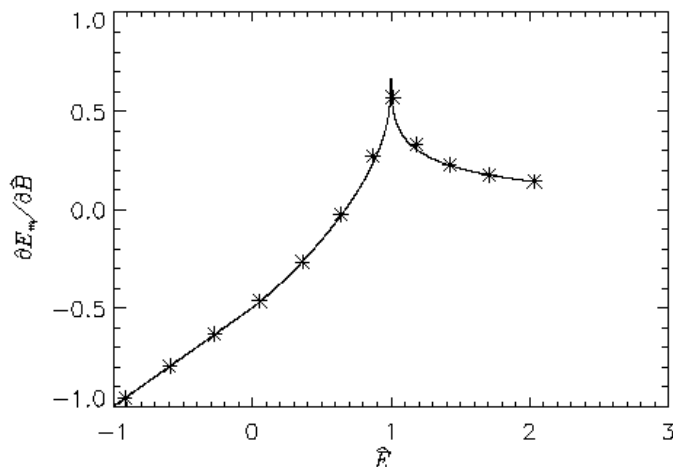


Figure 4.2:  $\partial E_m / \partial \hat{B}$  as a function of  $\hat{E}$ . The stars are at the  $(1, 1)$  resonance states  $n = 62$ ,  $m = 0, 2, \dots, m_{\max} = 14, \dots$ . Magnetic field  $B = 25$ . The continuous curve is given by Eq. (4.15).

$r = 0$  [Eq. (4.8)]. These are the states with either even  $n/2$  and odd  $m$  or odd  $n/2$  and even  $m$ .

A couple of comments on the calculation procedures are in order. In the perturbation theory the one-dimensional Schrödinger equation (4.2) was solved numerically. The two-dimensional wavefunction was constructed using Eq. (4.8). We call these results “theoretical.”

In the “numerical” calculations the two-dimensional Schrödinger equation was solved by diagonalization of the Hamiltonian in the basis of states in the square without magnetic field. The states with the required symmetry are

$$\Psi_{pq}(x, y) = \begin{cases} \sqrt{2} [\cos \pi px \cos \pi qy + \cos \pi qx \cos \pi py], & p \neq q \text{ odd} \\ 2 \cos \pi px \cos \pi qy, & p = q \text{ odd} \\ \sqrt{2} [\sin \pi px \sin \pi qy - \sin \pi qx \sin \pi py], & p \neq q \text{ even} \end{cases}. \quad (4.17)$$

The labels  $p, q$  should not be confused with the resonances. Expand  $\hat{\psi}_m(x) = \sum \bar{\psi}_{m,l} e^{i\pi l x}$  in Eq. (4.8) where  $l$  is integer for  $r$  even and half-odd integer for  $r$  odd. Also  $\bar{\psi}_{m,l} = (-1)^m \bar{\psi}_{m,-l}$ . We expect the largest weights in the state  $(n, m)$  come from the  $B = 0$  states with  $p = \frac{n}{2} + l$ ,

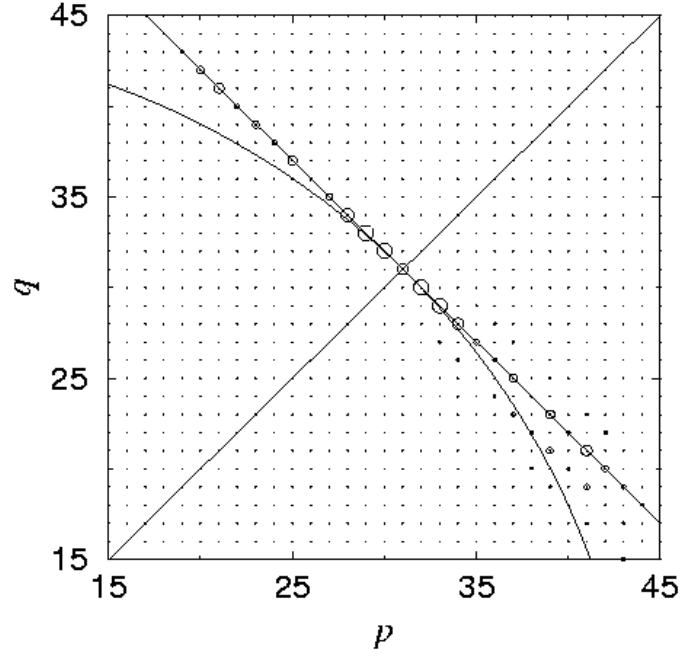


Figure 4.3: Decomposition of the state  $m = 14$ ,  $n = 62$ ,  $B = 25$  into  $B = 0$  basis states. The area of a circle is proportional to the square of the amplitude. The numerically exact results are shown below the diagonal  $p = q$ . Above the diagonal are the weights of theoretical wavefunction Eq. (4.8). A part of the constant energy circle  $p^2 + q^2 = \text{const}$  is shown as well.

$q = \frac{n}{2} - l$ . Figure 4.3 shows these states aligned along the diagonal in  $(p, q)$  plane. The energy of the basis states is  $p^2 + q^2 = \frac{n^2}{2} + 2l^2$  dropping a factor of  $\pi^2$ . If  $l^2 \ll n$ , it is much closer to the base energy  $n^2/2$  than the next base energy  $(n \pm 2)^2/2 \approx \frac{n^2}{2} \pm 2n$ . Nevertheless, there are basis states with other base energies lying near the constant energy circle (Fig. 4.3), for example, the states with  $p' = \frac{n+2}{2} + l'$ ,  $q' = \frac{n+2}{2} - l'$  where  $l'^2 \simeq n$ . However, the matrix elements of the Hamiltonian  $\mathcal{H}_{pq,p'q'}$  are small if the differences  $|p - p'|$ ,  $|p - q'|$ , etc., are large. When the condition  $n \gg l^2 \sim m^2$  breaks down, the basis states with other base energies will be contributing to the eigenstate. This is the case when the terms left out in the phase of Eq. (4.7) become important. The terms that shift  $n$  are of order  $(E_m - V_{\min})/k \sim m^2/n$ . Thus, for large  $m$  our perturbation theory is not too accurate.

The current density is given by

$$\mathbf{j}(x, y) = 2\text{Re}\Psi^*(x, y)[-i\nabla - \mathbf{A}(x, y)]\Psi(x, y). \quad (4.18)$$

The property  $\nabla \cdot \mathbf{j} = 0$  ensures that the streamlines are the closed loops. However, because of the approximate nature of both numerical and theoretical calculations, the small left-over divergence in the regions of small current density may have a big effect. This makes it problematic to construct a reasonable approximation for the streamlines. To overcome this difficulty we *imposed* the divergence-free character of the current by representing  $\mathbf{j}(x, y) = \nabla \times \hat{\mathbf{z}}\chi(x, y)$  where the function  $\chi(x, y) = \int_{1/2}^y j_x(x, y') dy'$ . Then the streamlines of  $\mathbf{j}$  are the contour lines of  $\chi$ . In the exact problem  $\chi(x, y) = \chi(y, x)$ . To see this, note that the Hamiltonian has a symmetry  $\mathcal{H}(x, y) = \mathcal{H}^*(y, x)$ , which means that for a non-degenerate state the wavefunction has the same symmetry (up to a phase factor). From this follows the symmetry for the current  $j_x(x, y) = -j_y(y, x)$ . Then  $\chi(y, x) = -\int_{1/2}^x j_y(x', y) dx' = \int_{1/2}^x \frac{\partial \chi(x', y)}{\partial x'} dx' = \chi(x, y)$ , using the condition  $j_x(\frac{1}{2}, y') = 0$ . In practice, however,  $\chi$  is not symmetric. This is the pay-off for making the approximate current non-divergent. Therefore in our calculations we used the symmetrized version  $\frac{1}{2}[\chi(x, y) + \chi(y, x)]$ . In the figures below we have a good agreement between thus obtained streamlines and other types of current density representations.

Qualitatively, the (1, 1) resonance states can be divided in four classes. The first class consists of the states of the low transverse modes with  $E_m - V_{\min} \ll Bk$ . These states are strongly localized along the stable orbit and have relatively simple paramagnetic current patterns. In Figs. 4.4-4.8 the magnetic field is  $B = 31.4$ . Figure 4.4 shows a three-dimensional representation of the numerical wavefunction  $n = 62$ ,  $m = 0$ . The theoretically estimated wavenumber is  $k \approx 2\pi 62/\mathcal{L} \approx 140$ . The parameter  $k\sqrt{\epsilon} = \sqrt{Bk} \approx 66$  is large indicating the strong localization due to the resonance. Because of the localization only one of the four terms in Eq. (4.8) dominates each side of the square periodic orbit. For example, near  $x = -y = 1/4$  only the  $s = 0$  term is appreciable. Here  $|\Psi(x, y)|^2 \approx \left| \hat{\psi}_0\left(x - y - \frac{1}{2}\right) \right|^2$  which is well approximated by a Gaussian. Near the square boundary there is interference between two terms. For example, near  $y = -1/2$  the  $s = 0, 3$  terms are large, so

$$\begin{aligned} |\Psi(x, y)|^2 &\approx \left| e^{i(\pi n/2)y} \hat{\psi}_0\left(x - y - \frac{1}{2}\right) + e^{-i(\pi n/2)y} \hat{\psi}_0\left(-x - y - \frac{1}{2}\right) \right|^2 \\ &= 4 \left| \hat{\psi}_0(x) \cos\left(\frac{\pi n}{2}y\right) \right|^2. \end{aligned} \quad (4.19)$$

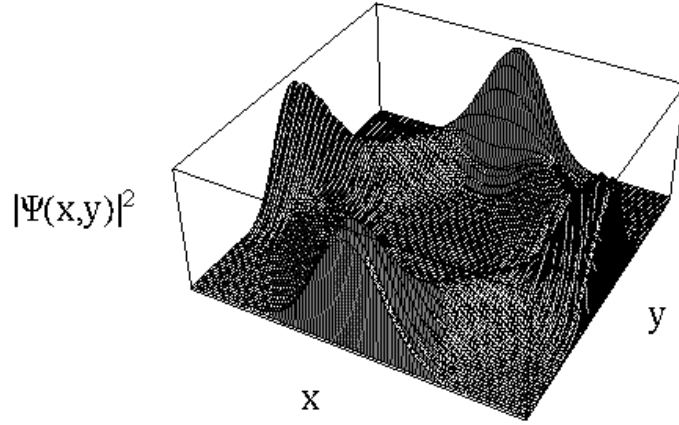


Figure 4.4: Absolute square of the numerical wavefunction for the localized paramagnetic state  $m = 0$ ,  $n = 62$ ,  $B = 31.4$ . According to Eq. (4.19), the profile along the side of the billiard is proportional to  $|\hat{\psi}_0|^2$  and there are fast interference oscillations in the transverse direction.

The cosine factor produces interference fringes parallel to the border. At the first maximum  $|\Psi(0, -\frac{1}{2} + \frac{1}{n})|^2$  is four times larger than  $|\Psi(\frac{1}{4}, -\frac{1}{4})|^2$ . The cross-section  $|\Psi(x, -\frac{1}{2} + \frac{1}{n})|^2$  is also a Gaussian. The interference pattern can be seen in the density plot in the lower left quarter of Fig. 4.5. The rest of the figure shows the current for this state. Starting on the lower left and going counter-clockwise we show a density plot of  $|\Psi|^2$ , the streamlines, the absolute value of the current density  $|\mathbf{j}(x, y)|$ , and the vector field  $\mathbf{j}(x, y)$  (the dot is at the calculated point and the stick size and direction represent the current density magnitude and direction). Of course, close to the boundary the current is parallel to the boundary. Its interference fringes mimic those of the wavefunction.

Figures 4.6-4.8 show another state of the same class  $n = 60$ ,  $m = 1$ . Its surface of section wavefunction is close to the first excited state of a harmonic oscillator. Clearly, the probability and current densities are very small near the point  $x = -y = 1/4$ . They are not exactly zero, however, because the terms with  $s = 1-3$  in Eq. (4.8) have exponentially small tails there. Figures 4.6, 4.7 were obtained numerically and Fig. 4.8 shows the results of theoretical calculations. We see that the theory works well in the low  $m$  case.



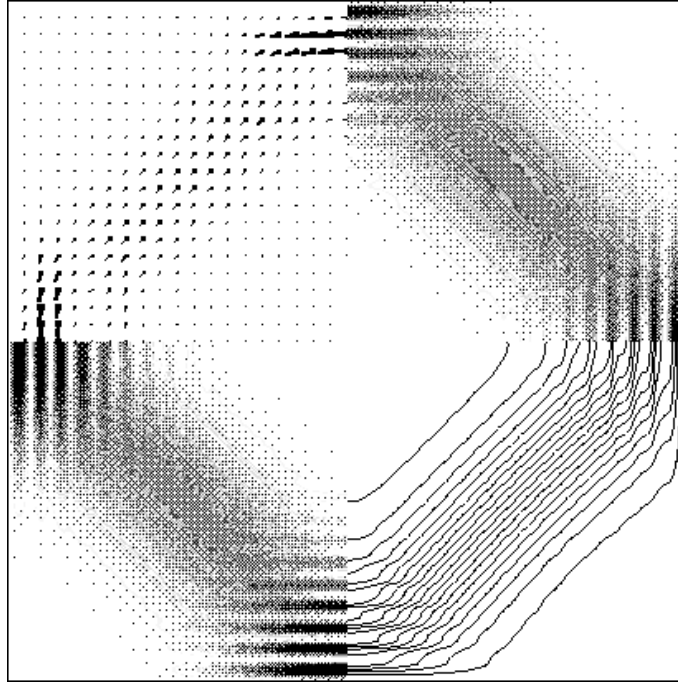


Figure 4.5: Numerical wavefunction and current for the state in Fig. 4.4. The state is symmetric under the  $90^\circ$  rotation. Counter-clockwise from the lower left: a density plot of  $|\Psi|^2$ , current streamlines, a density plot of  $|\mathbf{j}|$ , and a vector field representation of the current (the dot is at the calculated point, the size and direction of the stick represents the current density magnitude and direction).

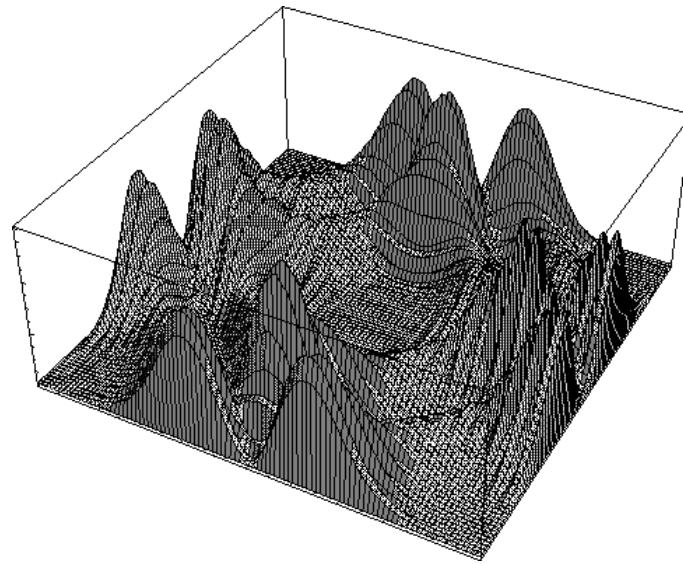


Figure 4.6: Absolute square of the numerical wavefunction for the state  $m = 1$ ,  $n = 60$ ,  $B = 31.4$ .

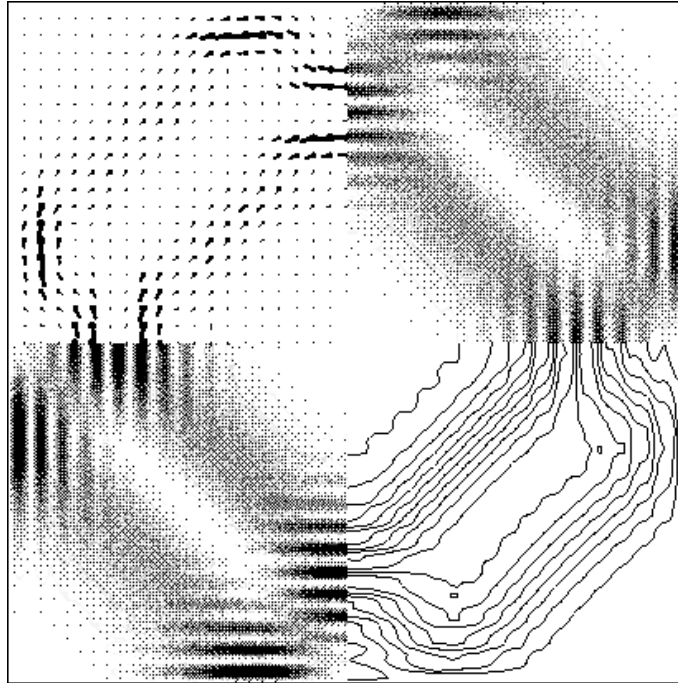


Figure 4.7: Numerical wavefunction and current for the state in Fig. 4.6. The same representation as Fig. 4.5.

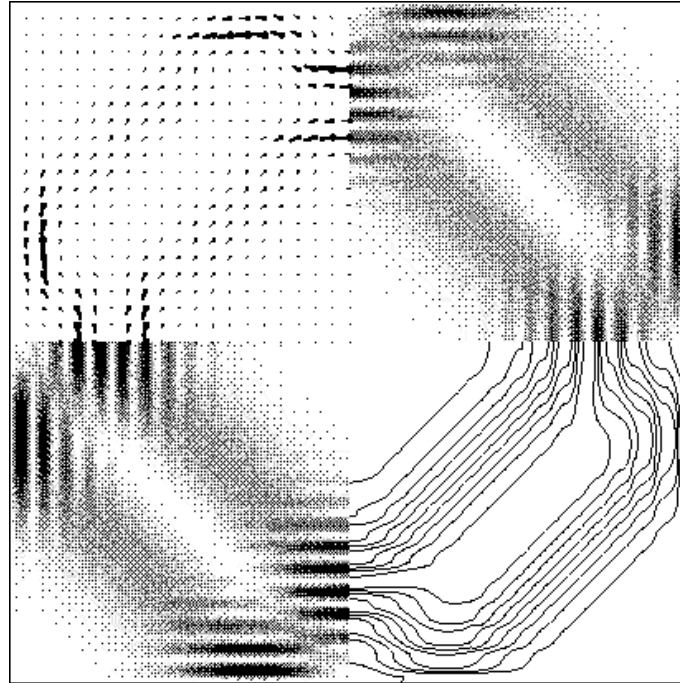


Figure 4.8: Theoretical wavefunction and current for the state in Fig. 4.6. The same representation as Fig. 4.5.

The states with  $|E_m| \ll V_{\max} = Bk/2\mathcal{L}$  belong to the second class. These states are delocalized and have rather complicated probability and current distributions because all four terms in Eq. (4.8) are important throughout the square. These states lie on the border of para- and diamagnetism and are weakly magnetic. Figure 4.9 shows such state  $n = 62$ ,  $m = 10$ ,  $B = 25$ . It has very small magnetization (Fig. 4.2) because the loops of rather strong diamagnetic and paramagnetic currents nearly cancel each other. The figure shows the numerical results as before, except for the upper left corner, where the theoretical streamlines are shown. The theory and numerics differ primarily in the lower current regions. To understand the complexity of the higher  $m$  states and the lack of localization consider the normal derivative  $|\partial\Psi_{62,10}/\partial y|_{y=-1/2}$  on the boundary (Fig. 4.10). In the low  $m$  state it would be proportional to  $|\hat{\psi}_m(x)|$  [cf. Eq. (4.19)]. When  $m$  becomes larger  $\hat{\psi}_m(x)$  extends significantly beyond the physical domain  $[-\frac{1}{2}, \frac{1}{2}]$  (Fig. 4.10), so it has to be “folded” back to this domain with an additional rapidly varying phase factor  $e^{i\kappa x}$ . Formally, it means that the terms with  $s = 1, 2$  in Eq. (4.8) cannot be neglected.

The third class includes the diamagnetic states with  $E_m$  near the top of the potential. The state at the maximum of the magnetization curve (Fig. 4.2) with  $n = 62$ ,  $m = 14$ ,  $B = 25$  is shown in Figs. 4.11 (numerics) and 4.12 (theory). In the case of large  $m$  the theory does relatively poorly, although it is still qualitatively correct. The unperturbed basis states beyond the diagonal  $p + q = n$  appear in the Hamiltonian matrix (Fig. 4.3, below the line  $p = q$ ), while the theory does not reflect this (Fig. 4.3, above the line  $p = q$ ). This state is localized near the unstable orbit, i.e. this is a scar state that we predict. One can even see the two channels in Fig. 4.11 because if  $E_m$  is just below  $V_{\max}$  the wavefunction  $\hat{\psi}_m(x)$  has the excessive weight near the turning points on both sides of the maximum of the potential at  $x = 1$ . In this case we find  $E_m = 628.57$  and  $V_{\max} = 648.64$ . For comparison, we show the state  $n = 62$ ,  $m = 14$ ,  $B = 31.4$  (Fig. 4.13). Here  $E_m = 703.4$  is much lower than  $V_{\max} = 792.2$ , so the two channels are further apart.

One can observe the change of the topology of the current from paramagnetic to diamagnetic by looking at the sequence of states  $m = 6, 8, 10, 12$ ,  $n = 62$ , and  $B = 25$  (Fig. 4.14). Similar effect could be achieved by the change of magnetic field.

The states with  $E_m \gg V_{\max}$  belong to the fourth class. The magnetic field is a small

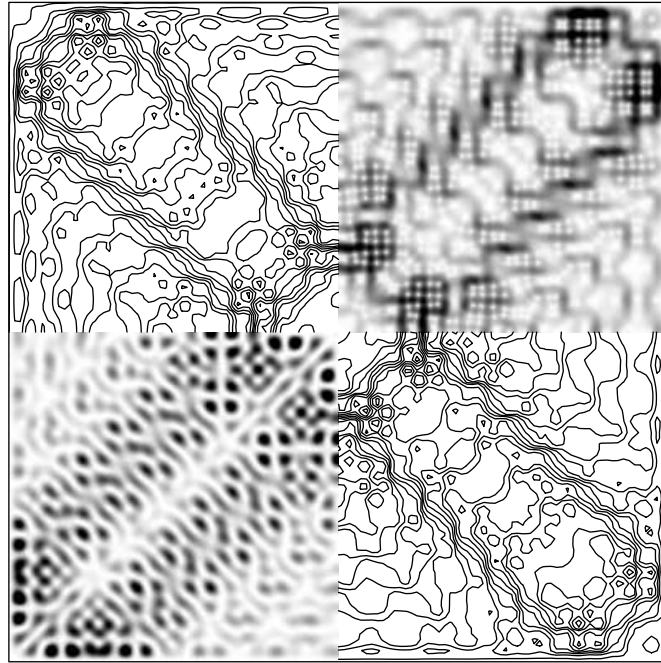


Figure 4.9: Almost non-magnetic state  $m = 10$ ,  $n = 62$ ,  $B = 25$ . The numerical results are shown as before, except for the upper-left corner, where the theoretical streamlines are shown. The theory and numerics disagree mainly in the low-current regions. The diamagnetic loops close to the diagonals nearly cancel the paramagnetic loops in the triangular wedges between the diagonals.

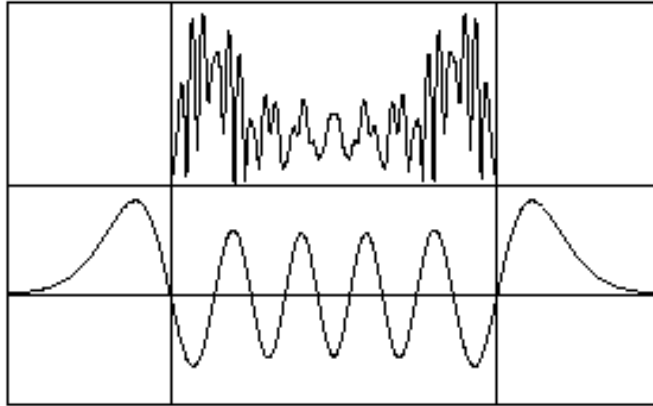


Figure 4.10: Normal derivative  $|\partial\Psi_{nm}/\partial y|_{y=-1/2}$ , obtained numerically (upper plot), and the theoretical surface of section function  $\hat{\psi}_m(x)$  (lower plot) for the state of Fig. 4.9. When  $m$  is large,  $\hat{\psi}_m(x)$  extends considerably outside the domain  $[-\frac{1}{2}, \frac{1}{2}]$  (indicated by the vertical lines). In order to construct the normal derivative, the tails have to be “folded” back with an additional phase factor. For small  $m$  both functions are proportional.

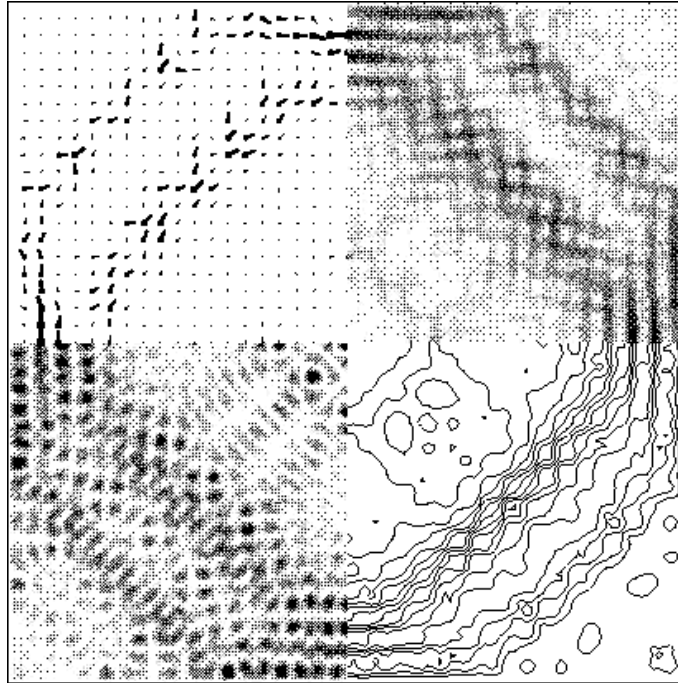


Figure 4.11: Numerical wavefunction and current for the state of maximum diamagnetism  $m = 14$ ,  $n = 62$ ,  $B = 25$ . The same representation as Fig. 4.5.



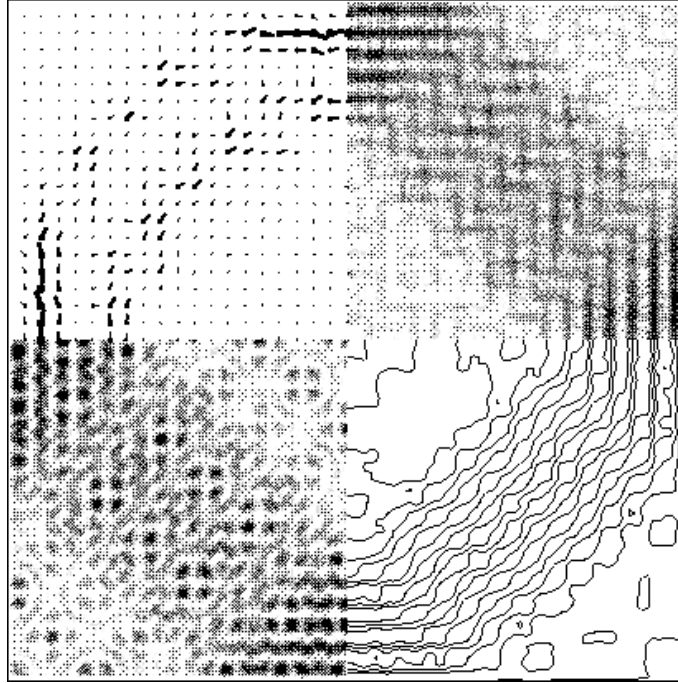


Figure 4.12: Theoretical wavefunction and current for the state in Fig. 4.11. The same representation as Fig. 4.5.

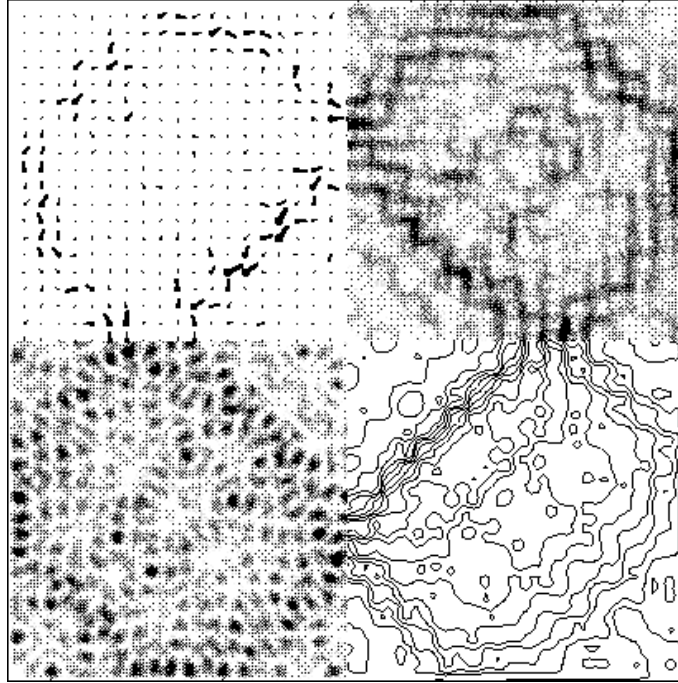


Figure 4.13: Numerical wavefunction and current for the diamagnetic state  $m = 14$ ,  $n = 62$ ,  $B = 31.4$ . The same representation as Fig. 4.5.

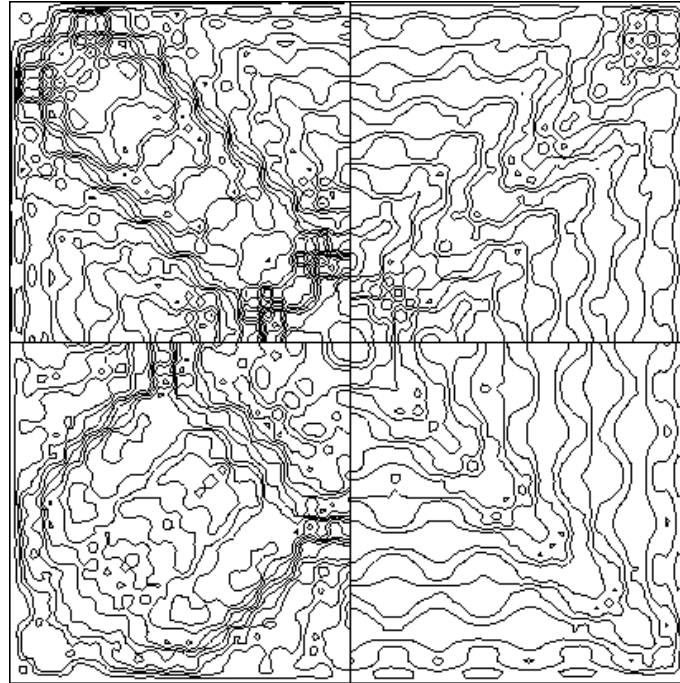


Figure 4.14: Streamlines for the sequence of states  $m = 6, 8, 10, 12$ ,  $n = 62$ ,  $B = 25$ , counter-clockwise from the lower right.

perturbation in this case and the states are weakly diamagnetic. The expansion near  $(1, 1)$  resonance will eventually break down and higher resonances become involved.

## 4.2 Aharonov-Bohm flux line

The theory laid out in the previous sections can be extended to non-uniform flux configurations. If the Lorentz force is neglected then the problem is reduced to finding the flux enclosed by a periodic orbit. Of course, if the flux distribution is not smooth enough, like the ABFL case, we have to worry about the diffraction. To estimate the effect of diffraction consider a finite size flux line of radius  $\rho$  and flux  $\phi$ . An orbit that goes through the flux region is subjected to the Lorentz force produced by the magnetic field  $B = \phi/\pi\rho^2$  and gets deflected by an angle

$$\delta\theta \sim \frac{\phi/\phi_0}{k\rho} \quad (4.20)$$

where  $\phi_0$  is the flux quantum. The diffraction can be neglected if  $\delta\theta \ll 1$ . Clearly, in the zero radius flux line the diffraction effects cannot be neglected. If we define the perturbation parameter  $\epsilon = (\phi/\phi_0)/k$ , i.e. the ratio of the perturbed part of the action to the unperturbed action, then the condition is  $\epsilon/\rho \ll 1$ . This means that the limit  $\rho \rightarrow 0$  cannot be taken before  $\epsilon \rightarrow 0$  if we want to neglect the diffraction. Therefore we have to consider a finite size flux line. In the numerical examples we take  $\phi/\phi_0 = 0.1$  and  $\rho = 0.01$ , while  $k > 120$ . Instead of one flux line, four quarter-strength lines symmetrically located were used in order to reduce the amount of calculations. Within the approximation of our theory it gives essentially the same result as a single line. Note that for the ideal ABFL the matrix elements of the Hamiltonian are infinite if the basis functions do not vanish on the flux line. One can avoid this problem by making the substitution  $\Psi \rightarrow r^{|\phi/\phi_0|}\bar{\Psi}$  where  $r$  is the distance from the flux line [56, 61]. The new wavefunction  $\bar{\Psi}$  satisfies the equation  $\bar{\mathcal{H}}\bar{\Psi} = E\bar{\Psi}$  with the same energy as  $\bar{\Psi}$ . The most singular term of the non-hermitian Hamiltonian  $\bar{\mathcal{H}}$  is of order  $r^{-1}$  instead of  $r^{-2}$ .

We consider the states near the  $(1, 1)$  resonance. A periodic orbit of this family may either enclose the flux line and have  $\pm 2\pi\phi/\phi_0$  added to its action, or pass by the flux line and have no extra action. Hence the one-dimensional wavefunction satisfies the Schrödinger equation (4.2) with a step-wise effective potential. Strictly speaking, the walls of the potential will have a finite width  $\rho$ , because when the orbit goes *through* the flux line there is an additional action

between 0 and  $\pm 2\pi\phi/\phi_0$ . Of course, the profile of the walls depends on the flux distribution within the line. If we are not going beyond the second order of the perturbation theory (Sec. 2.2), we may disregard the finite width of the walls, since the wavefunction does not change much. This way the results would be independent of  $\rho$ . The third order contains the derivative of the potential. In order to neglect it we must require  $k\epsilon^{3/2}/\rho \ll 1$ . Since  $\epsilon/\rho \ll 1$ , we have the condition  $k\sqrt{\epsilon} \lesssim 1$ , or  $k\epsilon \ll 1$ .

The width and position of the square well and barrier depend on the location of the flux. If the flux is located at  $x = 0, y = -\frac{1}{2} + a$ , where  $0 \leq a \leq 1/2$ , the potential is

$$V(x) = \begin{cases} -2\pi\frac{\phi}{\phi_0}\frac{k}{\mathcal{L}}, & x \in [-a, a] \\ +2\pi\frac{\phi}{\phi_0}\frac{k}{\mathcal{L}}, & x \in [1-a, 1+a] \\ 0, & x \in [a, 1-a] \end{cases} \quad (4.21)$$

extended periodically by  $V(x+2) = V(x)$ . Hence, assuming  $\phi > 0$ , the potential consists of the well of width  $2a$  and depth  $2\pi\frac{\phi}{\phi_0}\frac{k}{\mathcal{L}}$  in the interval  $[-\frac{1}{2}, \frac{1}{2}]$  (counter-clockwise orbits) and the same size barrier in  $[\frac{1}{2}, \frac{3}{2}]$  (clockwise orbits). For sufficiently large  $\frac{\phi}{\phi_0}\frac{k}{\mathcal{L}}$  the eigenfunctions are approximately  $\hat{\psi}_m(x) = \cos[(m+1)\pi x/2a + m\pi/2]$ ,  $|x| < a$ , and zero elsewhere. This expression holds for sufficiently small  $m$ . The energy  $E_m \approx -2\pi\frac{\phi}{\phi_0}\frac{k}{\mathcal{L}} + \frac{\pi^2(m+1)^2}{4a^2}$ .

The function  $\hat{\psi}_0$  for  $a = 1/4$  and  $n = 86$  is shown in Fig. 4.15 (a). We include the exponentially small portion of the function for  $|x| > 1/4$ . The upper curve is  $\hat{\psi}_0(x)$  and the lower curve is  $\hat{\psi}_0(-1-x)$ . The PSS wavefunction  $\psi(x) = e^{i\kappa x}\hat{\psi}_0(x)$  should be compared to the normal derivative of the two-dimensional wavefunction  $|\partial\Psi/\partial n|$  at  $y = -1/2$  [curve (b), Eq. (4.8)]. The oscillations appear because of interference of  $\psi(x)$  and  $\psi(-1-x)$ , they scale as  $\hat{\psi}_0(-1-x)$ . The other four curves show the normal derivative calculated numerically. Curve (c) is from full numerical diagonalization, (d) is from the diagonalization in the reduced basis that includes only the unperturbed states along the diagonal  $p = \frac{n}{2} + l, q = \frac{n}{2} - l$  (Sec. 4.1.4). The latter result is very close to the theoretical. Curves (e) and (f) are the numerical results for the ideal single ABFL ( $\rho = 0$ ) with  $n = 82$  and  $n = 70$ . Although there are strong diffraction corrections, the overall shape is given well by the theory. The two-dimensional wavefunction is localized along the stable orbit. The strength of localization is characterized by  $\hat{\psi}_0$ . Figure 4.16 shows  $|\Psi(x, y)|$  for an ideal ABFL,  $n = 58$ . Although the localization is not very strong, the wavefunction has little support in the center and the corners of the square.

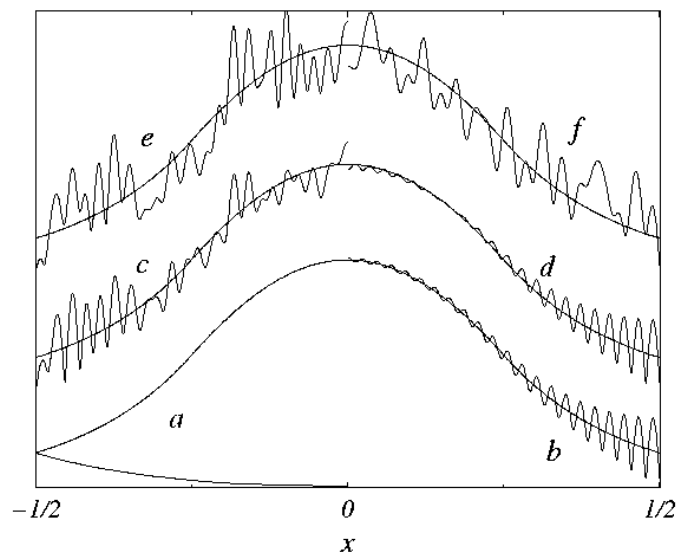


Figure 4.15: State  $m = 0$ ,  $n = 86$  in the square with the flux line,  $a = \frac{1}{4}$ ,  $\phi = 0.1\phi_0$ ,  $\rho = 0.01$ . (a) Upper curve  $\hat{\psi}_0(x)$ , lower curve  $\hat{\psi}_0(-1-x)$ . This function is superimposed on the other plots that show the normal derivative  $|\partial\Psi/\partial n|_{y=-1/2}$ : (b) is the theoretical result from Eq. (4.8), (c) is from the full numerical diagonalization, (d) is from the diagonalization in the reduced basis that consists of the states along the diagonal  $p = \frac{n}{2} + l$ ,  $q = \frac{n}{2} - l$  (Sec. 4.1.4). For comparison, curves (e) and (f) show the numerical results for the ideal single flux line with  $n = 82$  and  $n = 70$ , respectively. Although there are strong diffraction effects, the overall shape is given correctly by the theory.

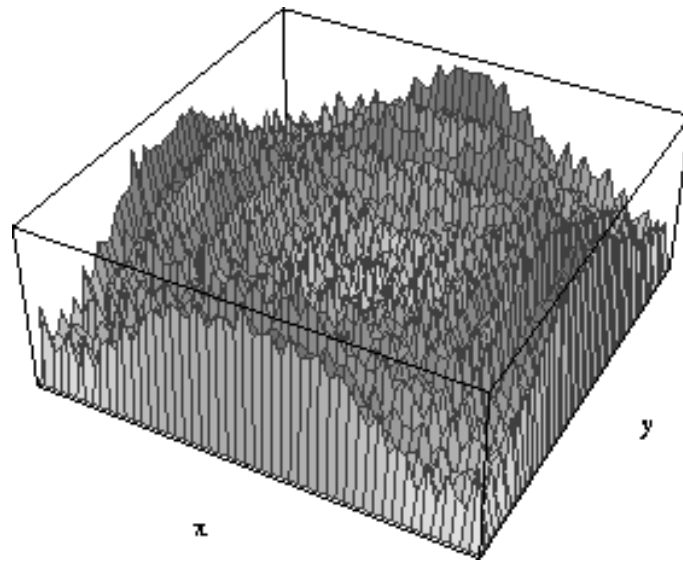


Figure 4.16: Absolute value of the wavefunction,  $n = 58$ ,  $m = 0$ , for an ideal single flux line,  $a = \frac{1}{4}$ ,  $\phi = 0.1\phi_0$ . Note that  $|\Psi(x, y)|$  is almost but not strictly symmetric under the  $90^\circ$  rotation due to the higher order effects.

If the flux is located at the center of the square ( $a = 1/2$ ), the potential well extends to the whole side of the square and there is no spatial localization. For small  $m$  the counter-clockwise orbits are preferred and there is a strong paramagnetic current. The upper part of Fig. 4.17 shows the streamlines for the state  $n = 82$ ,  $m = 0$ , symmetric under the  $90^\circ$  rotation. The lower part of the figure gives the current density along the line  $y = 0$ ,  $x \in [-\frac{1}{2}, 0]$ . Neglecting the  $A$ -term in Eq. (4.18) we have an approximate formula for it,  $j_y(x, 0) \propto -(\cos \pi n x / 2)^2 \left[ \hat{\psi}_m(-x - \frac{1}{2})^2 - \hat{\psi}_m(x - \frac{1}{2})^2 \right]$ . For low  $m$  the second term in the square brackets is small when  $x < 0$ , so  $j_y \leq 0$ . It has equally spaced double zeros at  $x = (2l + 1)/n$ . The factor depending on  $\hat{\psi}_m$  has a zero at  $x = 0$ .

It is interesting to compare the square with ABFL with the “step” billiard. This is a square with the step-wise boundary perturbation. For example, suppose the lower side is perturbed by  $\xi(x) = -\epsilon$ ,  $|x| < a$ , and  $\xi(x) = 0$ ,  $\frac{1}{2} > |x| > a$ . Then for the  $(0, 1)$  resonance (bouncing ball states with the large  $y$ -momentum) the effective potential is proportional to Eq. (4.21) limited to  $x \in [-\frac{1}{2}, \frac{1}{2}]$  with the periodicity  $V(x + 1) = V(x)$  (the system has the time-reversal symmetry). When  $k\epsilon \ll 1$  and  $k\sqrt{\epsilon} \sim 1$ , our theory predicts localization within  $|x| < a$ . If  $k\epsilon = \pi/2$ , i.e.  $2\epsilon$  is a half-wavelength, the classical action for the  $(0, 1)$  orbits within  $|x| < a$  and outside of this region differ by  $\pi$ . This is equivalent to the case  $\phi/\phi_0 = 1/2$ . Since the action enters the phase of the  $T$ -operator, this difference becomes ambiguous, it can be made  $-\pi$  by adding the phase  $2\pi$  for  $|x| > a$ . (This would be impossible in the case of continuous perturbation.) Thus the effective potential is undetermined when  $k\epsilon \gtrsim 1$ . The preliminary numerical results [61] show that in this case there are states localized within  $|x| < a$  and the states localized outside of this region.

### 4.3 Experimental suggestions

Some of the experimental methods mentioned in Sec. 2.3.6 could conceivably be adapted to the billiard with a magnetic flux. The mesoscopic systems like the quantum corrals [27] or the GaAs squares [51] are directly related to our theoretical model, though accurately measuring the wavefunction may be a challenge.

In the liquid surface wave experiments the effect of the flux can be modeled by the flow of



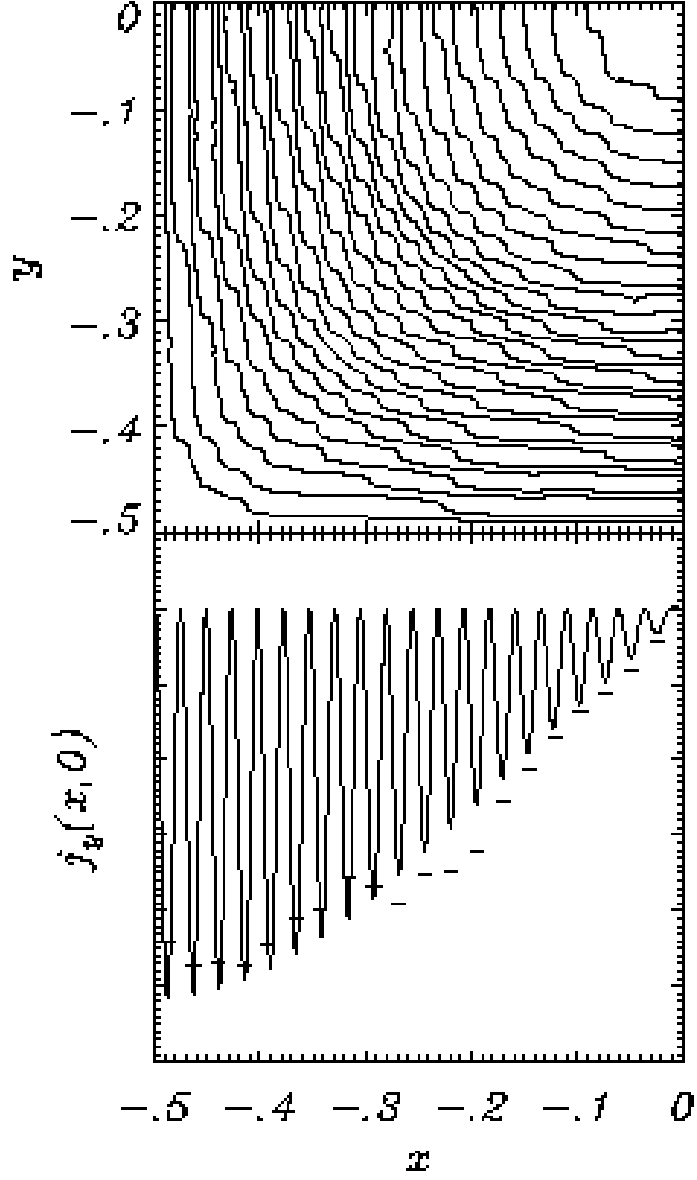


Figure 4.17: Ideal flux line at the center of the square,  $\phi = 0.1\phi_0$ . Current in the state  $n = 82$ ,  $m = 0$ , symmetric under the  $90^\circ$  rotation. Upper figure: numerical streamlines for a quarter of the square. Lower figure: theoretical current density  $j_y(x, 0)$ , dashes indicate the numerical minima.

the medium [10]. If  $\mathbf{V}(\mathbf{r})$  is the velocity of the liquid then there is a correspondence

$$\frac{e\mathbf{A}(\mathbf{r})}{c\hbar} \longleftrightarrow \frac{-k\mathbf{V}(\mathbf{r})}{v_g(k, \mathbf{r})} \quad (4.22)$$

where the group velocity  $v_g \ll |\mathbf{V}|$ . (This analogy neglects the  $A^2$  term in the Hamiltonian.) Thus, rotating the tank with a constant angular velocity is equivalent to applying the uniform field to a quantum billiard. The flux

$$2\pi \frac{\phi}{\phi_0} \longleftrightarrow -\frac{k}{v_g} \oint \mathbf{V} \cdot d\mathbf{r} \quad (4.23)$$

in the case of homogeneous medium. A flux line would be analogous to a vortex formed by the water pouring through a small hole on the bottom of the tank. Reference [10] reports the experiments on scattering of the surface waves on a vortex.

In the microwave field experiments [73, 35, 72] a ferrite strip of length  $2a$  can be embedded in the wall  $y = -1/2$  (Fig. 4.18). If one applies the static magnetic field to the ferrite, the wave will acquire an additional phase upon reflection from the strip. The phase is different for the forward and backward directions, i.e. the time reversal symmetry is broken. This system is analogous to the ABFL square billiard with the flux line located distance  $a$  from the bottom. Suppose the square cavity is in  $xy$ -plane, and the ferrite is under the magnetic field in  $z$ -direction. Then the permeability of the ferrite in the absence of losses is

$$\hat{\mu} = \begin{bmatrix} \mu_{\parallel} & -i\chi & 0 \\ i\chi & \mu_{\parallel} & 0 \\ 0 & 0 & \mu_z \end{bmatrix}. \quad (4.24)$$

Consider a plane wave with electric field  $\mathbf{E}_i = E\hat{\mathbf{z}}e^{i(k_x x - k_y y)}$  ( $k_y > 0$ ) propagating in the cavity. Suppose this wave is incident on the ferrite layer of width  $\delta$ . Assuming the Dirichlet conditions on the metal wall to which this layer is attached, one can show that upon reflection the wave becomes  $\mathbf{E}_r = -E\hat{\mathbf{z}}e^{i(k_x x + k_y y + \phi)}$  where the phase<sup>2</sup>

$$\phi = 2 \tan^{-1} \left[ \frac{k_y (\mu_{\parallel}^2 - \chi^2) \sin(k_y^f \delta)}{k_y^f \mu_{\parallel} \cos(k_y^f \delta) - k_x \chi \sin(k_y^f \delta)} \right]. \quad (4.25)$$

Here  $k_y^f = \sqrt{k_f^2 - k_x^2}$  where  $k_f = k\sqrt{\mu_{\parallel} - \chi^2/\mu_{\parallel}}$  is the wavenumber inside the ferrite. The time-reversal is achieved by reversing the sign of  $k_x$ . Then  $\phi$  changes. In the quantum billiard

<sup>2</sup>This differs from the result reported in Ref. [72].

the phase changes sign but keeps the magnitude when time is reversed. Here it is not the case because  $\phi$  includes the phase that the wave acquires by traveling through the bulk of the ferrite. In order to separate the effect of the magnetic field from the effect of the width we may remove a metal layer from the wall outside of the strip, i.e. for  $|x| > a$  (Fig. 4.18). The width of the removed layer  $\delta'$  is determined by the condition

$$2k_y\delta' = \frac{1}{2} [\phi(k_x) + \phi(-k_x)] \quad (4.26)$$

meaning that the phase the wave acquires outside of the ferrite strip should be equal to the average phase on the strip. Then the effective phase  $\phi_{\text{eff}} = \phi - 2k_y\delta'$  is odd in  $k_x$ . In the experiments the wavenumber in the ferrite  $k_f$  was about ten times larger than  $k$ , so we expect  $\delta' > \delta$  to compensate for the phase.

## 4.4 Conclusions

The classically weak magnetic field acts as a perturbation in an integrable square billiard. In this system there are special states that are localized near the short stable periodic orbits that enclose a finite flux. The perturbation breaks the time-reversal symmetry and there is a preferred current direction. Not surprisingly, the states carry persistent currents. We observed a variety of probability and current distributions. The overall magnetic response ranges from the paramagnetic for the well-localized states to the diamagnetic. The short periodic orbits dominate the susceptibility. The localization also takes place for an off-center Aharonov-Bohm flux line. Although there is no direct classical effect in this case, the vector potential changes the action and enters the phase of the wavefunction. The diffraction effects are quite important for the flux line and limit the preciseness of the semiclassical results.

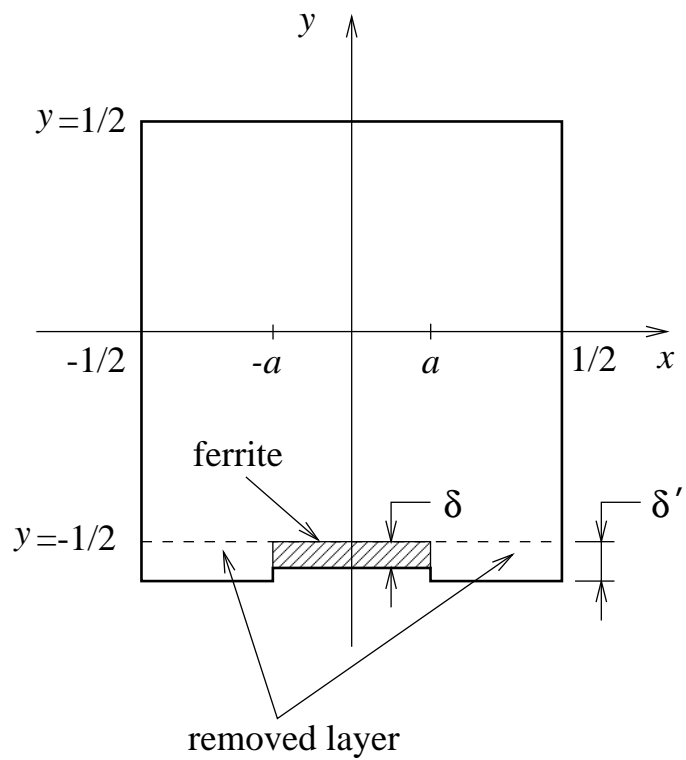


Figure 4.18: Possible microwave experiment with ferrite. The ferrite layer of width  $\delta$  and length  $2a$  is mounted on the wall. Part of the wall of width  $\delta'$  is removed to compensate for the width of the ferrite. The dashed line indicates the boundary of the original square.

## Chapter 5

# Quasiclassical Born-Oppenheimer approximations

Up to now all our results followed from the Bogomolny equation. It gives the natural semiclassical formulation and reduces the dimensionality of the problem through the use of Poincaré’s surface of section (PSS). The perturbation theory allows one to make an asymptotic expansion in the phase of the wavefunction in a controllable way and relate the quantum states to the classical phase space. The method has certain shortcomings. To find the full two-dimensional wavefunction an additional trivial, but lengthy, step is required. The resulting function is inaccurate near the caustics and in the classically forbidden regions.

There are cases, on the other hand, when the equivalent results can be obtained by the adiabatic, or Born-Oppenheimer, approximation (BOA) [22]. In general, the BOA is appropriate when a subset of the system’s coordinates varies in time slower than the remaining coordinates. This allows an approximate separation of variables in the partial differential equation describing the system. We will see in the examples below that such separation of variables is possible sometimes even if the notion of “fast” and “slow” is not well defined (Sec. 5.5). In any case, the conditions for the separation always follow from the differential equation itself, and we refer to all such cases as the BOA.

The relationship between the BOA and the  $T$ -operator method is quite complex [80]. Both methods are usually equivalent in the leading order. Unlike the  $T$ -operator, the BOA directly generates the two-dimensional wavefunction. If the PSS is chosen along the slow direction, the one-dimensional PSS wavefunction will be a part of the BOA result. The  $T$ -operator method

often produces an asymptotic form of the BOA solution. It is not always clear whether the BOA can be constructed for a given problem. For instance, we were unable to formulate the BOA in a simple form for a perturbed circle, apart from the states near the (1, 2) resonance (Sec. 5.4). The  $T$ -operator, once constructed, treats all resonances uniformly. The purpose of this chapter is to illustrate the above remarks on several examples.

## 5.1 Textbook example

We remind the reader of the standard example where the BOA can be used [7]. In the molecules or solids the electrons' positions  $\mathbf{r}_e$  can be treated as “fast” compared to the “slow” ionic positions  $\mathbf{R}_i$ . This is based on the small electron-ion mass ratio  $m_e/M_i$ . In the Schrödinger equation

$$\left[ -\frac{\hbar^2}{2m_e}\nabla_e^2 - \frac{\hbar^2}{2M_i}\nabla_i^2 + V(\mathbf{r}_e, \mathbf{R}_i) \right] \Psi(\mathbf{r}_e, \mathbf{R}_i) = E\Psi(\mathbf{r}_e, \mathbf{R}_i) \quad (5.1)$$

we make the Born-Oppenheimer ansatz

$$\Psi(\mathbf{r}_e, \mathbf{R}_i) = \Phi(\mathbf{r}_e|\mathbf{R}_i) \psi(\mathbf{R}_i). \quad (5.2)$$

Here we assume that  $\Phi(\mathbf{r}_e|\mathbf{R}_i)$  is the  $N$ th electronic eigenstate for fixed ionic variables which solves

$$\left[ -\frac{\hbar^2}{2m_e}\nabla_e^2 + V(\mathbf{r}_e, \mathbf{R}_i) \right] \Phi(\mathbf{r}_e|\mathbf{R}_i) = U(\mathbf{R}_i) \Phi(\mathbf{r}_e|\mathbf{R}_i) \quad (5.3)$$

where  $\mathbf{R}_i$  is treated as a parameter. The eigenenergy  $U(\mathbf{R}_i)$  then acts as a potential for the slow variable:

$$\left[ -\frac{\hbar^2}{2M_i}\nabla_i^2 + U(\mathbf{R}_i) \right] \psi(\mathbf{R}_i) = E\psi(\mathbf{R}_i). \quad (5.4)$$

The adiabatic invariance provides that the electronic eigenstate label  $N$  does not change as  $\mathbf{R}_i$  is slowly varied. The approximation made to the Schrödinger equation implies that

$$\left| \frac{\nabla_i \psi \nabla_i \Phi}{M_i} \right|, \left| \frac{\psi \nabla_i^2 \Phi}{M_i} \right| \ll \left| \frac{\psi \nabla_e^2 \Phi}{m_e} \right|. \quad (5.5)$$

In the case of the ground state of hydrogen molecule one can estimate  $|\nabla_i \Phi| \sim |\nabla_e \Phi| \sim |\Phi|/a_B$  where  $a_B$  is the Bohr radius. The ions will oscillate with frequency  $\omega \sim e/\sqrt{M_i a_B^3}$  and amplitude  $\delta R_i \sim \hbar/M\omega \sim (m_e/M_i)^{1/4} a_B$ . Hence we estimate  $|\nabla_i \psi| \sim |\psi|/\delta R_i \sim |\psi|(M_i/m_e)^{1/4}/a_B$ . Therefore the first term on the left of Eq. (5.5) is the biggest and it

is  $(M_i/m_e)^{3/4}$  times smaller than the *r.h.s.* This example shows that the BOA amounts to neglecting certain derivatives in the differential equation. The higher order corrections can also be written down.

It was shown that the interaction between the fast quantum electronic and the slow classical ionic degrees of freedom may lead to chaotic behavior [17].

## 5.2 Bouncing ball states

In Sec. 3.2 we have shown how to derive the bouncing ball (BB) states in a Bunimovich stadium (Fig. 3.10) using the  $T$ -operator. We obtained an almost square well effective potential which made the states localized within the straight part of the billiard. Equivalently, we could use the BOA [6] since there is a separation between the fast and slow motion. We have also mentioned a generalization of this problem: the stadium with the endcaps of slightly different radii (Fig. 3.11). In the latter case the effective potential is a square well with a sloped bottom, and the states are spatially shifted towards the wider part of the billiard. In both cases the wavefunction stays away from the semicircular regions, so the exact shape of the boundary there is of little consequence for the states with the low transverse quantum number  $m$ . Another interesting example is the  $\pi/3$ -rhombus billiard [16], which has two degenerate families of the BB states.

In this section we apply the BOA method to the  $(0, 1)$  resonance states in the tilted unit square introduced in Sec. 3.1.4. The lower side of the square has a slope,  $y = \epsilon x$ , and the states of interest have a small  $x$ -momentum compared to the  $y$ -momentum. These are, of course, the BB modes, and, as we just explained, they are similar to the BB states in a tilted stadium (the effective potential is twice as large in the latter case, because two sides are tilted).

We solve the Helmholtz equation  $(\nabla^2 + k^2)\Psi = 0$  with the BOA ansatz  $\Psi(x, y) = \Phi(y|x)\psi(x)$ . The fast equation is

$$\frac{\partial^2 \Phi}{\partial y^2} = -U(x)\Phi. \quad (5.6)$$

The solution

$$\Phi(y|x) = \sqrt{\frac{2}{1-\epsilon x}} \sin\left(\pi n \frac{1-y}{1-\epsilon x}\right) \quad (5.7)$$

vanishes at  $y = \epsilon x$  and  $y = 1$  and is normalized. From this we find the function  $U(x) = [\pi n / (1 - \epsilon x)]^2 \approx \pi^2 n^2 + 2\epsilon \pi^2 n^2 x$ . Then the slow function satisfies the equation

$$-\psi'' + \alpha^3 x \psi = \mathcal{E}_m \psi \quad (5.8)$$

where  $\mathcal{E}_m = k^2 - \pi^2 n^2$  and  $\alpha = (2\epsilon \pi^2 n^2)^{1/3}$ . Note that  $\alpha^3 x$  is in the leading order  $k^2 \epsilon$  times the effective potential  $2x$  of the  $T$ -operator method if the lower side is chosen as the PSS. Hence  $\psi(x)$  is the surface of section wavefunction given by Eq. (3.11) with  $E_m = \mathcal{E}_m / k^2 \epsilon$ . The energy  $k^2$  and the two-dimensional wavefunction are also given correctly.

Equation (5.8) has a solution

$$\psi(x) = \text{Ai}(\alpha x - z_m) \quad (5.9)$$

for large  $\alpha$ . Here  $z_m$  is a root of  $\text{Ai}(-z)$ , so that  $\psi(0) = 0$ . If  $\alpha - z_m \gg 1$ ,  $\psi$  also effectively vanishes at  $x = 1$ . The transverse energy  $\mathcal{E}_m = \alpha^2 z_m$  must be much smaller than the maximum potential  $\alpha^3$ , i.e.  $\alpha \sim (k^2 \epsilon)^{1/3} \gg z_m$ . The wavefunction  $\Psi(x, y)$  is localized within  $x \lesssim z_m / \alpha$ . If this condition is not satisfied, Eq. (5.8) still can be solved by a linear combination of Ai and Bi functions. In the opposite case,  $k^2 \epsilon \ll 1$ , the slope of the side can be neglected in the leading order. This is the situation when the non-resonant perturbation theory applies and there is no localization. The BOA is applicable if  $|\Phi^{-1}(\partial\Phi/\partial x)| |\psi^{-1}\psi'| \ll |\Phi^{-1}(\partial^2\Phi/\partial y^2)|$ . When  $z_m / \alpha \ll 1$ , we estimate  $|\psi^{-1}\psi'| \sim \alpha$ , and the above condition gives  $\epsilon^4 \ll k$ , which is always true. For larger  $m$ , i.e. when  $z_m / \alpha \sim (m/k\sqrt{\epsilon})^{2/3} \gtrsim 1$ , we have  $|\psi^{-1}\psi'| \sim m$ , so the condition becomes  $\epsilon m \ll k \sim n$ . This shows that the BOA is valid even if  $m \sim n$ .

Figure 5.1 shows the cross-sections of the numerically obtained wavefunctions  $\Psi_{nm}$ : (a)  $\Psi_{55,1}(x = 0.01, y)$  [this is proportional to  $\Phi(y|x = 0.01)$ ], (b)  $\Psi_{55,1}(x, y = 0.99)$  compared with  $\text{Ai}(\alpha x - z_1)$ , and (c)  $\Psi_{55,2}(x, y = 0.99)$  compared with  $\text{Ai}(\alpha x - z_2)$ . Here  $\epsilon = 0.01$  is less than the wavelength  $\lambda = 0.036$  which in turn is less than  $\sqrt{\epsilon} = 0.1$ . This results in sufficiently strong localization. The two-dimensional representation of  $|\Psi_{55,2}(x, y)|^2$  is shown in Fig. 5.2.

One concludes that in the case of the (0,1) resonance in the tilted square the BOA is straightforward and readily provides the two-dimensional wavefunction, while the  $T$ -operator method would require more work. The BOA method is not, however, directly generalizable to the higher resonances (Sec. 3.1.4), although the next section suggests a possible approach.



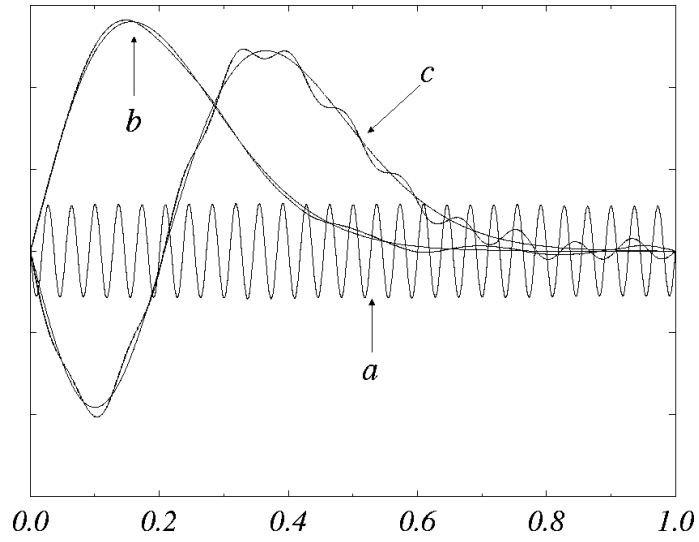


Figure 5.1: Cross-sections of the numerical wavefunctions  $\Psi_{nm}$  for the  $(0,1)$  resonance in the tilted square,  $\epsilon = 0.01$ . (a)  $\Psi_{55,1}(x = 0.01, y)$ ; (b)  $\Psi_{55,1}(x, y = 0.99)$  compared with  $\text{Ai}(\alpha x - z_1)$ ; (c)  $\Psi_{55,2}(x, y = 0.99)$  compared with  $\text{Ai}(\alpha x - z_2)$ . The magnitude of the states has been normalized.



Figure 5.2: Density plot of  $|\Psi_{55,2}(x,y)|^2$ , the state of Fig. 5.1 (c). The lower part of the billiard ( $0 < y < 0.25$ ) is shown and the graph is expanded in the  $y$  direction by a factor of three in order to display more details of the wavefunction. The dashed line is at  $y = 0$ .

### 5.3 Channeling approximation

The necessity to find the coordinates in which the fast and slow motion separate may prevent us from treating generic resonances by the BOA. In some cases the method of images resolves this problem. Consider, for example, a rectangular billiard perturbed by a potential or a magnetic flux. The copies of the rectangle obtained by reflection about its sides will cover the whole two-dimensional plane, forming a lattice. (The magnetic flux has opposite signs in the neighboring rectangles.) Suppose that the perturbation is classically weak, that is the classical orbit does not deviate much from the straight line after one passage across the billiard. (For the estimate in uniform magnetic field see Sec. 4.1.1.) An orbit in the original rectangle extends along a straight line with minor deviations in the extended scheme (cf. Fig. 4.1). Now the fast and slow directions separate and the BOA can be used. The BOA in this case is related to the channeling method for the energetic particles traveling through the crystal lattice [53].

For definitiveness, consider the uniform magnetic field  $B$  as a perturbation. We start with the  $(1, 1)$  orbits. We rotate the coordinate system to make one variable  $\xi = (ax + by)/d$  run along the fast  $(1, 1)$  direction and the other variable  $\eta = (-bx + ay)/d$  along the slow perpendicular direction. Here  $a \times b$  are the dimensions of the rectangle and  $d = \sqrt{a^2 + b^2}$ . The Schrödinger equation in these coordinates in the units  $\hbar = c = e = 2m = 1$  is

$$\left\{ [-i\partial_\xi - A_\xi(\xi, \eta)]^2 + [-i\partial_\eta - A_\eta(\xi, \eta)]^2 \right\} \Psi(\xi, \eta) = E\Psi(\xi, \eta). \quad (5.10)$$

In the channeling approximation we assume that the particle moving fast in the  $\xi$  direction “sees” only the averaged vector potential. We may neglect  $A^2$  comparing to the linear  $kA$  terms (since  $\epsilon = B/k \ll 1$ ) and substitute the average vector potential  $\bar{A}_\xi(\eta)$  for  $A_\xi(\xi, \eta)$ , where

$$\bar{A}_\xi(\eta) = L_\xi^{-1} \int_0^{L_\xi} d\xi A_\xi(\xi, \eta) \quad (5.11)$$

and  $L_\xi = 2d$ , the period in  $\xi$ . Note that  $\bar{A}_\xi L_\xi = \oint \mathbf{A} \cdot d\mathbf{l}$  is the flux enclosed by the periodic orbit in the original billiard. Similarly,  $\bar{A}_\eta L_\xi = \oint d\mathbf{l} \times \mathbf{A} = 0$  in the gauge where  $\text{div} \mathbf{A} = 0$ . Now Eq. (5.10) becomes separable.

The same result can be obtained on a more formal basis. Namely, we make an ansatz  $\Psi(\xi, \eta) = \Phi(\xi|\eta) \psi(\eta)$  and consider the vector potential as a small perturbation in the fast equation for  $\Phi$ . Then, according to the elementary perturbation theory, we can approximate

$\Phi(\xi|\eta) = e^{ik\xi}$  and find the fast eigenenergy  $U(\eta)$  after multiplying the fast equation by  $\Phi^*$  and integrating over  $\xi$ . Again neglecting  $A^2$  we find that

$$U(\eta) = k^2 - 2k\bar{A}_\xi(\eta). \quad (5.12)$$

The  $A_\eta\partial_\eta$  term automatically disappears in the BOA approach. The slow equation is

$$-\psi'' - 2k\bar{A}_\xi(\eta)\psi = (E - k^2)\psi. \quad (5.13)$$

Now we can rewrite the results in the  $x, y$  coordinates. Suppose the origin is chosen at the center. Define the function  $\hat{\psi}(x - ay/b - a/2) = \hat{\psi}(-d\eta/b - a/2) = \psi(\eta)$ . This definition relates  $\hat{\psi}$  to the function in Eq. (4.7) when  $a = b = 1$ . The above equation turns into Eq. (4.2),

$$\hat{\psi}_m''(x) + [E_m - V(x)]\hat{\psi}_m(x) = 0, \quad (5.14)$$

with  $V(x) = -2\frac{b^2}{d^2}k\bar{A}_\xi(-\frac{bx}{d} - \frac{ab}{2d})$ . It has the symmetries  $V(x) = V(-x)$  and  $V(-a/2 + x) = -V(-a/2 - x)$  and has a period  $2a$ . For uniform field

$$\bar{A}_\xi(\eta) = \begin{cases} -B\eta(1 + \frac{d}{ab}\eta), & 0 \leq \eta \leq \frac{ab}{d}, \\ B(\frac{2ab}{d} + \eta)(1 + \frac{d}{ab}\eta), & \frac{ab}{d} \leq \eta \leq 2\frac{ab}{d}, \end{cases} \quad (5.15)$$

with  $\bar{A}_\xi(\eta + 2ab/d) = \bar{A}_\xi(\eta)$ , and  $V(x) = -(Bkab^3/d^3) \left[ \frac{1}{2} - 2\left(\frac{x}{a}\right)^2 \right]$  for  $|x| < a/2$  repeated antiperiodically outside this region. An eigenfunction in this potential satisfies the Bloch condition

$$\hat{\psi}_m(x + 2a) = e^{i\beta}\hat{\psi}_m(x) \quad (5.16)$$

where  $\beta$  is to be determined.

The two-dimensional wavefunction has the form

$$\Psi_0(x, y) = e^{ik(ax+by)/d}\hat{\psi}_m(x - ay/b - a/2). \quad (5.17)$$

This is one of the four degenerate solutions. Another solution is obtained from this after the rotation by  $\pi$ ,  $\Psi_2(x, y) = \Psi_0(-x, -y)$ . The other pair comes from shifting to the neighboring square, where the magnetic field has the opposite direction, and considering the  $(-1, 1)$  orbit. These solutions are  $\Psi_1(x, y) = \exp[ik(-ax + by)/d]\hat{\psi}_m(-x - ay/b + a/2)$  and  $\Psi_3(x, y) = \Psi_1(-x, -y)$ . The wavefunction in the original rectangle is constructed from these

four solutions under the condition that it vanishes on the boundary. The state can be made even or odd under  $(x, y) \rightarrow (-x, -y)$ . With  $r = \pm 1$  it has the form

$$\Psi_{nm} = A(\Psi_0 + r\Psi_3) + B(\Psi_2 + r\Psi_4). \quad (5.18)$$

Requiring  $\Psi_{nm}(\pm \frac{a}{2}, y) = 0$ , we find that  $A = -Be^{-i\chi_a}$  and  $e^{i\beta} = e^{-i2\chi_a}$  where  $\chi_a = ka^2/d$ . And from  $\Psi_{nm}(x, \pm \frac{b}{2}) = 0$  we get  $A = -rBe^{i\chi_b}$  and  $e^{i\beta} = e^{i2\chi_b}$  where  $\chi_b = kb^2/d$ . Therefore  $\chi_a + \chi_b = \pi n$  where  $n$  is even for  $r = 1$  and odd for  $r = -1$ . This determines  $k = \pi n/d$ , and the energy can be expressed as

$$E_{nm} = (\pi n/d)^2 + d^2 E_m/b^2. \quad (5.19)$$

The phase shift  $\beta = 2\pi n(b/d)^2 - 2\pi n_b$ . If we assume  $|\beta| \leq \pi$  then  $n_b$  is an integer part of  $(nb^2/d^2 - 1/2)$ . For a square  $\beta = 0$  for even  $n$  or  $\pi$  for odd  $n$ . This is the case considered in Ch. 4. It is clear that the BOA and the  $T$ -operator theory agree at least to the order  $\sqrt{\epsilon}$  in the wavefunction and  $\epsilon$  in energy.

We were able to apply the BOA to the rectangular billiard by extending it to a bigger system and thus “unfolding” the trajectories. The method can be generalized to include the boundary perturbation. In this case we again extend the unperturbed rectangle by reflection to the whole plane and assume that the classical orbits are almost straight lines in the plane (actually, they will slightly bend on the boundary crossings). Then  $U(\eta) = k^2 - 2k^2\delta L(\eta)/L_\xi$ , where  $\delta L(\eta)$  is the additional path due to perturbed boundary for an unperturbed orbit of period  $L_\xi$ . In light of Eq. (5.10) we might say that the change in length is compensated by a change of momentum  $\delta k = -k\delta L/L$  that preserves the action. Notice also that the time it takes the particle to travel distance  $L$  with the modified momentum is equal to the time it travels distance  $L + \delta L$  with the old momentum. If the extension of a system to the whole plane in the original coordinates is not possible (like for a circle billiard), it can be done in the action-angle variables.

## 5.4 BOA in the asymptotic region

Now we return to the low angular momentum resonance in a perturbed unit circle (Sec. 2.2.2). In this example the separation of fast and slow coordinates holds only over a part of the billiard. The BOA wavefunction in this region is in agreement with the  $T$ -operator solution.

The Helmholtz equation in cylindrical coordinates has the form

$$\left( r \frac{\partial}{\partial r} r \frac{\partial}{\partial r} + k^2 r^2 + \frac{\partial^2}{\partial \theta^2} \right) \Psi = 0. \quad (5.20)$$

For the low angular momentum  $l$  states the angular coordinate is slow and the radial coordinate is fast everywhere except the region near the center  $r \lesssim l/k \sim \sqrt{\epsilon}$ . Outside of this area we can make the BOA ansatz  $\Psi(r, \theta) = \Phi(r|\theta) \psi(\theta)$ . The fast equation

$$r \frac{\partial}{\partial r} r \frac{\partial}{\partial r} \Phi + [k^2 r^2 - l^2(\theta)] \Phi = 0 \quad (5.21)$$

is the Bessel equation with the variable order  $l(\theta)$ . Since it is invalid for  $r \rightarrow 0$  the solution may include both Bessel and Neumann functions. It is convenient to invoke the asymptotic expansion for large  $kr$  and  $l$  but small  $l/kr$  [41]

$$\Phi(r|\theta) \approx \frac{1}{\sqrt{kr}} \cos \left[ kr + \frac{l^2(\theta) - \frac{1}{4}}{2kr} + \alpha(\theta) \right] \quad (5.22)$$

where  $\alpha(\theta)$  is the phase that mixes Bessel and Neumann functions. Function  $\Phi$  must vanish at the boundary  $r(\theta) = 1 + \epsilon \Delta R(\theta)$  which requires

$$k + k\epsilon \Delta R(\theta) + \frac{l^2(\theta) - \frac{1}{4}}{2k} + \alpha(\theta) = \pi \left( n - \frac{1}{2} \right). \quad (5.23)$$

Both functions  $l(\theta)$  and  $\alpha(\theta)$  are unknown, and we need some additional information to determine them. Consider the slow equation

$$\psi'' + l^2(\theta) \psi = 0. \quad (5.24)$$

The radial wavefunction  $\psi(\theta)$  is expected to coincide with the PSS wavefunction that solves Bogomolny's equation. Equation (2.10) implies that

$$l^2(\theta) = k^2 \epsilon [E_m - V(\theta)] \quad (5.25)$$

where  $V(\theta) = \Delta R(\theta) + \Delta R(\theta - \pi)$ . Since  $V(\theta)$  has period  $\pi$ , Eq. (5.24) is solved with the boundary condition  $\psi(\theta - \pi) = (-1)^m \psi(\theta)$ , and the eigenvalues  $E_m$  are determined. Now Eq. (5.23) enables us to find

$$\alpha(\theta) = -\frac{1}{2} k \epsilon [\Delta R(\theta) - \Delta R(\theta - \pi)] + \alpha_0 \quad (5.26)$$

and the quantization condition

$$k - \frac{1}{8k} + \frac{1}{2} k \epsilon E_m + \alpha_0 = \pi \left( n - \frac{1}{2} \right). \quad (5.27)$$

The constant  $\alpha_0$  is determined from the special case  $\Delta R = 0$ . Then  $l = m$  and  $\Phi(r|\theta) \propto J_m(kr)$ , which implies  $\alpha_0 = -\frac{\pi}{2}(m \bmod 2) - \frac{\pi}{4}$ . Figures 2.5, 2.6 show the states with  $m = 2, 3$ , respectively, in the short stadium.

In the considered example the BOA is not self-contained — we could not complete the solution without knowing the behavior of the wavefunction at the origin. Having obtained the radial wavefunction by other means (e.g. from Bogomolny's equation), we reconstructed the two-dimensional wavefunction [cf. Eq. (2.61)] and the quantization condition [cf. Eq. (2.11)] of the perturbation theory. It is remarkable that the fast wavefunction  $\Phi(r|\theta)$  becomes asymptotically the Bessel function  $J_{l(\theta)}(kr)$  only in an unperturbed circle, in all other cases it is mixed with the Neumann function  $N_{l(\theta)}(kr)$ .

In this section the phase of the wavefunction (5.22) and the quantization condition (5.23) contain a  $k^{-1}$  order corrections that were absent in the  $T$ -operator theory. These corrections are normally small in the semiclassical regime although they may begin to play a role when the angular momentum  $l \sim k\sqrt{\epsilon} \lesssim 1$ . There are several sources of the  $k^{-1}$  corrections in the  $T$ -operator method. First, the  $k^{-1}$  terms can be added to the phase of the  $T$ -operator itself. For example, in the boundary integral method these terms originate in the derivative of Hankel's function [cf. Eq. (1.13)]. Second, the Bogomolny equation  $\psi = T\psi$  should be solved to higher precision, namely, one has to retain the next order terms in the expansion of the unperturbed action and the prefactor near the stationary point [cf. Eq. (2.6)]. Similarly, the two-dimensional wavefunction can be found from Eq. (1.10) with the Hankel function as the kernel. Note that the more general kernel (2.54) is valid only in the leading order in  $k^{-1}$ .

The low angular momentum resonance in the perturbed sphere of Sec. 2.5.4 can be described by a similar technique. We start with a three-dimensional Helmholtz equation

$$\left( \frac{\partial}{\partial r} r^2 \frac{\partial}{\partial r} + k^2 r^2 - \hat{l}^2 \right) \Psi = 0, \quad (5.28)$$

where  $\hat{l}^2 \equiv -\frac{1}{\sin\theta} \frac{\partial}{\partial\theta} \sin\theta \frac{\partial}{\partial\theta} - \frac{1}{\sin^2\theta} \frac{\partial^2}{\partial\varphi^2}$ . The equation in the fast radial direction

$$\frac{\partial}{\partial r} r^2 \frac{\partial}{\partial r} \Phi + [k^2 r^2 - l(l+1)] \Phi = 0 \quad (5.29)$$

is an equation for a spherical Bessel function of order  $l = l(\theta, \varphi)$  [41]. Again, since the BOA is not valid near the center, the solution will include both Bessel and Neumann spherical

functions. Asymptotically,

$$\Phi(r|\theta, \varphi) \approx \frac{1}{kr} \sin \left[ kr + \frac{l(l+1)}{2kr} + \alpha(\theta, \varphi) \right] \quad (5.30)$$

where  $\alpha(\theta, \varphi)$  is the phase to be determined. The slow equation

$$-\hat{l}^2 \psi + l(l+1)\psi = 0 \quad (5.31)$$

implies that

$$l(l+1) = k^2 \epsilon [E_{lm} - V(\theta, \varphi)], \quad (5.32)$$

where  $V(\theta, \varphi) = \Delta R(\theta, \varphi) + \Delta R(\pi - \theta, \varphi + \pi)$ . The eigenfunctions  $\psi_{lm}$  [the quantum number  $l$  should not be confused with the function  $l(\theta, \varphi)$ ] will be even or odd under inversion,  $\psi_{lm}(\theta, \varphi) = (-1)^l \psi_{lm}(\pi - \theta, \varphi + \pi)$ , where we assume the state  $\psi_{lm}$  has the same symmetry as the unperturbed state  $Y_{lm}(\theta, \varphi)$ . As before, the Dirichlet condition for  $\Phi$  gives

$$\alpha(\theta, \varphi) = -\frac{1}{2} k \epsilon [\Delta R(\theta, \varphi) - \Delta R(\pi - \theta, \varphi + \pi)] - \frac{\pi}{2} (l \bmod 2) \quad (5.33)$$

and the quantization for  $k$

$$k + \frac{1}{2} k \epsilon E_{lm} = \pi n + \frac{\pi}{2} (l \bmod 2). \quad (5.34)$$

Clearly, the BOA is consistent with the  $T$ -operator approach and even improves on the angular differential equation.

## 5.5 Whispering gallery modes

The whispering gallery modes discussed in Sec. 3.3 can also be derived with the BOA. The adiabaticity comes from the slow variation of curvature of the boundary. This approach is related to the parabolic equation and the etalon methods [4] in the sense that in the former some derivatives in the partial differential equation are neglected and in the latter an ansatz involving the Bessel function with variable order is made. All these methods give the same leading order results.

The billiard boundary is locally a circle of radius  $R(s)$  where the variable  $s$  runs along the perimeter. Therefore the whispering gallery wavefunction is locally a wavefunction for a circle,

$$\Psi(\rho, s) = \Phi(\rho|s) \psi(s) = \alpha(s) J_{l(s)}(kr_s) \psi(s), \quad (5.35)$$



where  $\rho \ll R$  is the distance from the boundary,  $r_s = R(s) - \rho$  is the radius measured from the local center of curvature and  $\alpha(s)$  is the normalization for  $\Phi$ . The slowly changing angular momentum  $l(s)$  does not have to be integer and will be determined by the boundary conditions. The “slow” wavefunction  $\psi(s)$  satisfies the equation similar to Eq. (5.24) and is equal to

$$\psi(s) = \frac{\exp i \int^s l(s') ds' / R(s')}{\sqrt{l(s) / R(s)}} \quad (5.36)$$

where  $ds/R$  plays a role of  $d\theta$ . Since  $l \sim kR$ , the function  $\psi(s)$  is not really slow, varying approximately as  $e^{iks}$ . However,  $\Phi(\rho|s)$  depends only on the slow varying functions of  $s$ , like  $l(s)$  and  $R(s)$ , which justifies the BOA ansatz. Since the order of the Bessel function is large and close to its argument, it can be approximated by an Airy function. If we define a function  $f(s)$  by  $l = kR(1 - f')$  then [41]

$$\begin{aligned} J_{l(s)}\{k[R(s) - \rho]\} &= J_l \left[ l + l^{1/3} \left( \frac{kRf' - k\rho}{l^{1/3}} \right) \right] \\ &\simeq \left( \frac{2}{kR} \right)^{1/3} \text{Ai} \left[ -2^{1/3} \frac{kRf' - k\rho}{(kR)^{1/3}} \right]. \end{aligned} \quad (5.37)$$

( $l$  can be replaced by  $kR$  in the leading order in  $f'$  and  $\rho/R$ .) The Airy function must vanish at  $\rho = 0$  which makes

$$f'(s) = 1 - \frac{l}{kR} = \frac{z_n}{2^{1/3} (kR)^{2/3}} \quad (5.38)$$

where  $z_n$  is the  $n$ th root of  $\text{Ai}(-z)$ . The full wavefunction can now be written down as

$$\Psi(\rho, s) = (kR)^{-1/6} \text{Ai} \left( \frac{2^{1/3} k^{2/3}}{R^{1/3}} \rho - z_n \right) \psi(s) \quad (5.39)$$

where the normalization factor has been added. Note that the normalization ensures the same total current through any section  $s = \text{const}$ .

The  $T$ -operator theory produces the asymptotic form of this solution, Eq. (3.41).<sup>1</sup> There the function  $f(s)$  was defined via Eq. (3.33) as a part of the phase of the PSS wavefunction. Clearly, this is consistent with the current definition. The explicit expression for  $f'$ , Eq. (3.34), compares with Eq. (5.38) if  $z_n$  is used in its approximate form  $[\frac{3}{2}\pi(n - \frac{1}{4})]^{2/3}$  for large  $n$ . The BOA solution works both in the classically allowed and classically forbidden regions including

---

<sup>1</sup>Although denoted by the same symbol, the PSS wavefunction and the slow wavefunction  $\psi(s)$  differ by a factor  $R^{-1/3}(s)$ .

the caustic. It does not require the large number of wavelengths in the radial direction, which would be the condition for the asymptotic expansion of the Airy function.

It is possible to derive the Airy function solution directly, without referring to the Bessel function. The Helmholtz equation in the  $(\rho, s)$  coordinates for small  $\rho/R$  is

$$\left[ \frac{\partial^2}{\partial \rho^2} - \frac{1}{R(1-\rho/R)} \frac{\partial}{\partial \rho} + \frac{1}{(1-\rho/R)^2} \frac{\partial^2}{\partial s^2} + \frac{\rho(R^{-1})'}{(1-\rho/R)^3} \frac{\partial}{\partial s} + k^2 \right] \Psi = 0. \quad (5.40)$$

The second term can be neglected as compared to the first term since  $|\Phi^{-1}\partial\Phi/\partial\rho| \sim k^{2/3}R^{-1/3}$  [according to Eq. (5.39)] and  $kR \gg 1$ . The third term can be expanded in  $\rho/R$ . The fourth term can be neglected compared with  $\frac{\rho}{R} \frac{\partial^2}{\partial s^2}$  since  $|\psi'/\psi| \sim k$  and  $kR \gg R'$ . The simplified equation

$$\left[ \left(1 + 2\frac{\rho}{R}\right)^{-1} \left( \frac{\partial^2}{\partial \rho^2} + k^2 \right) + \frac{\partial^2}{\partial s^2} \right] \Psi = 0, \quad (5.41)$$

when solved by the BOA, yields Eq. (5.39). We can also estimate the limits of applicability of the BOA from this differential equation. When we make the BOA ansatz, the largest term that we drop is

$$\left| \frac{\partial\Phi}{\partial s} \psi' \right| \sim \left| kz_n \frac{R'}{R} \frac{\text{Ai}'}{\text{Ai}} \Phi \psi \right| \quad (5.42)$$

where we take the typical  $\rho \sim z_n R^{1/3} k^{-2/3}$ . We should compare it with

$$\left| \frac{\partial^2\Phi}{\partial \rho^2} \psi \right| \sim \left| \frac{k^{4/3}}{R^{2/3}} \frac{\text{Ai}''}{\text{Ai}} \Phi \psi \right|. \quad (5.43)$$

Estimating  $|\text{Ai}''/\text{Ai}'| \sim n/z_n$  we obtain the condition

$$(kR)^{1/3} \gg |R'| z_n^2/n \sim |R'| n^{1/3} \quad (5.44)$$

which is the same as the requirement (3.38) for the simple  $T$ -operator theory to work. In Sec. 3.4 we consider the case when this condition is not satisfied.

The classical caustic is given by the turning point of the radial equation, or a point where the argument of the Airy function vanishes,  $\rho(s) = \frac{z_n R^{1/3}(s)}{2^{1/3} k^{2/3}}$ . If the energy  $k^2$  is fixed, the possible caustics are quantized by  $z_n$ . In the classical picture the product  $\epsilon(s) R^{1/3}(s) \equiv I$ , where  $\epsilon(s)$  is an angle that the classical trajectory makes with the boundary, is an adiabatic invariant in the limit  $\epsilon \rightarrow 0$  [4] (see Sec. 3.4). Semiclassically,  $I = 2^{1/3} \sqrt{z_n}/k^{1/3}$  and, therefore, the caustics can be labeled solely by this parameter. This is not surprising since, apart from the energy which does not change the geometry of the orbits, this adiabatic invariant is the only (approximate) integral of motion.

## 5.6 Conclusions

The Born-Oppenheimer approximation can be used alongside the  $T$ -operator and other techniques to describe the perturbed integrable systems. When the separation of the fast and slow variables is possible it provides a convenient way to find a two-dimensional approximate wavefunction and energy levels. The BOA solution is usually valid near caustics and in the classically forbidden (shadow) regions where the semiclassical approximation often fails or needs modification. Whether the natural coordinates, in which the separation of fast and slow motion is possible, exist, depends on the geometry of the system or a family of orbits. In principle, the separation should always be possible in the action-angle variables, but then again the shadow regions are off limits. The adiabatic approximation may also be possible when there is a slowly changing parameter instead of the slowly changing position of the particle, as in the whispering gallery case.

## Chapter 6

### Trace formulas

The *trace formulas* are used to describe the density of states in terms of the classical periodic orbits of the system. The Gutzwiller trace formula [40] applies to the hard chaotic systems and the Berry-Tabor trace formula [13, 14, 39] works for the integrable systems. In the former case the periodic orbits are unstable and isolated, while in the latter case they form families. The intermediate situations include the perturbed integrable systems [59] and mixed systems.

The  $T$ -operator formalism (Sec. 1.4) adequately describes a system on a semiclassical level. In particular, one should be able to derive the trace formulas directly from the  $T$ -operator. We show in Sec. 6.1 how this can be done. In the following sections we apply the general formalism to the Gutzwiller and Berry-Tabor cases. Then we consider a perturbed integrable system, which interpolates between the two extremes. The interpolation formula can be parametrized. At least *four* parameters are needed to describe the perturbed family of periodic orbits correctly [79], not three, as Ref. [76] claims. We illustrate these points with the example of the coupled quartic oscillators in Sec. 6.5.

#### 6.1 General derivation of the trace formula

The energy spectrum of a system described by the Bogomolny operator  $T(E)$  is given by the zeros of the Fredholm determinant [cf. Eq. (1.32)]

$$D(E) = \det [1 - T(E)]. \quad (6.1)$$

The oscillatory part of the density of states can be expressed as a logarithmic derivative

$$d_{\text{osc}}(E) = d(E) - \bar{d}(E) = \frac{-1}{\pi} \text{Im} \left[ \frac{d \ln D(E + i\epsilon)}{dE} \right] \quad (6.2)$$

where  $d(E) = \sum_a \delta(E - E_a)$  and  $\bar{d}(E)$  is the smoothed (Weyl) density of states. To justify this result [60] we write  $D(E) = \prod_n [1 - e^{i\theta_n(E)}]$ . Here  $e^{i\theta_n(E)}$  are the eigenvalues of the  $T$ -operator which is approximately unitary. Then Eq. (6.2) yields

$$d_{\text{osc}} = -\frac{1}{2\pi} \sum_n \theta'_n \left( 1 + \text{Im} \cot \frac{\theta_n}{2} \right) = \sum_n \left[ -\frac{1}{2\pi} \theta'_n + |\theta'_n| \delta(\theta_n(E)) \right]. \quad (6.3)$$

With  $\theta'_n$  approximately independent of  $n$  the first sum gives the smoothed part  $-\bar{d} = -\frac{N}{2\pi} \theta'$  where  $N$  is the size of the  $T$ -matrix. The second sum is  $d(E)$ .

Using the relationship  $\ln \det(1 - T) = \text{Tr} \ln(1 - T)$  in Eq. (6.2) and expanding the logarithm in powers of  $T$ , we find

$$d_{\text{osc}}(E) = \frac{1}{\pi} \text{Im} \sum_{n=1}^{\infty} \frac{1}{n} \frac{d\tau_n(E)}{dE} \quad (6.4)$$

where

$$\tau_n(E) = \text{Tr} T^n(E) = \int dq_1 \cdots dq_n T(q_1, q_2) \cdots T(q_n, q_1). \quad (6.5)$$

The composition property for the  $T$ -operator (Sec. 1.5) gives for a two-dimensional system

$$\tau_n(E) = \int dq \sum_p \left( \frac{1}{2\pi i \hbar} \left| \frac{\partial^2 S_p(q, q'; E)}{\partial q \partial q'} \right| \right)_{q=q'}^{1/2} \exp \left[ \frac{i}{\hbar} S_p(q, q; E) \right]. \quad (6.6)$$

Here  $p$  denotes a “closed” orbit that leaves the Poincaré surface of section (PSS) from point  $q$  and arrives at the same point on its  $n$ th crossing of the PSS,  $S_p(q, q; E)$  is the reduced action for this orbit, and the Maslov index was omitted. In effect, we calculated  $n - 1$  out of  $n$  integrals in Eq. (6.5) by the stationary phase ( $S\Phi$ ). Whether the last integral can be done by the  $S\Phi$  as well, depends on the  $S_p(q, q; E)$ .

Since the exact density of states is a collection of  $\delta$ -functions, the formal series (6.4) diverges when  $E$  is on the spectrum. In practice, one includes only the first few terms that account for the short periodic orbits. This produces the density of states smoothed over some energy scale ( $\hbar$ /time). Such averaging can be experimentally relevant, say, due to the finite resolution of the spectrum because of non-zero temperature. For example, the susceptibility of a square in magnetic field is determined mostly by the shortest periodic orbit that encloses flux (Sec. 4.1.3). Thus, only one term in the trace formula is needed in this case [67]. When one is

interested in the energy level correlations on the scale of the average spacing, the orbits with periods up to the *Heisenberg time*  $\hbar\bar{d}$  should be included.

## 6.2 Gutzwiller trace formula

In the Gutzwiller case the periodic orbits are isolated, which means that  $S_p(q, q; E)$  has the well defined stationary points.  $[\partial S_p(q, q')/\partial q + \partial S_p(q, q')/\partial q' = p(q) - p'(q') = 0$  at  $q = q' = q^*$ , a  $S\Phi$  point of the integral (6.6).] Let  $q, q'$  be in the vicinity of  $q^*$  and expand in  $\delta q = q - q^*$  and  $\delta q' = q' - q^*$

$$S_p(q, q') \simeq S_p(E) + p^*(\delta q - \delta q') + \frac{1}{2}V_{11}\delta q^2 + V_{12}\delta q\delta q' + \frac{1}{2}V_{22}\delta q'^2 \quad (6.7)$$

where  $p^*$  is the momentum of the periodic orbit. The matrix of second derivatives  $V$  depends on  $q^*$  and the energy. Suppose the orbit  $p$  of “length”  $n$  (i.e. returning to the surface of section  $n$  times) consists of  $r$  repetitions of a *primitive* periodic orbit of length  $s$ , with  $n = rs$ . Then the contribution of orbit  $p$  to the integral (6.6) is

$$\tau_p = \left( \sum_1^s \left| \frac{V_{12}}{V_{11} + 2V_{12} + V_{22}} \right|^{1/2} \right) \exp \left[ \frac{i}{\hbar} S_p(E) \right]. \quad (6.8)$$

The summation is over the  $s$  stationary points, where the orbit crosses the PSS (each of them can be chosen as a starting/ending point for the periodic orbit).

The prefactor can be expressed in terms of the *monodromy matrix*  $M_p$  of orbit  $p$ , which relates the final momentum  $\delta p = p - p^* = V_{11}\delta q + V_{12}\delta q'$  and position  $\delta q$  to the initial  $\delta p' = -V_{12}\delta q - V_{22}\delta q'$  and  $\delta q'$ . With

$$M_p = \begin{pmatrix} -\frac{V_{11}}{V_{12}} & \frac{V_{12}^2 - V_{11}V_{22}}{V_{12}} \\ -\frac{1}{V_{12}} & -\frac{V_{22}}{V_{12}} \end{pmatrix} \quad (6.9)$$

the prefactor can be written as  $s|\det(M_p - 1)|^{-1/2}$ . The sum over the crossing points appears as a factor. [To see that  $\det(M_p - 1)$  is independent of the choice of the initial point  $q^*$ , express  $M_p = M_{12}M_{23}\cdots M_{n1}$ , where  $M_{i,i+1}$  is the monodromy matrix between the two consecutive crossings. Then  $\det(M_p - 1) = \det(M_{23}\cdots M_{n1}M_{12} - 1)$ .]

For a repeated orbit,  $S_p = rS_s$  and  $M_p = (M_s)^r$ . Only the rapidly varying phase needs to be differentiated when evaluating the derivative in Eq. (6.4). With  $dS_s(E)/dE = T_s$ , the

period of the primitive orbit, the density of states

$$d_{\text{osc}} = \sum_{s,r} \frac{T_s/\hbar}{|\det(M_s^r - 1)|^{1/2}} \cos \left\{ r \left[ \frac{S_s(E)}{\hbar} + \frac{\pi}{2} \nu_s \right] \right\} \quad (6.10)$$

where we restore the Maslov index.

### 6.3 Berry-Tabor formula

In the integrable systems the periodic orbits form continuous families, and therefore the  $S\Phi$  cannot be applied. On the other hand, since the action is constant within a family, the integral (6.6) can be easily done in the action-angle variables. For a two-dimensional system we define the variables  $I, \theta, J, \Theta$ , and choose the surface of section  $\Theta = 0$ . The action after the first return  $S(\theta - \theta', E)$  depends only on the difference of the angles (cf. Sec. 1.7). For an orbit  $p$  of length  $n$  the action  $S_p(\Delta\theta) = nS(\Delta\theta/n)$ . If  $p$  is a periodic orbit with a frequency ratio  $\omega_I/\omega_J = m/n$  then  $\Delta\theta = \theta - \theta' = 2\pi m$ . The derivative  $S_p'' = -(2\pi n g_E'')^{-1}$ , where  $J = g_E(I)$  (Sec. 1.7). Using these results in Eqs. (6.6) and (6.4) we arrive to the Berry-Tabor trace formula [13, 14]

$$d_{\text{osc}} = \sum_p \frac{T_p}{\pi \hbar^{3/2} n^{3/2} |g_E''|^{1/2}} \cos \left( \frac{S_p}{\hbar} + \frac{\pi}{2} \nu_p - \frac{\pi}{4} \right). \quad (6.11)$$

Note that a chaotic system may have a family of non-isolated periodic orbits. Among the examples are the bouncing ball orbits in the stadium [75, 71, 64] or Sinai billiard [9, 70].

### 6.4 Perturbed Berry-Tabor formula

In a perturbed integrable system the families of periodic orbits are broken with only a few isolated orbits remaining (Sec. 2.1). However, the action  $S_p(q, q'; E)$  in the integral (6.6) varies too slowly for the  $S\Phi$  to be applied. It may be convenient to express this one-dimensional integral in the action-angle variables. For an orbit of length  $n$

$$S_p(\theta, \theta') = nS(\Delta\theta/n) + \epsilon W(\theta, \theta') \quad (6.12)$$

where  $\epsilon W(\theta, \theta')$  is the perturbed part of the action that can be calculated by the standard technique. We may neglect the order  $\epsilon$  terms in the prefactor and take  $\theta' = \theta - 2\pi m$  for a

broken family with the winding number  $m/n$ . Then the integral that remains is

$$I_W = \frac{1}{2\pi} \int d\theta \exp \left[ \frac{i\epsilon}{\hbar} \hat{W}(\theta) \right] \quad (6.13)$$

where  $\hat{W}(\theta) = W(\theta, \theta - 2\pi m)$ .<sup>1</sup> The perturbed result for the  $d_{\text{osc}}$  is just the Berry-Tabor formula with the substitution  $\cos \phi \rightarrow \text{Re}[I_W \exp(i\phi)]$  where  $\phi$  is the argument of cosine in Eq. (6.11) [59]. One might say that the perturbed trace formula interpolates between the Berry-Tabor case, when  $\epsilon = 0$  and  $I_W = 1$ , and the Gutzwiller case, when  $\epsilon \hat{W}/\hbar$  is large and  $I_W$  can be done by the  $S\Phi$ .

When a family of periodic orbits is broken by the perturbation, at least one stable and one unstable periodic orbits remain, which means that  $\hat{W}(\theta)$  has at least one minimum and one maximum. Assume, for example, that  $\hat{W}(\theta)$  has a single maximum and minimum at  $\theta = 0, \pi$ , respectively. Often the perturbed action  $\hat{W}(\theta)$  can be approximated by a simple parametric expression that retains the essential information about its behavior. In the first attempts of this sort the function was approximated by the first terms of its Fourier series [59], e.g.,  $\hat{W}(\theta) \approx w_0 + w_1 \cos(\theta - \theta_0)$ . Then  $I_W \approx \exp(i\epsilon w_0/\hbar) J_0(\epsilon w_1/\hbar)$  where  $J_0$  is the Bessel function. However, this expression is, in general, incorrect in the limit of large  $\epsilon \hat{W}/\hbar$ . Indeed, the integral (6.13) can be done by the  $S\Phi$  and, therefore, depends on the values of  $\hat{W}$  and  $\hat{W}''$  at the extrema. This means that  $I_W$  must depend on four parameters.

Instead of increasing the number of terms in the Fourier expansion, it is more efficient to parametrize [76]  $\hat{W}(\theta) = W_0 + W_1 \cos[\xi(\theta)]$  where  $\xi(0) = 0$  and  $\xi(\pi) = \pi$ . The unknown function  $\theta(\xi)$  can be approximated by the first two terms of its Fourier expansion  $\theta = \xi - A \sin \xi - B \sin 2\xi$ . With  $d\theta/d\xi = 1 - A \cos \xi - 2B \cos 2\xi$  the integral (6.13) becomes

$$I_W = \frac{I_0}{2\pi} \int d\xi (1 - A \cos \xi - 2B \cos 2\xi) \exp \left[ \frac{i\epsilon}{\hbar} W_1 \cos \xi \right] \quad (6.14)$$

where  $I_0 = \exp[i(\epsilon/\hbar)W_0]$ . The integrals may be expressed in terms of Bessel functions  $J_m(\epsilon W_1/\hbar)$ , giving

$$I_W = I_0 (J_0 - iA J_1 + 2B J_2). \quad (6.15)$$

The four parameters  $W_0, W_1, A, B$ , can be related to  $\hat{W}$  and  $\hat{W}''$  evaluated at the extrema

---

<sup>1</sup>Note that  $\hat{W}(\theta) = r\bar{V}_q(\theta)$  for a periodic orbit  $(rp, rq)$ , where  $\bar{V}_q(\theta)$  is just the effective potential of the  $T$ -operator perturbation theory (cf. Sec. 2.5.3).  $p, q$  are relatively prime.



by

$$\begin{aligned}\hat{W}(0) &= W_0 + W_1, \quad \hat{W}(\pi) = W_0 - W_1, \\ \hat{W}''(0) &= -\frac{W_1}{(1 - A - 2B)^2}, \quad \hat{W}''(\pi) = \frac{W_1}{(1 + A - 2B)^2}.\end{aligned}\tag{6.16}$$

Thus, the above interpolation formula is correct in the limit of large  $\epsilon\hat{W}/\hbar$ , as well as for  $\epsilon \rightarrow 0$ . One can show that  $\det(M_p - 1)$  is proportional to  $\epsilon\hat{W}''$ .

The authors of Ref. [76] (UGT) take  $B = 0$ . They compensate the lack of another parameter by letting the function  $g_E''$  [Eq. (6.11)] depend on  $\epsilon$ . Although formally this method seems to be correct, it is physically misleading. The function  $g_E$  describes the constant energy surface in the action space  $(I, J)$ . When the system is perturbed, the topology of the invariant tori changes and the old actions are no longer the integrals of motion. Therefore  $g_E''$  does not have a clear physical interpretation for finite  $\epsilon$ . Secondly, UGT argue that “the independent evaluation of  $g_E''$  can be rather laborious and time consuming.” However, in order to explicitly evaluate this function in the limit  $\epsilon \rightarrow 0$  (which must be equal to the standard  $g_E''$ ) UGT would need to know the parameter  $W_1$  (in our notation) and the values of  $\det(M_p - 1)$  for the periodic orbits in this limit, which in effect requires the solution of the unperturbed problem. With this solution on hand it should not be hard to find the standard  $g_E''$ .

## 6.5 Example: coupled quartic oscillators

We study the correction to the trace formula for the coupled quartic oscillators, which are defined by the Hamiltonian

$$H = \frac{1}{2}(p_x^2 + p_y^2) + ax^4 + by^4 + \epsilon x^2 y^2.\tag{6.17}$$

When  $\epsilon = 0$  we may introduce the action-angle variables  $(I, \theta)$  in the  $x$  direction and  $(J, \Theta)$  in  $y$  direction. For a given energy  $E$  and winding number  $\alpha = \omega_I/\omega_J$

$$\begin{aligned}x &= \frac{1}{\sqrt{2}} \left( \frac{E/a}{1 + \frac{a}{b}\alpha^{-4}} \right)^{1/4} \text{sd}(\kappa\theta), \\ I &= \frac{2}{3}\kappa\sqrt{a} \left( \frac{E/a}{1 + \frac{a}{b}\alpha^{-4}} \right)^{-3/4}\end{aligned}\tag{6.18}$$

and similar for  $\Theta$  and  $J$ . Here  $\kappa = 2K/\pi$ , where  $K \equiv K(m = 1/2)$  is the complete elliptic integral of the first kind, and  $\text{sd}$  is one of the Jacobi elliptic functions [41]. The constant energy

surface is described by

$$g_E(I) = J = \left[ \left( \frac{2}{3}\kappa \right)^{4/3} E - \left( \frac{a}{b} \right)^{1/3} I^{4/3} \right]^{3/4}. \quad (6.19)$$

The action after the first return to the PSS  $\Theta = 0$  is

$$S(\theta - \theta', E) = \frac{2}{3}\kappa E^{3/4} \left[ \frac{(\theta - \theta')^4}{a} + \frac{(2\pi)^4}{b} \right]^{1/4}. \quad (6.20)$$

The perturbed part of the action  $\delta S = -\int \delta H dt$  in the leading order in  $\epsilon$ . The integral of the perturbed Hamiltonian can be evaluated along the unperturbed orbit. For a family of periodic orbits of winding number  $\alpha = m/n$  we find

$$\hat{W}(\theta) = -\frac{\kappa E^{3/4}}{8(ab)^{1/4}} \frac{\alpha}{[a + b\alpha^4]^{3/4}} \int_{-2\pi m}^0 d\theta'' \text{sd}^2[\kappa(\theta'' + \theta)] \text{sd}^2[\kappa\theta''/\alpha]. \quad (6.21)$$

Note that the shape of  $\hat{W}(\theta)$  is independent of  $a$ ,  $b$ , and  $E$ , and each is taken to be unity.

Figure 6.1 depicts  $\hat{W}(\theta)$  for the (1, 1) family,  $\alpha = 1$ . It is periodic with period  $\pi$  due to symmetries. The interpolation formulas of the previous section can be adjusted, when the period of  $\hat{W}(\theta)$  is  $2\pi/r$ , by changing  $\theta \mapsto r\theta$ . From the numerical values of  $\hat{W}$  and  $\hat{W}''$  at the extrema we find the interpolation parameters  $A = -1.49 \times 10^{-2}$ ,  $B = -1.04 \times 10^{-4}$  (independent of  $a$ ,  $b$ ,  $E$ ) and  $W_0 = -0.46$ ,  $W_1 = 0.27$ . The real part of  $I_W$  as a function of  $\epsilon/\hbar$  is shown in Fig. 6.2 and the imaginary part appears in Fig. 6.3. The deviation of the interpolation formula from the exact integral is given in the inset of Fig. 6.2. They agree to within a part in  $10^{-5}$ .

Note that the parameter  $B$  is relatively small. This may have worked in favor of UGT who assumed  $B = 0$ . In general, however, this assumption implies a relation between the curvatures at minimum and maximum of  $\hat{W}(\theta)$ , namely,

$$\sqrt{W_1/\hat{W}''_{\min}} + \sqrt{W_1/|\hat{W}''_{\max}|} = \frac{2}{r} \quad (6.22)$$

(in this case  $r = 2$ ). We find numerically that the *l.h.s.* of this equation is equal to 1.00021 for the (1, 1) resonance.

## 6.6 Conclusions

The oscillatory part of the density of states can be expressed in terms of traces of the powers of  $T$ -operator. The powers can be evaluated by the stationary phase. For their traces the  $S\Phi$  can

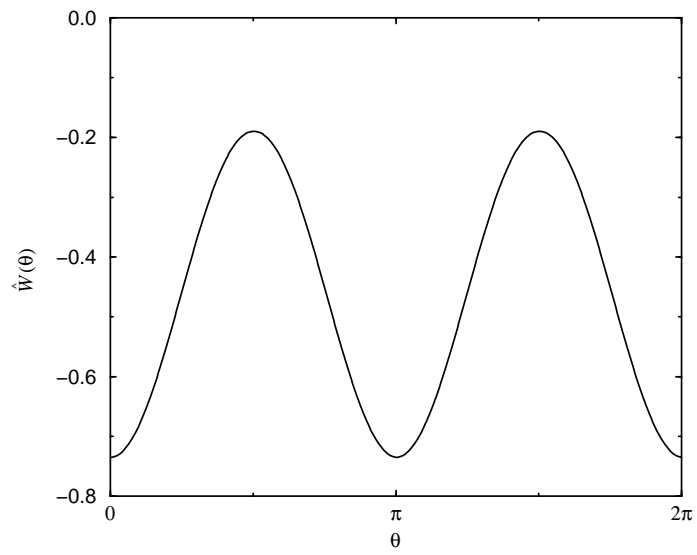


Figure 6.1:  $\hat{W}(\theta)$  for the (1, 1) family of orbits ( $\alpha = 1$ ) of the quartic oscillators with  $x^2y^2$  coupling. The parameters  $a = b = E = 1$ .

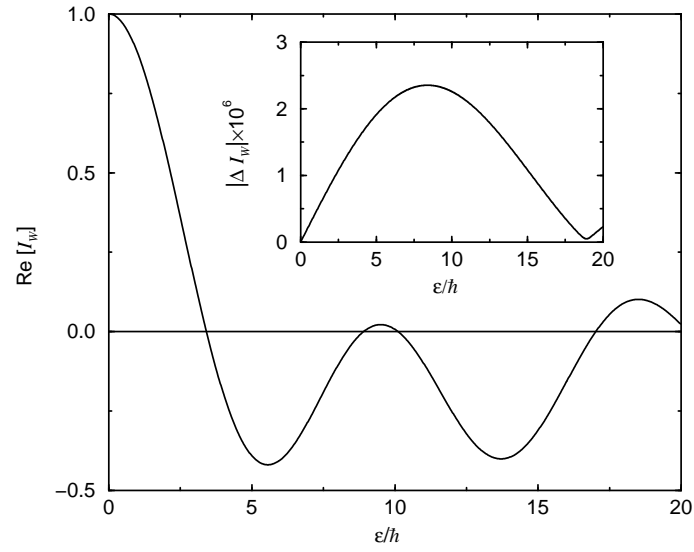


Figure 6.2: Real part of  $I_W$  as a function of  $\epsilon/\hbar$ . The difference between this function computed by numerical quadrature and from the interpolation formula,  $|\Delta I_W|$ , is shown in the inset.

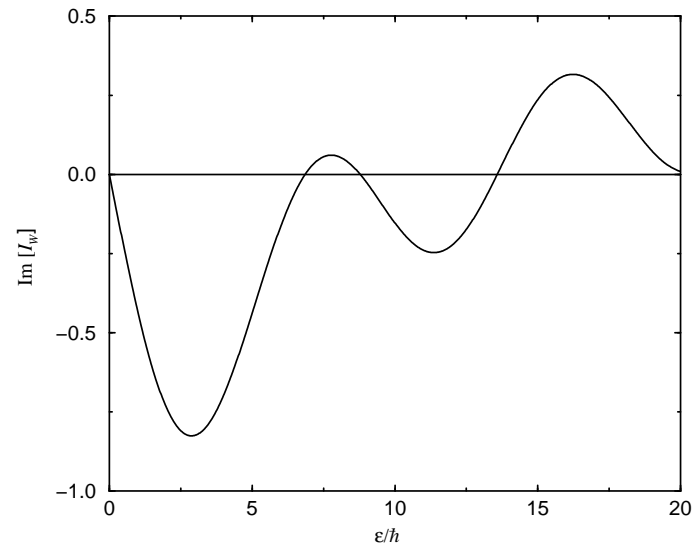


Figure 6.3: Imaginary part of  $I_W$  as a function of  $\epsilon/\hbar$ .

be used only when the periodic orbits are isolated and the action of the closed orbits in their neighborhoods divided by Planck's constant changes by order of one on the scale shorter than the distance between periodic orbits (Gutzwiller case). For an (almost) integrable system the whole family of (almost) periodic orbits contributes to the trace (Berry-Tabor case). When the perturbed action becomes large compared to the Planck constant, the surviving periodic orbits can be considered well isolated and the Gutzwiller formula is recovered.

## Chapter 7

### Summary

In this work we formulated the semiclassical theory for perturbed integrable systems, applied this theory in a number of cases, and compared it with other methods. The use of the Poincaré surface of section (PSS) allows to reduce the spatial dimensions by one. The Bogomolny  $T$ -operator connects the classical and semiclassical pictures on the surface of section. It is a kernel of an integral equation  $T\psi = \psi$  that determines the PSS wavefunction. It has a solution when the energy is on the spectrum, i.e. when  $\det(1 - T) = 0$ . The  $T$ -operator is unitary in the stationary phase approximation. When the boundary of a billiard is chosen as a surface of section, Bogomolny's equation follows from the boundary integral method in the semiclassical approximation. The  $T$ -operator contains the Maslov phases that come from the regions where the semiclassical approximation is not valid.

A classical resonance in a perturbed integrable system manifests itself in the quantum picture if the size of the resonant island is greater than the Planck constant. In a billiard with a perturbed boundary this translates to the condition  $\sqrt{L\delta L} \gtrsim \lambda$  where  $L$  is the size of the billiard,  $\delta L \sim \epsilon L$  is the magnitude of the perturbation, and  $\lambda = 1/k$  is the wavelength. When this is the case, the resonant perturbation theory is required. The theory can be constructed by expanding the phase of the PSS wavefunction  $\psi$  in  $k\epsilon^M$ , starting with  $M = \frac{1}{2}$ . In the leading order the perturbed part of the wavefunction satisfies the one-dimensional Schrödinger equation with the effective potential that scales as  $k^2\epsilon$ . Because of the above condition, the equation has bound state solutions that indicate the localized two-dimensional wavefunction. Usually the localization is in the neighborhood of a stable periodic orbit. The two-dimensional wavefunction can be found by propagating  $\psi$  from the PSS into the bulk of the

system, basically along the classical paths. The spread of the wavefunction in the momentum space scales as  $k\sqrt{\epsilon}$ . The non-resonant states are delocalized in the coordinate space, but are better localized (as  $k\epsilon$ ) in the momentum space. Our theory automatically takes into account the whole perturbed family of periodic orbits, not just the neighborhood of a stable orbit. The solutions of the one-dimensional Schrödinger equation include both bound and unbound and thus cover the transition from the resonant to non-resonant states, as long as the influence of other resonances can be neglected. In this work we considered two examples of billiards with a perturbed boundary: the circle, in particular, the short stadium, and the rectangle, in particular, the tilted square.

In some instances the perturbation theory can be applied to the non-perturbative systems. This can be done if the system is close to some integrable system in the regions where the wavefunction is large. We mentioned the ice-cream cone billiard that has the localized states in the circular part, the bouncing ball states in the stadium localized outside of the semicircles, the bouncing ball states near a period-2 orbit, and the whispering gallery modes. The system may have an additional perturbation. For example, the bouncing ball modes in the slanted stadium are shifted towards the wider end. The whispering gallery mode in a convex billiard follows from the standard EBK quantization procedure of the respective classical motion. However, when the boundary has a point or a region of zero curvature, there is no classical adiabatic invariant and the classical particle is not localized near the boundary. Still, the localized quantum state may exist. Outside of the region of zero curvature it is a superposition of the standard whispering gallery modes that are well-defined. The singular region acts like a scatterer that mixes the standard modes. The scattering matrix can be approximately expressed in terms of the  $T$ -operator. If the eigenstates of the scattering propagator are composed of the small number of the standard modes, they are localized near the boundary.

The magnetic field is a small perturbation for charged particle in a square billiard if its momentum  $p \gg eA/c$ , where  $A$  is the vector potential. Then, in the uniform field case, the cyclotron radius is greater than the size of the square. Thus, in the leading order, the shape of the orbits is unchanged. The resonant perturbation theory should be applied when  $kL\sqrt{\epsilon} \equiv \sqrt{(e/c\hbar)kBL^3} \gtrsim 1$  where  $B$  is the magnetic field. In this case there exist states that are localized near the stable periodic orbits. The unstable periodic orbits are the time-reversals

of stable orbits. The states associated with the  $(1,1)$  resonance dominate the susceptibility. Since the time-reversal symmetry is broken, the states carry the persistent currents. The low transverse modes are paramagnetic and the higher modes are diamagnetic. In the square with a flux line the localization also takes place but the diffraction effects are strong. The diffraction is smaller for a finite size tube.

When one of the system's coordinates changes much faster than the other, one can solve the two-dimensional Schrödinger equation in the Born-Oppenheimer approximation (BOA). The solution usually agrees with the perturbation theory in the leading order. The standard example are the bouncing ball states where there is a natural separation of the fast and slow motion. The rectangular geometry is easy to deal with as well, if one employs the method of images. In this case the BOA is similar to the channeling approximation. On the other hand, in the circular geometry only the low angular momentum states are suitable for the BOA. Even then it fails in the polar coordinates near the center. Thus the BOA solution cannot be completed in this case since it lacks the boundary condition at the center. At the same time, it agrees with the perturbation theory in the asymptotic region if the missing information is provided. In the whispering gallery mode the slow variable is the curvature of the boundary. In this instance the BOA solution is valid also near the caustic and in the classically forbidden region where the perturbation theory is not applicable.

The  $T$ -operator contains all the information about the energy spectrum in the semiclassical approximation. In particular, the oscillatory part of the density of states can be expressed in terms of the traces of the powers of  $T$ -operator. Depending on the dynamics of the system the traces can be evaluated to yield the Gutzwiller trace formula in the hard chaotic case or the Berry-Tabor formula in the integrable case. In the former the periodic orbits are isolated and in the latter they form families. The perturbed integrable system connects the opposite situations and provides an interpolation formula. The interpolation formula can be parametrized. The parametrization depends on four parameters: the perturbed part of the action and the monodromy determinant for the stable and unstable periodic orbits. When the action difference between the stable and unstable orbits is greater than  $\hbar$ , these orbits are well isolated, when the actions are equal, the system is integrable. In the case of the coupled quartic oscillators the parametrization works very well.



The results of this work may be hard to verify experimentally, since it is the energy spectrum, not the probability density, that is usually measured. Nevertheless, there are experimental techniques available. The simplest would be to measure the electric field distribution in a microwave cavity. The experiments have already been done for a chaotic shape cavity, so there is no principal difficulty to make it almost integrable. The electric field in a cavity and the electron wavefunction in a billiard satisfy the same differential equation. The magnetic billiard can be modeled by adding a ferrite strip on the walls of the cavity. In this case the analogy holds only in the leading order in vector potential. It should also be possible to measure the electron wavefunction in quantum corrals, but the effect may be diminished due to a substantial leakage through the walls. Another class of experiments involves the surface waves in water, although here the dissipation may be a big problem.

## Bibliography

- [1] Agam O. and B. L. Altshuler, e-print cond-mat/0004190 (2000).
- [2] Aharonov Y. and D. Bohm, Phys. Rev. **115**, 485 (1959).
- [3] Arnol'd V. I., Funktsional. Anal. i Prilozhen. **6**, 12 (1972) [Functional Anal. Appl. **6**, 94 (1972)].
- [4] Babich V. M. and V. S. Buldyrev, *Short Wavelength Diffraction Theory* (Springer-Verlag, Berlin, 1991).
- [5] Bäcker A., R. Schubert, and P. Stifter, J. Phys. A **30**, 6783 (1997).
- [6] Bai Y. Y., G. Hose, K. Stefański, and H. S. Taylor, Phys. Rev. A **31**, 2821 (1985).
- [7] Baym G., *Lectures on Quantum Mechanics* (W. A. Benjamin, N.Y., 1969); A. B. Migdal and V. Krainov, *Approximation Methods in Quantum Mechanics* (W. A. Benjamin, N.Y., 1969).
- [8] Berglund N. and H. Kunz, J. Stat. Phys. **83**, 81 (1996).
- [9] Berry M. V., Ann. Phys. **131**, 163 (1981).
- [10] Berry M. V., R. G. Chambers, M. D. Large, C. Upstill, and J. C. Walmsley, Eur. J. Phys. **1**, 154 (1980).
- [11] Berry M. V. and K. E. Mount, Rep. Progr. Phys. **35**, 315 (1972).
- [12] Berry M. V. and M. Robnik, J. Phys. A **19**, 649 (1986); M. Robnik and M. V. Berry, *ibid.* **19**, 669 (1986).
- [13] Berry M. V. and M. Tabor, Proc. R. Soc. London, Ser. A, **349**, 101 (1976).

- [14] Berry M. V. and M. Tabor, J. Phys. A **10**, 371 (1977).
- [15] Birkhoff G. D., *Dynamical Systems* (American Math. Society, N.Y., 1927).
- [16] Biswas D. and S. R. Jain, Phys. Rev. A **42**, 3170 (1990).
- [17] Blümel R. and B. Esser, Phys. Rev. Lett. **72**, 3658 (1994).
- [18] Boasman P. A., Nonlinearity **7**, 485 (1994).
- [19] Bogomolny E. B., Nonlinearity **5**, 805 (1992).
- [20] Borgonovi F., Phys. Rev. Lett. **80**, 4653 (1998).
- [21] Borgonovi F., G. Casati, and B. Li, Phys. Rev. Lett. **77**, 4744 (1996).
- [22] Born M. and J. R. Oppenheimer, Ann. Phys. (Leipzig) **4-84**, 457 (1927).
- [23] Boyd G. D. and J. P. Gordon, Bell Syst. Tech. J. **40**, 489 (1961).
- [24] Bunimovich L. A., Comm. Math. Phys. **65**, 295 (1979).
- [25] Casati G. and T. Prosen, Phys. Rev. E **59**, R2516 (1999).
- [26] Creagh S. C., J. M. Robbins, and R. G. Littlejohn, Phys. Rev. A **42**, 1907 (1990).
- [27] Crommie M. F., C. P. Lutz, and D. M. Eigler, Science **262**, 218 (1993).
- [28] Date G., S. R. Jain, and M. V. N. Murthy, Phys. Rev. E **51**, 198 (1995).
- [29] Dembowski C., H.-D. Gräf, A. Heine, R. Hofferbert, H. Rehfeld, and A. Richter, Phys. Rev. Lett. **84**, 867 (2000).
- [30] Fishman S., B. Georgeot, and R. E. Prange, J. Phys. A **29**, 919 (1996).
- [31] Fishman S., D. R. Grempel, and R. E. Prange, Phys. Rev. Lett. **49**, 509 (1982).
- [32] Frahm K. M. and D. L. Shepelyansky, Phys. Rev. Lett. **78**, 1440 (1997); *ibid.* **79**, 1833 (1997).
- [33] Georgeot B. and R. E. Prange, Phys. Rev. Lett. **74**, 2851 (1995).
- [34] Georgeot B. and R. E. Prange, Phys. Rev. Lett. **74**, 4110 (1995).

- [35] Gokirmak A., D.-H. Wu, J. S. A. Bridgewater, and S. M. Anlage, *Rev. Sci. Instrum.* **69**, 3410 (1998).
- [36] Goodings D. A. and N. D. Whelan, *J. Phys. A* **31**, 7521 (1998).
- [37] Gradshteyn I. S. and I. M. Ryzhik, *Table of integrals, series, and products* (Academic Press, Boston, 1994).
- [38] Gustavson F. G., *Astron. J.* **71**, 670 (1966).
- [39] Gutzwiller M. C., *J. Math. Phys.* **11**, 1791 (1970).
- [40] Gutzwiller M. C., *J. Math. Phys.* **12**, 343 (1971); *Chaos in Classical and Quantum Mechanics*, (Springer-Verlag, N.Y., 1990).
- [41] *Handbook of Mathematical Functions*, edited by M. Abramowitz and I. Stegun (Dover, N.Y., 1965).
- [42] Heller E. J., *Phys. Rev. Lett.* **53**, 1515 (1984).
- [43] Heller E. J., M. F. Crommie, C. P. Lutz, and D. M. Eigler, *Nature* **369**, 464 (1994).
- [44] Kaplan L. and E. J. Heller, *Physica D* **121**, 1 (1998).
- [45] Keller J. B., *Ann. Phys. (N.Y.)* **4**, 180 (1958).
- [46] Keller J. B. and S. I. Rubinow, *Ann. Phys. (N.Y.)* **9**, 24 (1960); *ibid.* **10**, 303(E) (1960).
- [47] Khinchin A. Ya., *Continued Fractions* (University of Chicago Press, Chicago, 1964).
- [48] Kudrolli A., M. C. Abraham, and J. P. Gollub, e-print nlin.CD/0002045 (2000).
- [49] Landau L. D. and E. M. Lifshitz, *Quantum Mechanics. Non-relativistic Theory* (Pergamon Press, London, 1958).
- [50] Lazutkin V. F., *KAM Theory and Semiclassical Approximations to Eigenfunctions* (Springer-Verlag, Berlin, 1993).
- [51] Lévy L. P., D. H. Reich, L. Pfeiffer, and K. West, *Physica B* **189**, 204 (1993).

- [52] Lichtenberg A. J. and M. A. Lieberman, *Regular and Chaotic Dynamics* (Springer-Verlag, N.Y., 1992).
- [53] Lindhard J., Dan. Mat. Fys. Medd. **34(14)** (1965).
- [54] Maslov V. P. and M. V. Fedoriuk, *Semi-Classical Approximation in Quantum Mechanics* (Reidel, Boston, 1981).
- [55] Mather J. N., Ergod. Th. and Dynam. Sys. **2**, 397 (1982).
- [56] Narevich R., private communication.
- [57] Narevich R., R. E. Prange, and O. Zaitsev, Phys. Rev. E **62**, 2046 (2000); Physica E (to be published).
- [58] Nöckel J. U. and A. D. Stone, Nature **385**, 45 (1997).
- [59] Ozorio de Almeida A. M., *Hamiltonian Systems: Chaos and Quantization* (Cambridge University Press, Cambridge, 1988); in *Quantum Chaos and Statistical Nuclear Physics*, edited by T. H. Seligman and H. Nishioka, Lecture Notes in Physics, Vol. 263 (Springer, Berlin, 1986).
- [60] Prange R. E., Phys. Rev. Lett. **77**, 2447 (1996).
- [61] Prange R. E., private communication.
- [62] Prange R. E., R. Narevich, and O. Zaitsev, Phys. Rev. E **59**, 1694 (1999); e-print chaodyn/9802109 (1998).
- [63] Prange R. E., R. Narevich, and O. Zaitsev, e-print nlin.CD/0010001 (2000); Physica Scripta (to be published).
- [64] Primack H. and U. Smilansky, J. Phys. A **27**, 4439 (1994).
- [65] Rahav S. and S. Fishman, Foundations of Physics (to be published).
- [66] Rayleigh Lord, Phil. Mag. **20**, 1001 (1910); *ibid.* **27**, 100 (1914); *The Theory of Sound*, v. 2 (MacMillan, London, 1894).

- [67] Richter K., D. Ullmo, and R. A. Jalabert, Phys. Rep. **276**, 1 (1996), and references therein.
- [68] Robnik M., J. Phys. A **17**, 109 (1984).
- [69] Robnik M. and M. V. Berry, J. Phys. A **18**, 1361 (1985).
- [70] Sieber M., H. Primack, U. Smilansky, I. Ussishkin, and H. Schanz, J. Phys. A **28**, 5041 (1995).
- [71] Sieber M., U. Smilansky, S. C. Creagh, and R. G. Littlejohn, J. Phys. A **26**, 6217 (1993).
- [72] So P., Ph.D. thesis, University of Maryland, 1995.
- [73] So P., S. M. Anlage, E. Ott, and R. N. Oerter, Phys. Rev. Lett. **74**, 2662 (1995); D. H. Wu, J. S. A. Bridgewater, S. M. Anlage, and A. Gokirmak, Phys. Rev. Lett. **81**, 2890 (1998); S.-H. Chung, A. Gokirmak, D.-H. Wu, J. S. A. Bridgewater, E. Ott, T. M. Antonsen, and S. M. Anlage, Phys. Rev. Lett. **85**, 2482 (2000).
- [74] Tabor M., *Chaos and integrability in nonlinear dynamics: an introduction* (Wiley, N.Y., 1989).
- [75] Tanner G., J. Phys. A **30**, 2863 (1997).
- [76] Ullmo D., M. Grinberg, and S. Tomsovic, Phys. Rev. E **54**, 136 (1996); S. Tomsovic, M. Grinberg, and D. Ullmo, Phys. Rev. Lett. **75**, 4346 (1995).
- [77] Wallraff A., A. V. Ustinov, V. V. Kurin, I. A. Shereshevsky, and N. K. Vdovicheva, Phys. Rev. Lett. **84**, 151 (2000).
- [78] Zaitsev O., unpublished.
- [79] Zaitsev O., R. Narevich, and R. E. Prange, e-print chao-dyn/9902019 (1999); R. E. Prange, O. Zaitsev, and R. Narevich, Physica E (to be published).
- [80] Zaitsev O., R. Narevich, and R. E. Prange, e-print nlin.CD/0009054 (2000); Foundations of Physics (to be published).